Response to Comments of Referee#1

Dear Reviewer:

We would like to thank you for the valuable and constructive comments/suggestions which helped to improve our manuscript. We have carefully revised the manuscript accordingly. Please find our point-to-point responses below (line numbers and figure numbers refer to the new version of manuscript; reviewer comments and suggestions are in italics, responses are in plain font; revised sections in the manuscript text in response to the comments are marked with red color).

1. In Section 3, was the WRF simulation nudged towards FNL analysis data? If so, is it fair to compare nudged model results with observations? Please clarify on this.

Response: We thank the reviewer for pointing out this missing information. In this study, a nudging towards FNL analysis data was used for the domain1 (75 km) and domain2 (15 km) to provide a more accurate meteorological boundary for domain3 (3 km). The innermost domain was driven one-way by initial and boundary inputs from the outer domain. No nudging was used in the domain3 (3 km). To evaluate the impact of aerosol-induced perturbations, we used only the meteorological fields in domain 3.

We have added clarifications on this point (Page 6, line 156): 'No nudging was used in the innermost domain. The aerosol-induced perturbations were estimated with the meteorological fields simulated in domain3.'

2. Is the conclusion sensitive to different plume rise parameterizations? Can the authors provide some validations on the simulated plume rise heights?

Response: Thanks for drawing attention to this point. The plume rise height is indeed an important factor for investigating aerosol-radiation-cloud interaction. For example, Johnson et al. (2004) showed the vertical distribution of light-absorbing aerosols could significantly affect the aerosol radiative effect. The plume rise parameterization used in this study is the only option provided in WRF-Chem (Grell et al., 2011; Freitas et al., 2007), which has shown commendable performance in simulating the plume height in the Amazon (Wu et al., 2011). To demonstrate the performance of the plume rise scheme in our study, we have conducted a comparison of the aerosol vertical distribution using CALIPSO observations.

The clear-sky monthly mean aerosol extinction profiles at 532 nm, provided by the CALIPSO Level 3 aerosol product (Tackett et al., 2018), was used here. The simulation data

was processed to align with the observation by using outputs corresponding to the passing time of the satellite, excluding cloudy grid cells with a cloud criterion of 1 g/kg and interpolating the extinction coefficient at 550 nm to 532 nm. The averaged aerosol extinction profiles from the model results of domain 3 and observation were then compared (Fig. R1a).

The observed vertical profile of the aerosol extinction coefficient is basically reproduced by the model. The model well captures the peaks of the aerosol extinction coefficient at the surface and near 2 km. Similar to our study, an overestimation of the aerosol extinction coefficient above 3 km was also simulated by Wu et al. (2011, Fig. R1b). The phenomenon found in both studies may be caused by an overestimated exchange between PBL and the free atmosphere by turbulent mixing and convective transport, an underestimation of precipitation scavenging, and/or an overestimated plume rise at some fire spots. Generally, the vertical distribution of aerosols is captured reasonably by the model, which illustrates an acceptable performance of the plume rise parameterization and indicates the reliability of the conclusions about aerosol-radiation-cloud interactions obtained by the model.

We have added the comparison of the aerosol extinction coefficient profile to the aerosol evaluation section in the SI (Page 6, Line 142).

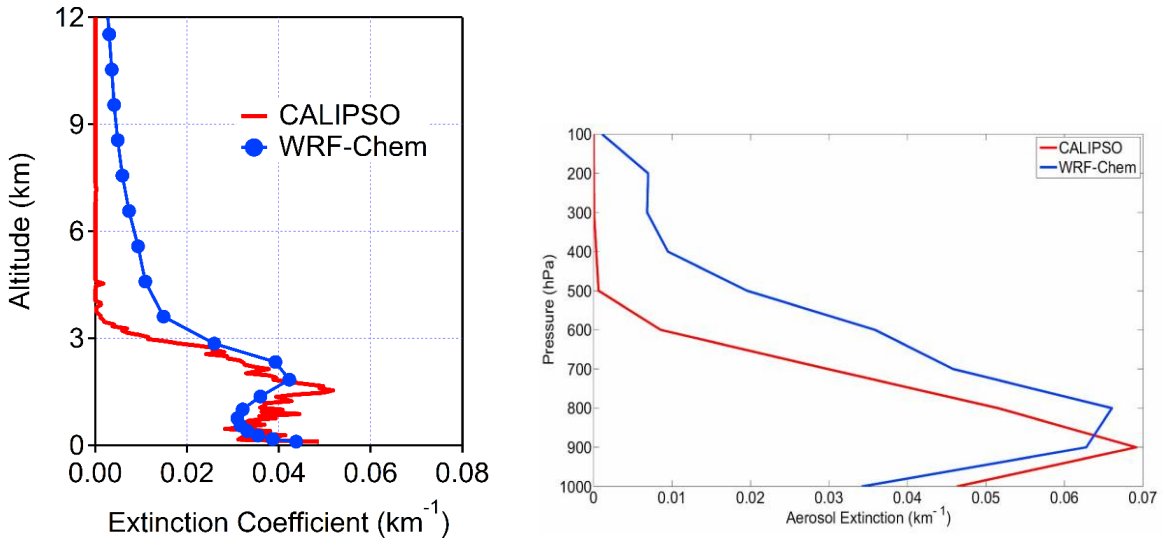

(a) (b)

Figure R1. (a) Monthly mean clear-sky aerosol extinction coefficient at 532 nm averaged over domain3. (b) Clear-sky aerosol extinction coefficient at 532 nm averaged over the Amazon Basin (Figure 3 from Wu et al. 2011).

3. Is the conclusion sensitive to the choice of the period? One month seems to be quite short. Why not consider multi-month or multi-year analysis?

Response: We acknowledge the reviewer's concern and we agree that longer term simulation (multi-month and/or multi-year) may add to the robustness of the conclusions. Currently, the simulations for this study were conducted for one month but not for a longer time mainly because of the limitation of the computing resources. As the WRF-Chem model itself is computation-demanding due to many coupled modules, and since additionally the simulations included 3-nested domains with fine resolution (3 km) at the innermost domain of 161*161 grids, and a set of 10 parallel sensitivity cases for 5 emission scenarios, the simulations are highly computational intensive. Previous WRF-Chem simulations using such fine resolution to estimate the aerosol-radiation-cloud interaction were limited to 3-day to 8-day periods (Archer-Nicholls et al., 2016; Wu et al., 2011). The authors made an attempt in this study to expand the simulation time in order to include more cloud and precipitation cases and to give more robust constraints on the aerosol effect assessments compared to previous simulations. Limited by current computing resources, we chose a simulation period of 1 month, which has been shown to be a timescale that has short-term climatic significance (Becker et al., 2013).

The one-month simulation period targets September 2014 in order to make sure the study is conducted under typical dry season conditions. Pöhlker et al. (2016) comprehensively compared the meteorology over 18 years (1998-2016) and found that 2014 is a typical year and September is a typical month of the dry season for the Amazon area, e.g., the precipitation rates on September 2014 were found comparable to the 18-year average data and showed no pronounced hydrological anomalies (Fig. R2). Hence, this sensitivity study based on September 2014 can serve to reveal the typical sensitivity behavior of the dry season radiation, cloud, and precipitation over the central Amazon to BB aerosols. To address the questions of the representativeness of the simulation period and sensitivity of the results to other dry season periods, we added a statement on Line 91 and included a longer period simulation as a suggestion for future investigation on Line 460, respectively:

'Comparison of the precipitation in central Amazonia in the year 2014 with that averaged over 18 years (1998–2016) indicates that the atmospheric conditions in this region in 2014 are climatically representative (Pöhlker et al., 2016). Therefore, the present study based on September 2014 may serve to represent the typical sensitivity behavior of the dry season climate to BB aerosol concentration variations.'

'Furthermore, the sensitivity of the climate response to the concentration of BB aerosols may be influenced by the meteorological conditions, and as this study is based on September 2014, continuing model investigations based on varying and longer periods are needed to characterize the influence of variations in meteorology and to provide climatic assessments.'

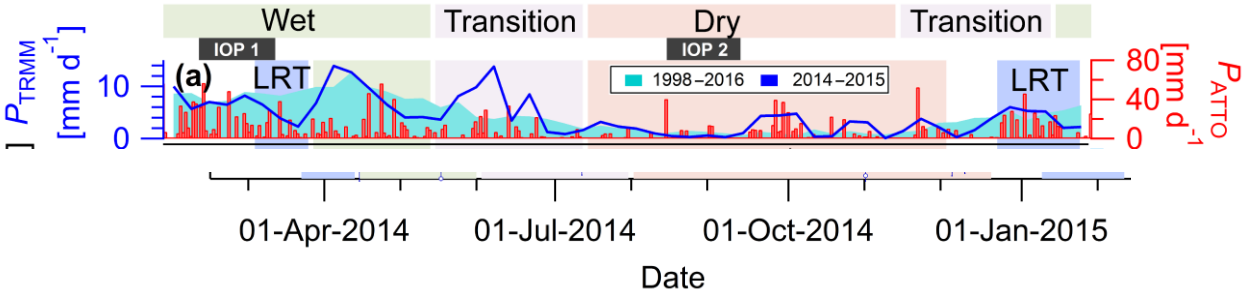

Figure R2. Precipitation rates from tropical rainfall measuring mission (TRMM) PTRMM and in situ measurements at the ATTO site PATTO. The P_{TRMM} seasonal cycles are derived from an area upwind of the ATTO site (59.5 W, 2.4 N, 54.0 W, 3.5 S), covering a long-term period from 1 January 1998 to 30 June 2016 (aqua shading), and the period of the CCN measurements from 1 March 2014 to 28 February 2015 (blue line). (Figure 1 from Pöhlker et al., 2016)

4. The main conclusion is that lower precipitation is expected with biomass burning aerosols. Do historical observations support this conclusion?

Response: The authors appreciate this insightful comment. Practically, the inconsistent methodologies used in observational data analysis and model simulation make it difficult to reconcile observation and model results. The modelling study uses strict control experiments by increasing/decreasing aerosol concentration on a fixed meteorology field. In contrast, satellite and in-situ observations usually use a method of sampling spatial and/or temporal correlation between aerosol and precipitation, and therefore other factors such as concurrent meteorological influence may bring in uncertainties. Besides, mismatched domain, study period, and convection stage between observation and model, e.g., that satellites usually measure at a specific time of day, should also be considered. Observational studies on the impact of biomass burning aerosols on precipitation, especially in-situ observations, are still scarce. The authors did find satellite observations in Rosenfeld et al. (1999) and Koren et al. (2012) showing overall consistent results with the conclusions in this study. Satellite measurements of a biomass burning episode in the tropical area by Rosenfeld et al. (1999) found that the rain formation process was shut down by biomass burning aerosols. This is consistent with our model results that biomass burning aerosols cause decreased precipitation occurrence and consequently lower precipitation amount. Another satellite measurement over the Amazon from June to August 2007 by Koren et al. (2012) showed a trend of decreasing precipitation due to biomass burning aerosols at an aerosol loading similar to this study (AOD >0.2). Yet, due to uncertainties caused by uncoordinated observation measurement and model simulation, the authors would be cautious and conservative about directly comparing the observations with the modelling results. More

observation measurements and observation conducted in coordination with modelling might still be needed to provide constraints on aerosol-precipitation interactions in the model.

5. Why did an underestimation of precipitation during Sept 17 & 18 lead to much lower temperature and higher RH, compared to the observations? Why did the temperature vary little these days? Maybe it would be worthy to check the synoptic pattern and assure that this is not a model bug.

Response: Compared to the observations, the model underestimated the precipitation at the ATTO site during Sept 17 & 18 (Fig. S3), and meanwhile the temperature (Fig. S2a) in the model (red line) is higher than the observations (dot) and the RH (Fig. S2b) in the model (red line) is lower than the observations (dot). This may be associated with the fact that the precipitation itself moistens the soil, enhances the latent heat flux, and therefore leaves less net energy in the ground to heat the surface air, so low surface air temperature occurs during precipitation. Hence, the underestimation of precipitation in the model was accompanied by higher modelled temperature. As the RH is inversely related to air temperature, a lower modelled RH was found when precipitation was underestimated. We have added more explanation about the relationship between the bias in precipitation and in temperature and RH (Line 78 in SI): 'This is expected since precipitation enhances surface evaporation and latent heat flux, leaves less net energy in the ground to heat the surface air (Zhuang et al., 2017), and therefore corresponds to a cool and moistened near-surface atmospheric state as can be found in the ATTO observation (Fig. S2). Consequently, the precipitation underestimation in the model was accompanied by higher biased simulated temperature and lower biased RH.'

The discrepancy of precipitation, temperature, and RH on Sept 17 & 18 between model and observation is obvious at the ATTO site but is not evident for the domain averaged precipitation (Fig. S6, comparison between simulated domain precipitation and TRMM observation). As suggested by the reviewer, a check of the synoptic pattern against the NCEP reanalysis was conducted (Fig. R3, shown below) and it shows the model basically captured the synoptic patterns. This means the model simulated the synoptic patterns and regional precipitation well but underestimated the precipitation at the ATTO site. The reason for this precipitation underestimation at the ATTO site could be associated with a location bias of rainfall. We then extracted the air temperature and RH from the grid (north of ATTO) where significant precipitation occurred on Sept 17&18 and compared it with the ATTO observations (Fig. R4, shown below). The air temperature (RH) at the precipitating grid dropped (increased) comparably to the observation during the rainfall period. It also serves as an indicator that the location bias of the rainfall on Sept 17 & 18 could account for the discrepancy of the meteorological factors between the simulation and the ATTO observation. We have added

more explanation for the underestimation of precipitation at ATTO (Line 113 in SI): 'The regional rainfall events on 6, 8, 17 and 18 Sep are well predicted by the model with a slight underestimation, which reflects a better model performance compared with the evident model underestimation of precipitation at the ATTO site on these four days. Moreover, the modelled synoptic patterns corresponding to the precipitation episodes are consistent with the NCEP reanalysis data (not shown). The well-reproduced regional synoptic and precipitation conditions in the model serve to corroborate that the precipitation underestimation at the ATTO site is likely induced by a local bias of rainfall location and neglecting precipitation of sub-grid convection by the model.'

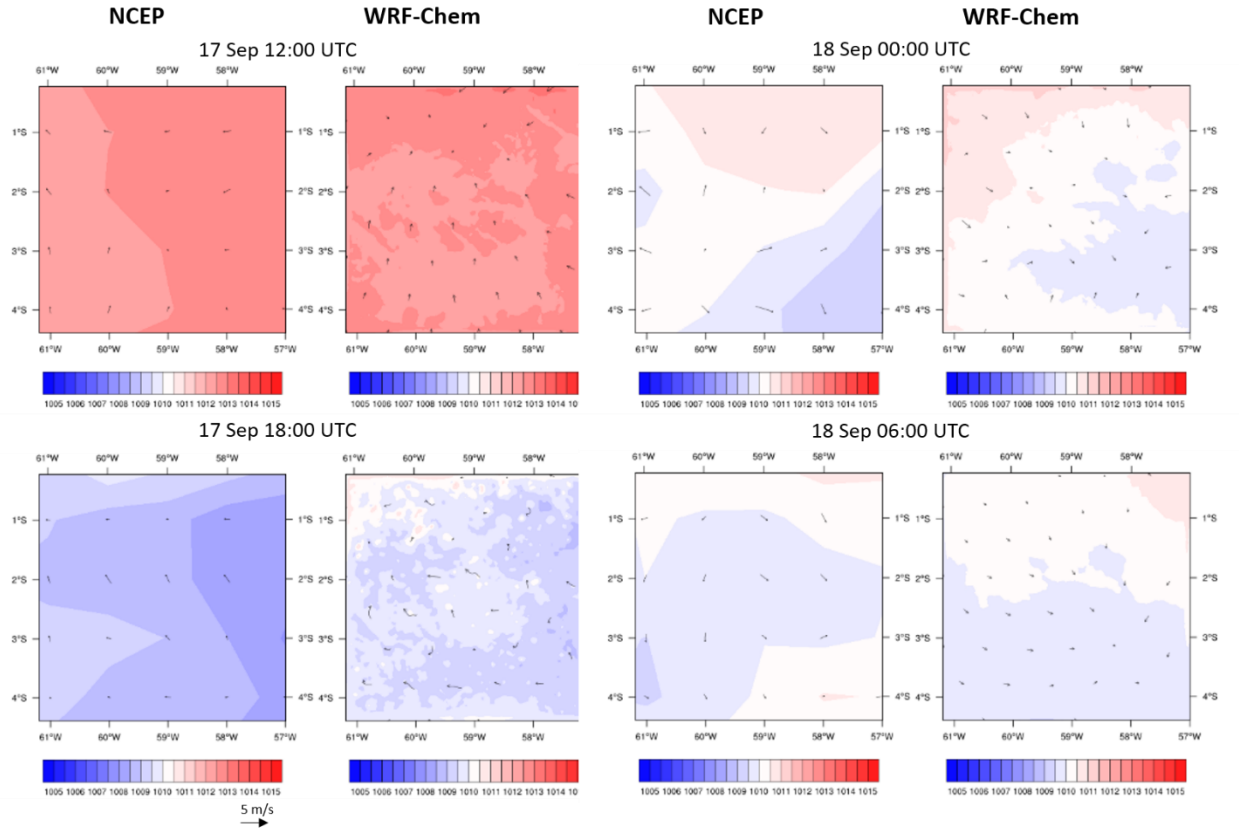

Figure R3. Surface air pressure and horizontal wind from NCEP reanalysis and WRF-Chem model.

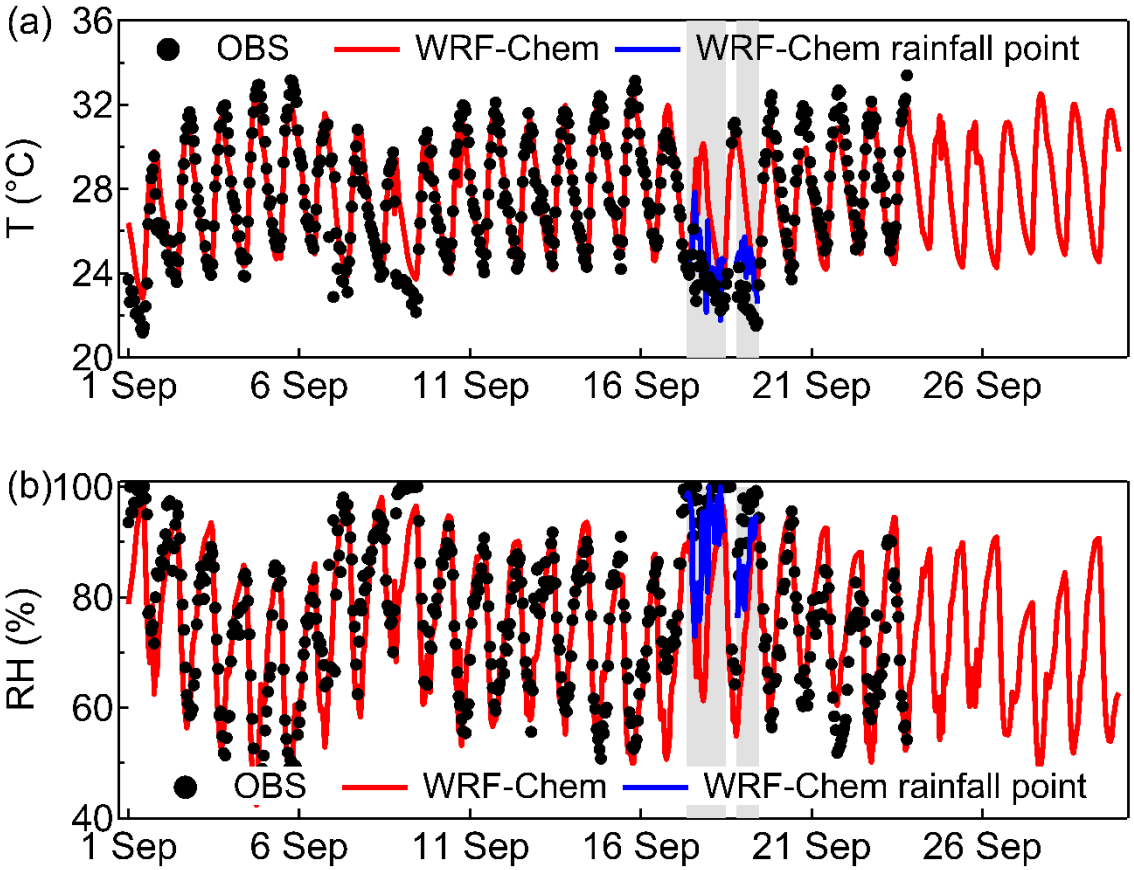

Figure R4. Time series of surface air temperature (a), relative humidity (b) from ATTO observation (black dot) and the domain3 simulation at ATTO (red line) and at significant precipitaiton point (blue line) during September 2014.

6. The validations of AOD simulation are not so impressive, it would be helpful to show: 1. the mean absolute bias & correlation between simulation and observation, making the validation more quantitative; 2. Reference other papers for the bias between simulated and observed AOD in South America and other regions, quantitatively.

Response: Thanks for the suggestion. We have revised the AOD evaluation in the studied domain according to the reviewer's suggestion to make it more clear and quantitative (Line 123 in SI).

'Table S3 shows the comparison of the modelled AOD against the AERONET observation at Manaus_EMBRAPA, a forest reservation site representative of the central Amazon environment (Artaxo et al., 2013). The model simulation generally captures the absolute value and the temporal variation of the observed AOD, with the mean bias and correlation coefficient being -0.03 and 0.54, respectively (Table S3). This is basically consistent with the AOD prediction accuracy in the Amazon by global models using the same fire emission inventory (Reddington et al., 2019; Pan et al., 2020). The slightly low bias in the AOD value could be related to an underestimated BB emission intensity due to errors in the detection of fires by satellite (Rosario et al., 2013) and/or an underestimation of the transatlantic transport from Africa (Holanda et al., 2020). Besides, the lack of SOA production in the model may also account for the bias in the AOD simulation (Bond and Bergstrom, 2006).'

Table S3. Comparison of AOD and SSA at 550 nm obtained from model simulation in domain3 and observation.

	Observation	Model[a]
	AOD	
Manaus_EMBRAPA (AERONET)	0.24±0.10 (average of Sep 2014)	0.21±0.05 (R^b=0.54)
	SSA	
TT34[c] (Rizzo et al., 2013)	0.87±0.06 (average of Jul–Dec 2008–2010)	0.89±0.01
ATTO[d] (Saturno et al., 2018b)	0.88 (average of Aug–Nov 2012–2017)	0.90±0.01

a) Model results with EMIS1, averaged for September 2014.
b) R represents the correlation coefficient between the observation and model simulation.
c) The SSA values at this site are for 637 nm. Calculation of SSA at 550 nm is not conducted due to incomplete information on Angstrom exponent in Rizzo et al. (2013).
d) The SSA observation for the ATTO site is obtained from Saturno et al. (2018b) by extrapolating the original value at 637 nm to that at 550 nm using the Angstrom exponents in Saturno et al. (2018b).

7. The authors may consider to move Section 3 to supplement to make the manuscript less length and more focused.

Response: Very good suggestion. We have moved Section 3 to SI and added a short summary of the evaluation before the results section (Line 208).

'The WRF-Chem simulation with the EMIS1 scenario was evaluated for the meteorological conditions and the aerosol field using ground-based, radiosonde, and satellite remote sensing measurements (see Supplement Text S1–S3). The results show that the model simulation at 3 km resolution reasonably reproduces the metrological field in terms of surface conditions, vertical atmospheric structure, and regional precipitation. The total cloud fraction and liquid cloud amount are well captured by the model while the simulated ice water amount shows lower magnitude than the observations. The model generates close agreement of the predicted aerosol properties with the observations, including the aerosol optical properties

(AOD and SSA) and the CCN concentrations at different supersaturation conditions. Details of the model evaluation are provided in the Supplement. The satisfactory performance of the model enables it to provide reliable assessments of the BB aerosol effects on the regional climate through aerosol-radiation-cloud interactions.'

8. Technical comments: Line 27: 'which enables them' -> 'which enable them'

Response: Accepted.

9. Technical comments: Line 151: Need a reference

Response: Accepted. The reference has been added at Line 158 of the revised manuscript:

'Anthropogenic emissions were from the EDGAR-HTAPv2, a global gridded air pollution emission dataset with a resolution of 0.1° × 0.1° (http://edgar.jrc.ec.europa.eu/htap_v2; Janssens-Maenhout et al., 2015).'

Janssens-Maenhout, G., Crippa, M., Guizzardi, D., Dentener, F., Muntean, M., Pouliot, G., Keating, T., Zhang, Q., Kurokawa, J., Wankmüller, R., Denier van der Gon, H., Kuenen, J. J. P., Klimont, Z., Frost, G., Darras, S., Koffi, B., and Li, M.: HTAP_v2.2: a mosaic of regional and global emission grid maps for 2008 and 2010 to study hemispheric transport of air pollution, Atmos. Chem. Phys., 15, 11411–11432, https://doi.org/10.5194/acp-15-11411-2015, 2015.

Reference

Becker, E. J., H. van den Dool, and M. Peña, 2013: Short-Term Climate Extremes: Prediction Skill and Predictability. J. Climate, 26, 512–531, https://doi.org/10.1175/JCLI-D-12-00177.1.

Response to Comments of Referee#2

Dear Reviewer:

We would like to thank you for the valuable and constructive comments/suggestions which helped us to improve our manuscript. We have carefully revised the manuscript accordingly. Please find our point-to-point responses below (line numbers and figure numbers refer to the new version of manuscript; reviewer comments and suggestions are in italics, responses are in plain font; revised sections in the manuscript text in response to the comments are marked with red color).

1. To assess ARI, why not contrasting the experiment PC3_EMISX and PCNR3_EMISX? The current way to obtain ARI has an underlying assumption that that the total aerosol effects are a linear combination of ACI and ARI, which may not be the case because of the complexity of the nonlinear microphysics-dynamics-thermodynamics interactions of the system. Such an uncertainty should be discussed in the paper.

Response: We thank the reviewer for this insightful comment. This paper focuses on assessing the ARI of biomass burning aerosols (BBA), but the PC3_EMISX and PCNR3_EMISX include aerosols from biomass burning origin and other sources such as anthropogenic. Contrasting the experiment PC3_EMISX and PCNR3_EMISX results in the ARI of all aerosols (biomass burning plus other sources). In the studied domain, the contribution of non-BBA to the bulk aerosol optical property, although not dominant, is noticeable, e.g. the black carbon emission rate in the EMIS1 scenario is 1.8 mg m^{-2} s^{-1} for biomass burning emissions and 0.4 mg m^{-2} s^{-1} for anthropogenic emissions, and the non-BBA proportion is even accentuated in the EMIS0.5 case. The method used in this study to assess the ARI of BBA refers to the same method used in Archer-Nicholls et al. (2016) for separating BBA's indirect effect, i.e. ACI in this study, and radiative effect (direct+semi-direct), i.e. ARI in this study. This method assumed a closure relationship between the total aerosol effect and individual effects (ARI and ACI) and calculated the ARI as all the BBA-induced perturbations except those induced by the ACI pathway. This assumption was also found conventionally applied in assessing the radiative forcing of specific aerosols by indirect, direct and semi-direct effects separately and jointly (Ghan et al., 2012). By this method, the ARI of BBA can be obtained without the influence from non-BBA since the ARI from non-BBA (CC3-CCNR3) was deducted from the ARI of all aerosols (PC3_EMISX- PCNR3_EMISX).

On the other hand, the authors acknowledge the reviewer's concern that the nonlinear nature of the cloud system may make ARI assessed in the present way different from the results by contrasting the simulations with and without BBA radiative feedback. We calculated the difference between these two definitions of ARI, based on the EMIS6 scenario, since the non-BBA proportion could be neglected at high biomass burning emission intensity (the

black carbon emission rate in the EMIS6 scenario is 10.8 mg m^{-2} s^{-1} for biomass burning emissions and 0.4 mg m^{-2} s^{-1} for anthropogenic emissions). The results (Table S1) show that the difference between these two definitions of ARI is small (within the range of standard error) and does not influence the conclusions about the relative importance of ACI and ARI in this study.

The discussion about this uncertainty has been added (Page 7, Line 199):

'Due to the nonlinear nature of the cloud system, which involves complicated microphysics-dynamics-thermodynamics feedbacks (Stevens and Feingold, 2009), the ARI effect calculated as the residual component of the aerosol total effect aside from the ACI part may be different from directly contrasting the simulations with and without the radiative effect from BB aerosols. To assess this uncertainty, we compared the ARI effect on clouds obtained here with its counterpart, i.e., the difference between PC3_EMIX and PCNR3_EMISX, which directly computes the effect associated with aerosol-radiation interactions from all aerosols, based on the EMIS6 scenario to minimize the influence of aerosols not from BB (Table S1). It shows that the uncertainty in the ARI quantification associated with the cloud nonlinear microphysics-dynamics-thermodynamics feedbacks is very small and would not have a significant influence on the ARI assessment in this study.'

Table S1. Monthly mean perturbations caused by the ARI of BB aerosols for the EMIS6 emission scenario.

	ARI in this study	PC3_EMISX - PCNR3_EMISX	difference
LWP (g m^{-2})	–3.8	–3.9	–0.1 (3%)
IWP (g m^{-2})	0.26	0.24	–0.02 (8%)

2. It is unclear how the model treats the BC aging process. According to the present model description in Section 2.1, it seems the fresh BC are immediately mixed with other types of aerosols after emission. Such a simplified treatment could result in overestimation of the BC absorption and associated radiative forcing [Wang et al., 2018; Peng et al., 2016].

Response: Thanks for pointing out this issue. For calculating the aerosol optical properties, the model uses the Maxwell-Garnett mixing rule, which treats the BC as small particles distributed randomly within a mixture of the other chemical components. The BC aging process has not yet been implemented in the WRF-Chem available to the community. We have added a clarification about the treatment of BC aging in the model:

'Note that the process of BC aging (Peng et al., 2016; Wang et al., 2018) has not been implemented in the model. In the future, it would be desirable to implement BC aging (Peng

et al., 2016; Wang et al., 2018) in order to more accurately simulate the mixing state of BC-containing aerosols.'

The immediate mixing of BC with other aerosols after emission did not cause obvious overestimation of BC absorption in the studied domain, as shown from the comparable single scattering albedo (SSA) between the model output and the observation (Table. S3). This could have benefited from the improved mixing rule used here, because the Maxwell-Garnett mixing rule was proven to overcome the unrealistic absorption enhancement of BC by the direct internal mixing to some extent and was found to provide reasonable BC absorption (Bond and Bergstrom, 2006). Besides, the fact that the studied domain is away from the intensive biomass burning source and is impacted by the fire plumes transported there hours after being emitted could also lower the influence of BC aging on the studied domain. The evaluation of simulated SSA and AOD (Table S3) shows that the model can generally capture the aerosol optical features in this region, and therefore is reliable for estimating the aerosol radiative effect.

3. According to Fig. 6, the month-long simulations include a couple of deep convective systems with heavy precipitation (Sept. 9, 17-18). For the precipitation response analyses in Fig. 15, can the authors take a further step to assess the deep convective systems and the rest separately? Maybe a threshold of 3 mm/3hr can be applied to categorize those cases.

Response: Thanks for the insightful suggestion. Accordingly, we have separated the precipitation responses for deep convective systems and the rest as the reviewer suggested and added corresponding figures and discussion to the revised manuscript.

'To examine the precipitation responses at different precipitation intensities (Fig. 10), a threshold of daily maximum 3-hour accumulated precipitation exceeding 3 mm, the upper boundary of the domain averaged amount (Fig. S6), is used to distinguish the intensive precipitation grids from the light precipitation ones. High convective strength indicated by larger CAPE (Fig. 10) corresponds to intensive precipitation, whereas relatively weaker convection is associated with the light precipitation regime. Intensive precipitation shows a significant nonlinear ARI response, whereas light precipitation tends to be reduced monotonically by the ARI. The precipitation reduction by ACI at low aerosol concentration is less prominent in heavy than in light rainfall, due possibly to the dynamic feedbacks in deep convection (Rosenfeld et al., 2008). By contrast, a stronger ACI effect at larger aerosol amounts is shown in heavy precipitation as a result of the larger potential for CCN activation in strong convection (Reutter et al., 2009). The dependence of precipitation change on aerosol concentration is greater for the intensive precipitation than the light precipitation

regime, given that the precipitation responses at the EMIS1 and EMIS6 scenarios are –1% and –27 % respectively for the intensive regime and –5% and –17% respectively for the light precipitation. This is consistent with the rainfall sensitivity to increasing aerosol concentration for strong and weak convection in Chang et al. (2015). The dominance role of ARI over ACI at high aerosol loadings is found at both regimes.'

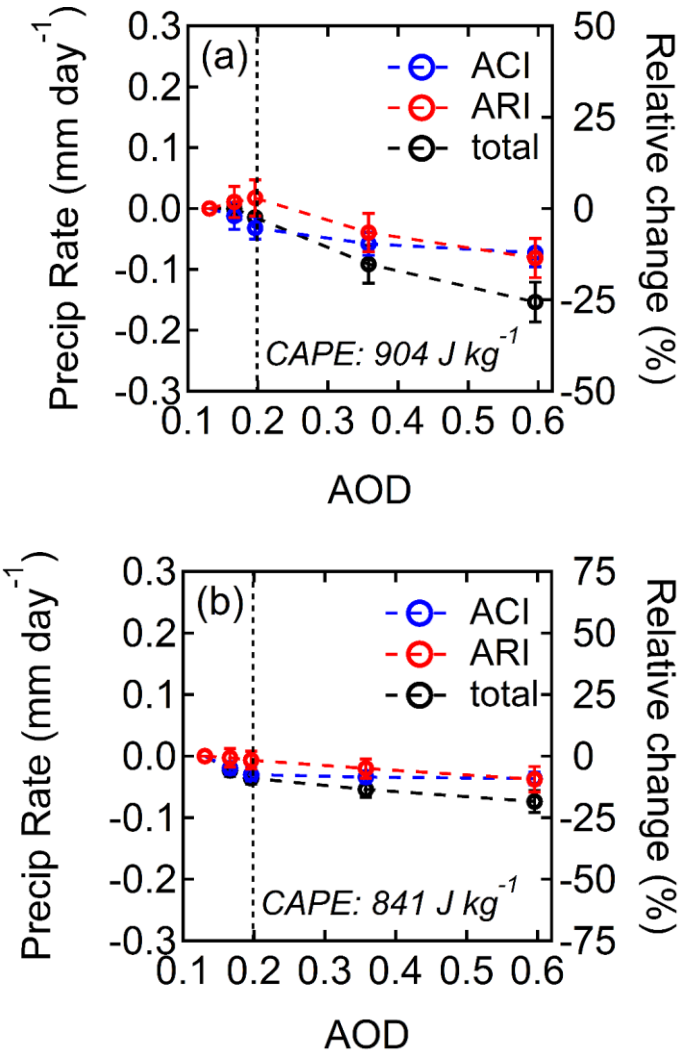

Figure 10. Changes in domain-averaged precipitation rate with increasing BB emission intensity (indicated by domain-averaged AOD in each emission scenario) at intensive precipitation regime (a) and light precipitation regime (b). The vertical dotted line in each plot indicates the EMIS1 scenario. Error bars denote the standard error.

4. For the IWP evaluation, how are the satellite data are averaged spatially? It seems the satellite observations shown in Fig. 5 are averaged over cloud points only. I doubt ice heterogeneous nucleation scheme can explain such a huge discrepancy. Even if the ice production scheme is not a function of INP concentration in this microphysics, it should still exist (most of time as function of temperature).

Response: Thanks for drawing attention to this point. The satellite datasets do have missing data points over the domain due to a combination of both unrecognized cloud ice signals and satellite technical problems such as the orbital gap (Remer et al., 2005). We calculated the countable proportion (the ratio of days when the ice water path data is not missing to the whole number of days in the study period) of each grid cell in the domain throughout the whole month (Figure R1). The countable proportion is approximately 0.5 with 6 out of 30 days having full data coverage. This can basically represent the magnitude of the IWP for the studied period and region. However, as the reviewer correctly points out, the elimination of the unrecognized weak ice signals would bias the observation results towards higher values and thus contribute to the discrepancy between the model and observation.

The ice production terms of the microphysical scheme used in the study include 1) homogeneous nucleation which occurs below -40°C and 2) depositional growth which is a function of temperature in the temperature range from -40°C to 0°C. With such an ice production parameterization, an underestimation of ice water content was found in Baro et al. (2018) by up to 80% and in this study by a similar magnitude (though the data quality contributes to some extent). A recent study by Su et al. (2018) found that introducing the ice nuclei source from dust particles into the microphysical scheme can improve the simulated ice water content by 15%. Analogous to dust particles, the biomass burning aerosols accompanied by biological material, soil dust, or ash particles was identified to efficiently improve the ice heterogeneous formation during the dry season (Seifert, P., et al., 2015). Based on these results, the missing parameterization of heterogeneous ice nucleation was listed in this study as one of the possible reasons for the IWP underestimation in the model.

We have reworded the discussion of the cloud ice comparison (Line 105 in SI). 'The uncertainties inherent in the satellite dataset, e.g., eliminating data points with unrecognized cloud ice, would bias the observation results towards higher values and thus to some extent account for the discrepancy between model and observation. Besides, uncertainties associated with the ice-phase microphysical processes, e.g., the lack of IN parameterization, may also be a potential reason for this discrepancy (Su et al., 2018).'

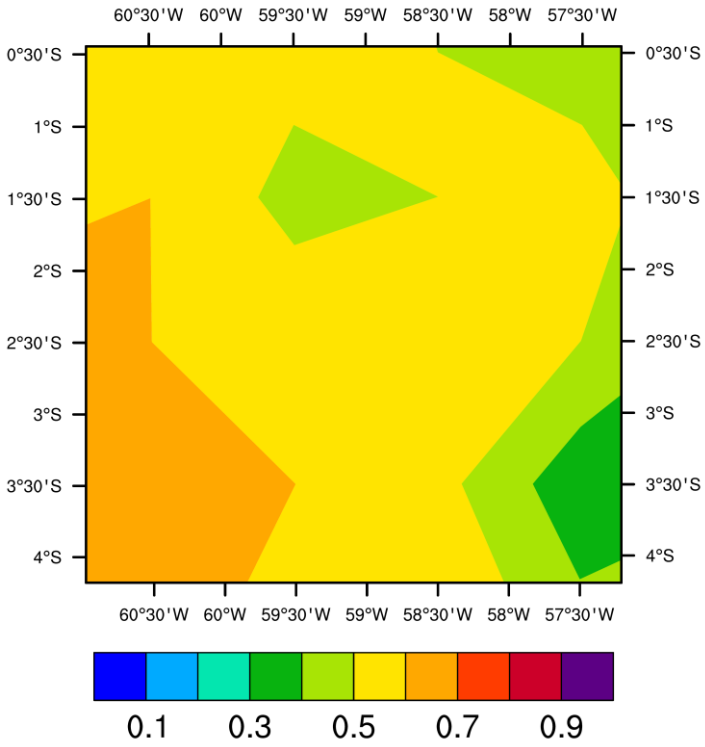

Figure R1. Fraction of countable data at each pixel throughout September 2014.

5. Line 62-65, similarly, a recent study using satellite data shows nonlinear response of deep convective clouds to smoke aerosol in South America [Jiang et al., 2017].

Response: Thanks for recommending the reference. This reference has been added.

6. Out of personal curiosity, to what extent the FDDA can reduce the meteorological biases? If the authors have the model free run available, I like to see a comparison of those two.

Response: In this study, FDDA was used in the outer domains to provide a more accurate meteorological boundary for domain 3. The simulated surface air temperature, relative humidity, and wind speed from the simulation of domain 2 with and without FDDA are compared against the observations at the ATTO site (Fig. R2). A notable improvement can be found in the run with FDDA compared to the free run.

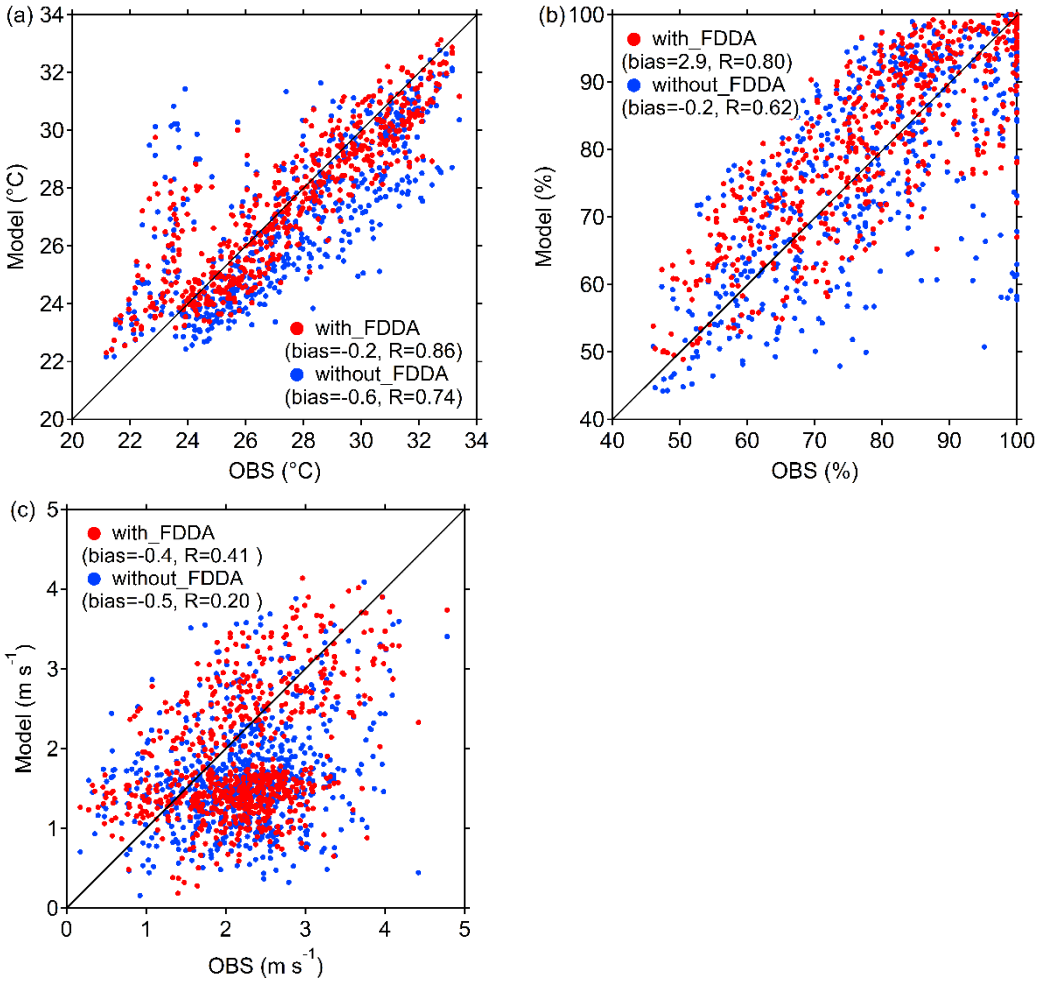

Figure R2. Scatter plot of surface air temperature (a), relative humidity (b) and wind speed (c) from observation and model simulation.

7. Fig. 4, what are the two dash lines in addition to the 1-to-1 line?

Response: The two dashed lines are 1:4 and 4:1 lines. We have clarified this in the caption.

'The dashed lines are 1:4, 1:1, 4:1 from top to bottom, respectively.'

8. Line 326-327, it doesn't make much sense to compare a regional aerosol forcing to the global values.

Response: Thanks, we agree. This comparison has been removed.

9. Fig. 11 is discussed after Figs. 12 and 13. Better to reverse their order.

Response: Accepted. The order has been reversed as the reviewer suggested.

10. In Fig. 11 and 12, the larger updraft velocity and IWP by absorbing aerosols corroborate the thermodynamic invigoration hypothesis by Wang et al. [2013] which suggested larger CAPE above PBL due to the presence of absorbing aerosols in the lower troposphere.

Response: Thanks for pointing out this connection. We have added this discussion at Line 329.

'This positive response of cloud ice and updraft velocity to ARI corresponds to the thermodynamic invigoration mechanism proposed in Wang et al. (2013) which suggested larger convective available potential energy (CAPE) above PBL could be induced by the absorbing aerosols in the lower troposphere.'

11. Title is too long. Maybe remove "dependence of aerosol-cloud and aerosol-radiation interactions on aerosol loading".

Response: We appreciate the reviewer's suggestion. We intended to use the subtitle to highlight the dependence mechanism studied in the paper and think it would help the readers to catch the key points effectively. We have shortened the title to 'Impact of biomass burning aerosols on radiation, clouds, and precipitation over the Amazon: relative importance of aerosol-cloud and aerosol-radiation interactions'

Reference

Remer, L. A., Kaufman, Y. J., Tanre, D., Mattoo, S., Chu, D. A., Martins, J. V., Li, R. R., Ichoku, C., Levy, R. C., Kleidman, R. G., Eck, T. F., Vermote, E., and Holben, B. N.: The MODIS aerosol algorithm, products, and validation, J. Atmos. Sci., 62, 947–973, 2005.

Seifert, P., Kunz, C., Baars, H., Ansmann, A., Bühl, J., Senf, F., Engelmann, R., Althausen, D., and Artaxo, P.: Seasonal variability of heterogeneous ice formation in stratiform clouds over the Amazon Basin, Geophysical Research Letters, 42, 5587–5593, https://doi.org/10.1002/2015GL064068, 2015.

Impact of biomass burning aerosols on radiation, clouds, and precipitation over the Amazon: relative importance of aerosol-cloud and aerosol-radiation interactions

Deleted: during the dry season

Deleted: dependence of aerosol-cloud and aerosol-radiation interactions on aerosol loading

Lixia Liu[1], Yafang Cheng[1], Siwen Wang[1], Chao Wei[1], Mira Pöhlker[1], Christopher Pöhlker[1], Paulo Artaxo[2], Manish Shrivastava[3], Meinrat O. Andreae[1,4], Ulrich Pöschl[1] and Hang Su[1]

[1] Max Planck Institute for Chemistry, Mainz, Germany

[2] Institute of Physics, University of São Paulo, São Paulo 05508-900, Brazil

[3] Pacific Northwest National Laboratory, Richland, Washington, USA

[4] Scripps Institution of Oceanography, University of California at San Diego, La Jolla, California, USA

Correspondence to: *yafang.cheng@mpic.de* & *h.su@mpic.de*

Abstract. Biomass burning (BB) aerosols can influence regional and global climate through interactions with radiation, clouds, and precipitation. Here, we investigate the impact of BB aerosols on the energy balance and hydrological cycle over the Amazon Basin during the dry season. We performed WRF-Chem model simulations for a range of different BB emission scenarios to explore and characterize nonlinear effects and individual contributions from aerosol-radiation interactions (ARI) and aerosol-cloud interactions (ACI). The ARI of BB aerosols tend to suppress low-level liquid clouds by local warming and increased evaporation, and to facilitate the formation of high-level ice clouds by enhancing updrafts and condensation at high altitudes. In contrast, the ACI of BB aerosol particles tend to enhance the formation and lifetime of low-level liquid clouds by providing more cloud condensation nuclei (CCN), and to suppress the formation of high-level ice clouds by reducing updrafts and condensable water vapor at high altitudes (> 8 km).

For scenarios representing the lower and upper limits of BB emission estimates for recent years (2002–2016), we obtained total regional BB aerosol radiative forcings of –0.2 W m^{-2} and 1.5 W m^{-2}, respectively, showing that the influence of BB aerosols on the regional energy balance can range from modest cooling to strong warming. We find that ACI dominate at low BB emission rates and low aerosol optical depth (AOD), leading to an increased cloud liquid water path (LWP) and negative radiative forcing, whereas ARI dominate at high BB emission rates and high AOD, leading to a reduction of LWP and positive radiative forcing. In all scenarios, BB aerosols led to a decrease in the frequency of occurrence and rate of precipitation, caused primarily by ACI effects at low aerosol loading and by ARI effects at high aerosol loading. The dependence of precipitation reduction on BB aerosol loading is greater in a strong convective regime than under weakly convective conditions.

Deleted: -

Overall, our results show that ACI tend to saturate at high aerosol loading, whereas the strength of ARI continues to increase and plays a more important role in highly polluted episodes and regions. This should hold not only for BB aerosols over the Amazon, but also for other light-absorbing aerosols such as fossil fuel combustion aerosols in industrialized and densely populated areas. The importance of ARI at high aerosol loading highlights the need for accurately characterizing aerosol optical properties in the investigation of aerosol effects on clouds, precipitation, and climate.

1 Introduction

Biomass burning as a main source of fine particles can influence weather and climate through complex feedbacks with radiation and clouds on regional and global scales (Ramanathan et al., 2001; Kaufman and Koren, 2006; Rosenfeld et al., 2008; Shrivastava et al., 2017; Ditas et al., 2018). Aerosols emitted from biomass burning contain black carbon (BC) and brown carbon, which enable them to scatter and absorb solar radiation directly, the so-called 'direct radiative effect' (Charlson et al., 1992; Ackerman et al., 2000). Absorption and scattering of radiation can lead to spatial perturbation and redistribution of energy, therefore trigger subsequent changes in surface energy budget, ground-atmosphere flux exchange, atmospheric thermodynamic stability, and cloud evolution (Li, 1998; Feingold et al., 2005; Cheng et al., 2008a, 2008b; Ding et al., 2013; Huang et al., 2016; Johnson et al., 2004), the so called 'semi-direct effect' (Hansen et al., 1997; Ackerman et al., 2000). These processes, induced by the aerosol radiative effects, are referred to as aerosol-radiation interactions (ARI; IPCC, 2013). By acting as cloud condensation nuclei (CCN) and ice nuclei (IN; Crutzen and Andreae, 1990; Roberts et al., 2001; Spracklen et al., 2011), BB aerosols influence the number concentration and size distribution of cloud droplets (Rosenfeld, 2000; Reutter et al., 2009) and thereby change the cloud albedo, i.e., the 'first indirect radiative effect' (Albrecht, 1989; Kaufman and Fraser, 1997), and cloud lifetime, i.e., the 'second indirect radiative effect' (Twomey, 1977; Jiang and Feingold, 2006). The latent heat release that accompanies these internal microphysical processes may modify atmospheric stability and affect convection strength and even subsequent cloud development (Rosenfeld et al., 2008). Such adjustments driven by aerosol microphysical effects are classified as aerosol-cloud interactions (ACI; IPCC, 2013). Each class of interactions, and their interplay can affect the weather and climate system, leading to enhanced or buffered effects (Tao et al., 2007; Koren et al., 2008; Stevens and Feingold, 2009; Wang et al., 2013).

Mainly driven by deforestation and agricultural practices (Echalar et al., 1998; Reddington et al., 2015), biomass burning events prevail in the Amazon Basin (Setzer and Pereira, 1991) during the dry season, typically between July and October (Gan et al., 2004), injecting large amounts of aerosols into the atmosphere. Long-range transport of BB aerosols from Southern Africa further increases aerosol loadings during this period (Holanda et al., 2020). Particle numbers during the peak of the burning season in the Amazon may increase one order of magnitude compared to the concentration levels during seasons without biomass fires (Martins et al., 1998; Andreae et al., 2002; Roberts et al., 2003; Martin et al., 2010). As most of the

Deleted: s

Deleted:) (

Deleted:) (

Deleted:) (

Deleted: with

Amazon region is located in the equatorial and subequatorial area with the Intertropical Convergence Zone passing across it, the radiation budget and convection system there play important roles in the global energy balance, carbon storage, and transport of water vapor (Sengupta et al., 1990; Bony et al., 2006; Su et al., 2011) and aerosols (Freitas et al., 2005). During the dry season, precipitation amounts are relatively low, rendering the rainforest ecosystem more vulnerable to rainfall changes. Therefore, perturbations imposed by BB aerosols during the dry season are important for climate and ecology in Amazonia and even globally (Andreae et al., 2004).

Extensive investigations regarding the influence of BB aerosols on radiation and convection in this region by observation (Williams et al., 2002; Andreae et al., 2004; Lin et al., 2006; Goncalves et al., 2015; Braga et al., 2017; Cecchini et al., 2017) and modelling studies (Feingold et al., 2005; Liu, 2005; Zhang et al., 2008; Wu et al., 2011; Ten Hoeve et al., 2012; Kolusu et al., 2015) have been conducted. BB aerosols were reported to cause a negative direct radiative forcing ranging from several to tens of W m^{-2} at the top of atmosphere (TOA) over the Amazon area (Procopio et al., 2004; Zhang et al., 2008; Sena et al., 2013; Kolusu et al., 2015). Yet, their total radiative forcing varies in sign and magnitude between different modelling estimates (Ten Hoeve et al., 2012; Kolusu et al., 2015; Archer-Nicholls et al., 2016) because of uncertainties associated with the prescription of aerosol optical properties, cloud sensitivity to BB aerosols, model resolution (Archer-Nicholls et al., 2016), etc. The BB aerosols over the Amazon were observed to efficiently increase cloud droplet number and decrease cloud droplet radius (Andreae et al., 2004; Cecchini et al., 2017). However, satellite remote sensing measurements showed both suppression and enhancement of cloud fraction with the presence of BB aerosols in the Amazon (Kaufman and Fraser, 1997; Koren et al., 2004; Kaufman and Koren, 2006; Koren et al., 2008), and suggested a dependence of cloud response on aerosol concentrations (Koren et al., 2008; Jiang et al., 2018). Simulations by both cloud-resolving models and regional atmosphere-aerosol coupled models found enhanced cloud water burdens due to the microphysical effects of BB aerosols (Wu et al., 2011; Reutter et al., 2014; Chang et al., 2015). Their radiative effect was shown by large-eddy simulation to efficiently diminish liquid cloud amount by evaporating cloud droplets and suppressing vapor availability from land-atmosphere flux exchange (Feingold et al., 2005). Precipitation from convective clouds was also reported to be either inhibited or invigorated based on observations from in-situ, aircraft, and satellite remote sensing measurements (Andreae et al., 2004; Lin et al., 2006; Goncalves et al., 2015). Cloud-resolving modelling found nonlinear relationships between aerosol loading and precipitation through the microphysical effects of BB aerosols (Carslaw et al., 2013; Chang et al., 2015). Regional modelling studies showed that their radiative effect could cause an overall reduction in precipitation, but may increase nighttime precipitation (Wu et al., 2011) and intensify the extreme high precipitation rates (Kolusu et al., 2015).

Inter-annual variability is a prominent characteristic of the biomass burning intensity in the Amazon (Kaufman and Fraser, 1997; Bevan et al., 2009; Pöhlker et al., 2019). However, most previous studies assessed the climate response to the perturbation from BB aerosols based on the emission scenario of one specific year (Zhang et al., 2008, 2009; Wu et al., 2011; Ten Hoeve et al., 2012; Kolusu et al., 2015; Archer-Nicholls et al., 2016). Given the possible nonlinear relationship between convection and aerosol concentration and the sensitivity of aerosol radiative forcing to aerosol loading, the necessity of a

Deleted: b

Deleted: b

Deleted: the

Deleted: b

Deleted: b

thorough assessment of radiation, clouds, and precipitation response to BB aerosols over an extensive range of emissions is underscored. Although Thornhill et al. (2018) estimated the difference in cloud response between high and low emission intensity scenarios, this difference may not be adequate to serve as constraint for estimating BB aerosols' impact on background Amazon climate, since the perturbations due to BB aerosols may be nonlinear and have been proven to be strongly dependent on the reference emission setting (Wang, 2005; Martins et al., 2009). In this study, we performed WRF-Chem simulations over the Amazon Basin in September 2014 with a 'clean' condition, defined by the absence of influence from biomass burning, and a set of emission scenarios resembling the realistic inter-annual emission variability in the dry season, to investigate the effects of BB aerosols on the Amazon radiation budget, clouds, and precipitation quantitatively and mechanistically. Comparison of the precipitation in central Amazonia in the year 2014 with that averaged over 18 years (1998–2016) indicates that the atmospheric conditions in this region in 2014 are climatically representative (Pöhlker et al., 2016). Therefore, the present study based on September 2014 may serve to represent the typical sensitivity behavior of the dry season climate to BB aerosol concentration variations. Climatically significant estimates of BB aerosols' radiative forcing, which may require statistics of over 30 years (Fiedler et al., 2017), are out of the scope of this study. As case study simulations imply that the initial convection response may influence secondary convection (Khain et al., 2005), monthly averaged effects of BB aerosols were assessed here to demonstrate an overall characteristic for the whole month. Individual processes of ARI and ACI were disentangled in our simulations, based on which the relative significance of the two pathways and their sensitivity to emission intensity were quantified. In this paper, the model description and experiment design are documented in Sect. 2. The overall impacts of BB aerosol emissions on radiation, meteorological conditions, clouds, and precipitation are shown in Sect. 3. Conclusions are in Sect. 4.

Deleted: An evaluation of the simulation results for the meteorological and chemical fields against observations is presented in Sect. 3.

Deleted: 4

Deleted: 5

2 Model and methods

Deleted: data

2.1 Model description

WRF-Chem is an online-coupled meteorology-chemistry model, which integrates meteorology and chemistry with aerosol-radiation-cloud feedbacks (Grell et al., 2005). WRF-Chem version 3.9.1 was used in this study to investigate the impact of BB aerosols on the energy budget and hydrological cycle over the Amazon Basin.

The Carbon-Bond Mechanism version Z (CBMZ) gas-phase chemistry mechanism (Zaveri and Peters, 1999) and the Model for Simulating Aerosol Interactions and Chemistry (MOSAIC) aerosol module (Zaveri et al., 2008) were selected. The aerosol size distribution is described by 8 discrete size bins defined by their lower and upper dry particle diameters ranging from 39 nm to 10 μm. Aerosols are assumed internally mixed in each bin to engage in microphysical processes. To participate in the radiative processes, each aerosol component is prescribed with a refractive index based on the values suggested in Barnard (2010). To avoid the overestimation of the particle absorption cross-section when using the internal mixing of BC with other aerosol components (Bond and Bergstrom, 2006), the Maxwell-Garnett mixing rule assuming spheres of BC

distributed randomly throughout a mixture of other aerosol components was applied in this study (Bond and Bergstrom, 2006). Note that the process of BC aging (Peng et al., 2016; Wang et al., 2018) has not been implemented in the model. In the future, it would be desirable to implement BC aging (Peng et al., 2016; Wang et al., 2018) in order to more accurately simulate the mixing state of BC-containing aerosols. With the mixed refractive indices, the aerosol extinction efficiency, single-scattering albedo, and asymmetry factor are computed using a Mie algorithm for each size bin and wavelength. The total optical properties are then obtained by integrating over all of the size bins and used as inputs to the RRTMG radiation transfer model for the shortwave (Fast et al., 2006) and longwave spectrum (Zhao et al., 2013). Aerosol-cloud interactions are accounted for in the model through three pathways: activation of aerosol particles to form cloud droplets as well as their resuspension from evaporating cloud droplets, aqueous chemistry, and wet deposition (Chapman et al., 2009). Aerosols are treated as 'interstitial' or 'cloud-borne' according to whether they are activated as CCN, and the calculation of the activation process follows the methodology of Abdul-Razzak (Abdul-Razzak and Ghan, 2002). The two-moment Lin microphysics scheme (Lin et al., 1983; Rutledge, 1984) was employed in this study, where prognostic cloud droplet number is treated based on activated aerosols following Ghan et al. (1997) and the autoconversion of cloud droplets to rain droplets is dependent on droplet number (Liu et al., 2005) so that aerosols are allowed to potentially influence the rain rate and liquid clouds (Ghan et al., 1997; Chapman et al., 2009). The aerosol-aware Lin microphysics scheme has been used previously in investigating aerosol impacts on synoptic cyclones (Ye et al., 2019), regional fog (Lee et al., 2016), and local convection systems (Wu et al., 2011). In order to validate the response of our model to increasing CCN, monthly mean domain-averaged cloud droplet radii and corresponding cloud-base CCN concentrations were calculated for simulations with different emission rates, shown in Fig. S1. The sensitivity of cloud droplet radius to increasing CCN concentration is pronounced at lower CCN concentrations, while the response tends to saturate at higher CCN concentrations. The saturation of the response of droplet radius to aerosol concentration has also been observed by satellite (Breon et al., 2002). These observations suggested a saturation point at AOD of 0.3, which corresponds to the relatively higher aerosol concentration scenario (EMIS3) in our study. 'Cloud-borne' aerosols and trace gases dissolved in cloud water interact through aqueous chemistry, which may modify aerosol composition and content. The aqueous-phase chemistry is based on the Carnegie-Mellon University (CMU) bulk aqueous phase chemical mechanism (Fahey and Pandis, 2001). Wet deposition of aerosols includes in- and below cloud removal through being collected by rain, graupel, and snow (Chapman et al., 2009) and through being scavenged by precipitation washout (Easter et al., 2004), respectively. Other major schemes utilized, e.g., the RRTMG longwave and shortwave radiation scheme (Mlawer et al., 1997; Pincus et al., 2003), the Yonsei University (YSU) boundary layer scheme (Hong, 2010), the Rapid Update Cycle (RUC) land surface scheme (Smirnova et al., 1997; Smirnova et al., 2000), the Grell-Devenyi cumulus parameterization (Grell and Devenyi, 2002), and the Fast-J photolysis rate scheme (Wild et al., 2000), are described in Table 1.

In this study, three nested domains with horizontal resolutions of 75 km, 15 km, and 3 km were set up over South America, as shown in Fig. 1. Domain1 covers most of the South American continent, with the biomass burning source region included. Domain3 centers around the ATTO site to represent the typical climate and environment of the central Amazon Basin (Andreae et al., 2015), and uses cloud-resolving grid spacing with the Grell cumulus parameterization turned off (Table 1). Vertical

Deleted: b
Deleted: b
Deleted: 5
Deleted: aerosol optical depth (
Deleted:)
Deleted: 2

layers of 29 levels extending from ground to 50 hPa were employed for all domains. The outer domains were two-way coupled with initial and boundary meteorological and chemical conditions from the 6-hour National Centers for Environmental Prediction (NCEP) Final Analysis (FNL) data and Model for Ozone and Related Chemical Tracers, version 4 (MOZART-4) global chemical transport model output (Emmons et al., 2010), respectively. The Four Dimensional Data Assimilation (FDDA) of temperature, horizontal wind and moisture was applied for the outer domains to reduce meteorological biases (Otte et al., 2012). The innermost domain was driven one-way by initial and boundary inputs from the outer domain. No nudging was used in the innermost domain. The aerosol-induced perturbations were estimated with the meteorological fields simulated in domain3. Anthropogenic emissions were from the EDGAR-HTAPv2, a global gridded air pollution emission dataset with a resolution of 0.1° × 0.1° (http://edgar.jrc.ec.europa.eu/htap_v2; Janssens-Maenhout et al., 2015). The biogenic emissions were generated online by Model of Emissions of Gases and Aerosols from Nature (MEGAN; Guenther et al., 2006). The Fire Inventory from NCAR version 1.5 (FINNv1.5; Wiedinmyer et al., 2011), which provides global estimates of the trace gas and particle emissions from open fires updated daily with 1 km resolution, was used to provide the biomass burning emissions. The primary organic matter (POM) emission rate was converted from OC emission based on an observed ratio of 1.5 between the mass of POM and OC (Reid et al., 2005). The conversion factor 1.5, broadly used in WRF-Chem simulations for biomass burning emission (Ge et al., 2014; Archer-Nicholls et al., 2015), represents the lower end of the range of POM/ OC ratios for fresh aerosol emissions from biomass burning (Yokelson et al., 2009; Takahama et al., 2011; Brito et al., 2014; Collier et al., 2016; Andreae, 2019). Plume ascent from fire emission sources is calculated by a plume rise parameterization (Grell et al., 2011; Freitas et al., 2007). The simulation spans from 24 Aug to 30 Sep 2014, when the Amazon Basin was undergoing its dry season with biomass burning prevalent. The simulation was conducted at 72-hour time slots, with the last 48 hours being used for analysis. In each recycle, the meteorological field was reinitialized, while the chemical field was restarted from the preceding run. The first 6 days of the simulation were used as spin up. Details on model configurations are listed in Table 1.

Deleted: ,

Deleted:)

Deleted: (

Deleted:)

Deleted: (

Deleted: was conducted

2.2 Design of numerical experiments

In order to quantitatively investigate the impact of BB aerosols on radiation, cloud, and precipitation, a set of BB aerosol emission scenarios generated by multiplying different aerosol emission factors (X) with the original BB aerosol emission scenario was applied to all domains. As sub-grid convective parameterization can cause uncertainties to the impacts from BB aerosols due to the lack of aerosol-cloud interactions in the sub-grid convective parameterization (Archer-Nicholls et al., 2016), the analysis of BB aerosol effects in Sect. 3 is based on the domain3 simulation where convections are explicitly resolved at 3 km resolution. Simulations of domain3, namely PC3_EMISX, were conducted using the BB aerosol emission scenario (EMISX) and chemical boundary conditions from the outer-domain simulation with the corresponding emission scenario. A control simulation CC3 was conducted without influence of biomass burning emissions. Then the total effects of BB aerosols can be evaluated from the difference between the PC3_EMISX and CC3 simulations.

Deleted: s'

Deleted: 4

Deleted: total effect

As shown in Fig. 2, the biomass burning emissions during September undergo large annual variations, e.g., the emission in 2007 is 6 times as much as that in 2014. The variation pattern of PM_{10} emitted from BB in September is consistent with an inter-annual variation of MODIS retrieved AOD over the Amazon (Sena et al., 2013). Based on the range of emission intensities from 2002 to 2016, we set three emission scenarios representing different emission strength: EMIS1 for emission in 2014, EMIS3 for an average intensity over all years, and EMIS6 for the emission intensity in 2007, which corresponds to the maximum emission intensity from 2002 to 2016. An addition, emission scenario EMIS0.5 was added to mimic the reduced BB emissions projected assuming the influence of enhanced government regulation policy (Streets, 2007). The domain3-averaged AOD in the simulations for the EMIS0.5, EMIS1, EMIS3, and EMIS6 emission scenarios is used to represent the aerosol concentration under the corresponding emission scenarios in the analysis in Sect. 3.

To assess the ACI and the ARI effect of BB aerosols separately and jointly, we calculated the ACI and ARI effect following the method used in Archer-Nicholls et al. (2016). Parallel simulations with PC3_EMISX and CC3 were performed in the absence of aerosol radiative feedbacks, namely PCNR3_EMISX and CCNR3, respectively (Table 2). The ACI effect of BB aerosols in each emission scenario can be assessed from the difference between PCNR3_EMISX and CCNR3, where aerosols were radiatively inactive and only the aerosol effect on cloud microphysics was included. Then the ARI effect of BB aerosols was obtained by deducting the ACI effect from the aerosol total effect (Archer-Nicholls et al., 2016). This way of calculating the ARI of BB aerosols enables assessments of the ARI solely from BB aerosols without the influence of aerosols from other origins (Ghan et al., 2012). Due to the nonlinear nature of the cloud system, which involves complicated microphysics-dynamics-thermodynamics feedbacks (Stevens and Feingold, 2009), the ARI effect calculated as the residual component of the aerosol total effect aside from the ACI part may be different from directly contrasting the simulations with and without the radiative effect from BB aerosols. To assess this uncertainty, we compared the ARI effect on clouds obtained here with its counterpart, i.e., the difference between PC3_EMIX and PCNR3_EMISX, which directly computes the effect associated with aerosol-radiation interactions from all aerosols, based on the EMIS6 scenario to minimize the influence of aerosols not from BB (Table S1). It shows that the uncertainty in the ARI quantification associated with the cloud nonlinear microphysics-dynamics-thermodynamics feedbacks is very small and would not have a significant influence on the ARI assessment in this study.

The WRF-Chem simulation with the EMIS1 scenario was evaluated for the meteorological conditions and the aerosol field using ground-based, radiosonde, and satellite remote sensing measurements (see Supplement Text S1–S3). The results show that the model simulation at 3 km resolution reasonably reproduces the metrological field in terms of surface conditions, vertical atmospheric structure, and regional precipitation. The total cloud fraction and liquid cloud amount are well captured by the model while the simulated ice water amount shows lower magnitude than the observations. The model generates close agreement of the predicted aerosol properties with the observations, including the aerosol optical properties (AOD and SSA) and the CCN concentrations at different supersaturation conditions. Details of the model evaluation are provided in the Supplement. The satisfactory performance of the model enables it to provide reliable assessments of the BB aerosol effects on the regional climate through aerosol-radiation-cloud interactions.

Deleted: To distinguish aerosol-cloud interactions (ACI) effect from aerosol-radiation interactions (ARI) effect, we adopted a similar method as in Wu et al. (2011). Parallel simulations with PC3_EMISX and CC3 were performed without aerosol radiative feedbacks, namely PCNR3_EMISX and CCNR3 (Table 2). The aerosol-cloud interactions (ACI) or aerosol microphysical effect of each BB aerosol emission scenario can be assessed from the difference between PCNR3_EMISX and CCNR3. Then the aerosol-radiation interactions (ARI) effect could be obtained by deducting the ACI effect from the aerosol total effect (Archer-Nicholls et al., 2016).¶

Deleted: remarkable

Deleted: 4

3 Results

3.1 Impact on radiation

Figure 3 shows the diurnal cycle of the BB aerosol impact on the domain-averaged all-sky shortwave radiation based on the EMIS1 emission scenario. The ACI effect, in which BB aerosols act as CCN, causes negative radiative perturbations to shortwave radiation both at TOA (Fig. 3a) and the surface (Fig. 3b) during the daytime. This can be attributed to the increased cloud albedo as a result of larger cloud LWP and smaller cloud droplet radius (Table 3) caused by the ACI (Twomey, 1977). The shortwave radiative forcing (RF) at TOA is estimated to be –0.7 W m^{-2} for the ACI effect.

The radiation perturbations due to the ARI effect are more complicated as they involve the direct radiative effect of BB aerosols themselves and subsequent cloud adjustments. Figures 3 and S10 show a clear difference in radiative forcing with and without considering clouds (all-sky versus clear-sky conditions). In clear-sky cases, BB aerosols reduce the shortwave radiation reaching the ground by directly scattering and absorbing incident solar radiation, leading to a reduction of shortwave radiation at the surface of –6.7 W m^{-2} (Fig. S10b). The clear-sky shortwave RF by ARI at TOA is negative for most of the day except at local noon (15:00 UTC to 17:00 UTC) when the planetary boundary layer (PBL) fully develops (Fig. S10a). This diurnal variation can be explained by the evolution of aerosol vertical distributions. The vertical location of absorbing aerosols is an important controlling factor for their absorptivity (Samset and Myhre, 2011). When aerosols are lifted higher by the vigorously grown PBL, the absorption of solar radiation by BB aerosols is amplified resulting in more heating and positive forcing. On average, the clear-sky shortwave RF by ARI at TOA is about –0.7 W m^{-2}, and corresponds to a cooling effect on the Earth-atmosphere systems, which is consistent in sign with observational and modelling results in this region (Sena et al., 2013; Archer-Nicholls et al., 2016; Thornhill et al., 2018). When taking clouds into consideration, the all-sky shortwave radiative perturbation by ARI is about –5.7 W m^{-2} and 0.4 W m^{-2} at the surface and TOA (Table 3), respectively. Compared with the clear-sky results, the positive shifts of radiative perturbation by ARI in all-sky condition at both the surface and TOA indicate less solar radiation reflected back to space. This can be accounted for by the decreased liquid cloud water content (Table 3) due to the BB aerosols' radiative effect, which results in more incident solar radiation (so-called 'semi-direct' effect). Seen from the diurnal cycle of shortwave forcing by the ARI (Fig. 3a), the time period when the radiative forcing is positive becomes longer, although negative values still exist in the early morning and late afternoon when the cloud response is negligible (Fig. 6b). In previous studies, the positive radiative forcing associated with the reduction of cloud cover was shown to be very strong (Zhang et al., 2008), even to the point of being able to reverse the sign of the BB aerosols' direct radiative forcing over the Amazon (Koren et al., 2004; Archer-Nicholls et al., 2016).

The total shortwave RF at TOA by BB aerosols is a result of the competing ACI and ARI effects. Figure 4a shows the total shortwave RF caused by BB aerosols from emission scenarios with different aerosol emission intensities (represented as the domain-averaged AOD). The relative importance of the ACI and ARI effects on shortwave RF varies with the aerosol

Deleted: 2.3 Data¶
2.3.1 Ground based measurements at ATTO¶
The Amazon Tall Tower Observatory (ATTO) site is located in the central Amazon, about 150 km northeast of Manaus, Brazil (Fig. 1), and represents a relatively clean rainforest background environment (Andreae et al., 2015). An 80-m tower, embedded within the canopy of about 35 m height, provides continuous measurements related to the research fields of meteorology, atmospheric trace gases, and aerosols (Andreae et al., 2015). Observational datasets used in this paper include meteorological variables, cloud condensation nuclei (CCN) number concentrations, and black carbon mass. Meteorology observations were obtained from a thermohygrometer and a 2-D sonic anemometer installed at 55 m on the tower. The data was averaged at 10-min resolution from raw observations taken at 1-min resolution. Air temperature and relative humidity (RH) measurements are only available from 1 Sep to 23 Sep 2014, while wind speed was observed over the complete simulation period. Aerosols were sampled at 60 m height. The CCN number concentration measurements by a CCN counter with supersaturation cycling through a set of levels ranging from 0.11% to 1.1% were used in this study. Detailed information on the CCN dataset can be found in Pöhlker et al. (Pöhlker et al., 2016, 2018). Equivalent black carbon (BCe) mass concentrations, M_{BCe}, were obtained from a multi-angle absorption photometer (MAAP) (μg m^{-3}). The mass concentration was calculated by dividing the absorption coefficients at 637 nm by the dry season mass absorption cross-section of 12.3 m^2 g^{-1} according to Saturno et al. (2018a). Specific details about the MAAP measurements of M_{BCe} can be found in Saturno et al. (2018a).¶
¶
2.3.2 Radiosonde measurements¶
Radiosonde observations from the Integrated Global Radiosonde Archive (IGRA) (Durre et al., 2006) at the site Manaus (3.15 °S, ...

Deleted: 4

Deleted: 4

Deleted: 9

Deleted: 9

Deleted: 9

Deleted: 5

Deleted: et al.

Deleted: The magnitude of –0.7 W m^{-2} for shortwave radiative forcing (RF) at TOA is comparable to the global indirect aerosol ...

Deleted: .

Deleted: 9

Deleted: 3

Deleted: 3

Deleted: 3

Deleted: Such a

Deleted: 5

Deleted: 5

Deleted: 9

Deleted: 13

Deleted: . 10

loading under the same atmospheric conditions. The total shortwave forcing is negative at lower aerosol loading, dominated by the ACI effect, but shifts to be positive at higher aerosol loading, driven by the ARI effect. This is expected because the addition of aerosols changes the cloud properties more severely at low background aerosol concentrations than at higher aerosol abundance where the microphysical effect tends to be saturated (Twomey, 1977; Roberts et al., 2003); and the ARI effect associated with aerosol extinction of radiation intensifies with increasing aerosol concentration (Koren et al., 2004).

Such nonlinear ACI and ARI effects of BB aerosols are consistent with their effects on cloud water (Fig. 5a), implying the importance of cloud adjustments for affecting BB aerosol RF. At TOA, the monthly mean shortwave RF by BB aerosols (ACI + ARI) is –0.3 W m^{-2} and 0.6 W m^{-2} for the EMIS1 and EMIS6 scenarios, respectively (Table 3). Similar in magnitude, a modelling study of the Amazon dry season using the HadGEM3-GA3 model showed a monthly mean shortwave RF of 1.35 W m^{-2} with AOD increasing from 0.19 to 0.67 (Thornhill et al., 2018). The longwave RF by BB aerosols is of comparable magnitude to the shortwave radiative forcing (Table S4). The ARI is the driving force for the positive longwave RF, as the outgoing infrared radiation can be directly trapped by black carbon contained within the BB particles (Ramachandran and Kedia, 2010). In addition, high clouds mainly comprised of ice are also efficient in blocking outgoing longwave radiation (Hartmann et al., 1992), yielding a positive longwave RF at TOA. Therefore, the ARI-induced larger amount of cloud ice content (Fig. 6b) can result in positive longwave RF as well. The positive longwave RF resulting from increased ice cloud is in agreement with the satellite observations of tropical deep convection, where a strong warming was caused by increased convective cloud anvils impacted by aerosols (Koren et al., 2010). However, it should be noted that, as the ice cloud response is a crucial factor for determining the longwave RF, the lack of parameterization of the aerosols' role as IN adds uncertainty to the simulated longwave RF by BB aerosols. The appreciable magnitude of longwave RF (Thornhill et al., 2018; Archer-Nicholls et al., 2016) underlines the necessity of further studies to constrain the BB aerosol effect on high clouds. The all-band RF (shortwave plus longwave) of BB aerosols changes sign with increasing emission intensity of BB aerosols, with values of –0.2 W m^{-2} and 1.5 W m^{-2} for the EMIS1 and EMIS6 scenarios, respectively.

At the surface, a reduction in shortwave radiation is induced by the presence of BB aerosols, which intensifies with higher emission intensity. Compared with previous model estimates, a –15.9 W m^{-2} shortwave reduction estimated from a multi-day biomass burning simulation in 2006 using WRF-Chem (Wu et al., 2011) is of similar magnitude as the –17.1 W m^{-2} in this study using the EMIS3 scenario, which is almost equivalent to the emission intensity of the year 2006. However, the magnitude of the estimates diverges in different models, e.g., –28.2 W m^{-2} was induced by an increase of AOD by about 0.4 using the GATOR-GCMOM model (Ten Hoeve et al., 2012), and –5.46±1.93 W m^{-2} was calculated with an increase of AOD by about 0.5 using HadGEM3-GA3 (Thornhill et al., 2018), which may result from different parameterizations of the aerosol optical properties and treatments of cloud response. The decreased solar radiation at the surface is balanced mostly (over 90%) by a reduced sensible and latent heat flux (Table 3) and marginally by the earth-emitted infrared radiation. Specifically, the ARI led to a decrease of –2.9% (–17.6%) and –2.0% (–12.0%) for sensible heat and latent heat, respectively, in the EMIS1 (EMIS6) scenario, which could impose an inhibiting effect on cloud formation (Yu et al., 2002; Feingold et al., 2005; Jiang and Feingold, 2006; Rosenfeld et al., 2008).

Deleted: changes in the
Deleted: loading will
Deleted: s
Deleted: the
Deleted: 12
Deleted: 5
Deleted: , respectively
Deleted: 1
Deleted: Besides
Deleted: 13
Deleted: b
Deleted: 5
Deleted: ads
Deleted: s

3.2 Impact on atmospheric stability

Figure 7 shows the diurnal and vertical distribution of the BB aerosol impact on the domain-averaged air temperature, relative humidity (RH), and vertical velocity for the EMIS1 scenario. Pronounced responses of air temperature and RH occur below 5 km, where aerosols are concentrated. Affected by the ARI, air temperature is reduced within the PBL, but is increased at the top of the PBL (Fig. 7b). As aforementioned, BB aerosols reduce the incident solar radiation at the surface and therefore decrease the heat flux from the ground to the atmosphere. Consequently, the air temperature within the PBL drops, with a diurnal maximum reduction of over –0.05 °C near the surface. The solar radiation absorbed by the black carbon in BB aerosols heats the atmosphere (Bond and Bergstrom, 2006), producing an increase in air temperature by about 0.03 °C near the top of the PBL. This vertical distribution of temperature responses tends to stabilize the PBL and suppress the upward velocity (Fig. 7b). On the other hand, the increased air temperature at the top of the PBL destabilizes the air above and stimulates updrafts (Feingold et al., 2005; Koch and Del Genio, 2010). The intensified upward airflow delivers more water vapor to higher altitudes, leading to a pronounced RH increase at altitudes above 10 km. The ACI effect acts opposite to the ARI effect in changing the thermodynamic structure. The air cools at the top of the PBL, since more evaporation-induced cooling is generated with more but smaller cloud droplets (Table 3). In contrast, higher air temperatures within the PBL can be the result of less evaporative cooling from precipitating hydrometeors (Fig. 8a). Overall, the thermodynamic response to BB aerosols is dominated by the ARI effect. The diurnal mean change of surface air temperature is –0.2 °C in the EMIS6 scenario (Table 3), in agreement with other modeling results for the Amazon area (Kolusu et al., 2015; Thornhill et al., 2018).

3.3 Impact on cloud

Figure 6 shows the diurnal and vertical distribution of domain-averaged changes in cloud water and cloud ice concentration caused by BB aerosols. By serving as CCN, BB aerosols create more cloud droplets and cause a reduction in the cloud droplet size (Table 3) due to competition for water vapor, which slows down the transfer rate from cloud to rain (Rosenfeld et al., 2008; Chang et al., 2015; Braga et al., 2017). Consequently, cloud water in the free troposphere is increased by the ACI effect throughout the day (Fig. 6a) at the expense of rainwater concentration, while the diminished cloud water within the PBL corresponds to the warmer air temperature (Fig. 7a) and suppressed moisture flux from the ground surface (Table 3).

The response of cloud water to ARI also varies with altitude. The increased RH within the PBL by the aerosol radiative effect (Fig. 7b) lowers the cloud base height (Table 3) and favors cloud persistence, resulting in higher cloud water content (Johnson et al., 2004). In contrast, the aerosol radiative heating near the top of the PBL (Fig. 7b) decreases the RH and therefore 'burns off' the liquid clouds (Feingold et al., 2005; Huang et al., 2016). Such contrasting cloud water responses to the BB aerosol radiative effect between different layers was also found by a large-scale RegCM3 simulation covering South America

Deleted: 4
Deleted: 11
Deleted: minent
Deleted: 11
Deleted: et al.
Deleted: es
Deleted: 11
Deleted: in the RH
Deleted: 5
Deleted: 14a
Deleted: 5
Deleted: 4
Deleted: 13
Deleted: 5
Deleted: 13a
Deleted: 11a
Deleted: 5
Deleted:
Deleted: the
Deleted: 11
Deleted: 5
Deleted: 11

(Zhang et al., 2008). The increased cloud water in the lower troposphere (0–2 km) was attributed to large-scale moisture convergence. Here, the simulation over a smaller region located in the central Amazon Basin shows that the local modification of the thermodynamic structure by BB aerosols is able to contribute to the effect as well.

Integrated over the atmosphere, the cloud LWP is enhanced by the ACI, but reduced by the ARI effect (Ackerman et al., 2000; Johnson et al., 2004; Feingold et al., 2005). Therefore, the overall change of cloud water amount by BB aerosols results from the competition between the ACI and ARI effects. Figure 5 displays the dependence of the overall response of cloud water on the emission intensity (represented as AOD). Weaker emission scenarios yield higher cloud water, driven by the ACI effect, while stronger emissions lead to an opposite response of cloud water, dominated by the ARI effect. The simulated dependence of cloud water change on aerosol amount agrees with satellite measurements of the total cloud fraction over the Amazon region (Koren et al., 2004).

The cloud ice content is invigorated by BB aerosols, driven by the ARI effect (Fig. 6b). Through radiation absorption, BB aerosols heat the air, evaporate liquid cloud, and promote upward flux of vapor and moisture to higher altitudes (Fig. 7b), facilitating cloud ice formation there. Similar ice enhancement due to aerosol radiative heating was also seen in simulations of dust-radiation interaction (Dipu et al., 2013). This positive response of cloud ice and updraft velocity to ARI corresponds to the thermodynamic invigoration mechanism proposed in Wang et al. (2013) which suggested larger convective available potential energy (CAPE) above PBL could be induced by the absorbing aerosols in the lower troposphere. In contrast, the ACI tend to act in opposition to the ARI effect, but at a minor magnitude, showing a moderate negative response (Fig. 6a). The ACI effect has been reported to invigorate deep convection when more abundant, smaller cloud drops are uplifted to boost the cloud microphysical processes at higher altitudes (Rosenfeld et al., 2008), which, however, is sensitive to the background environment (Khain et al., 2005; Fan et al., 2009). Hints of this effect are only seen during a narrow time span around 18 UTC and 22 UTC, as indicated by increased cloud ice (Fig. 6a) and precipitating hydrometeors (Fig. 8a). However, the enhancement is insignificant in magnitude and overwhelmed by the negative responses that persist during the rest of the diurnal cycle, which may result from different cloud types and environmental conditions from those in Rosenfeld et al. (2008). Generally, the monthly mean domain-averaged results show a negative effect of the ACI on cloud ice water path (IWP; Fig. 5b). However, the role of ACI could be more complicated than what is found here, because the ACI effect may potentially modulate the impact of ARI on the cloud ice (Shi et al., 2014; Huang et al., 2019), e.g., by influencing latent heat release, since the ACI effect is turned on when the ARI effect is assessed. The overall increase in cloud ice is in agreement with the fine-resolution simulation results over the biomass burning area by the GATOR-GCMOM model (Ten Hoeve et al., 2012). Although the absolute response of ice concentration is smaller compared to the cloud water change, the relative change in ice concentration is remarkable (Fig. 5b; Lee et al., 2017). It should be noted that uncertainties associated with BB aerosol effects on cloud ice exist, because of the lack of IN parameterization (Fan et al., 2018). Field observations suggested that the BC in the BB aerosols could contribute substantially to ice nucleation (McCluskey et al., 2014), which may influence the estimate of the response of cloud ice to BB aerosols.

Deleted:
Deleted: 12
Deleted: 13
Deleted: 11
Deleted: ,
Deleted: 13a
Deleted: 14a
Deleted: domain
Deleted: the
Deleted: with
Deleted: 12
Deleted:)
Deleted: (

3.4 Impact on precipitation

To show the response of precipitation, the diurnal and vertical distribution of domain-averaged changes in precipitating hydrometeors (sum of rain, snow, and graupel) based on the EMIS1 scenario is presented in Fig. 8. The domain-averaged rainwater below the freezing level height of about 5 km shows a prominent negative response to ACI during most of the daytime (Fig. 8a). As discussed before, by acting as CCN, the BB aerosols reduce cloud droplet radius, slow down the conversion rate from cloud to rain, and therefore inhibit warm rain formation. On the other hand, consistent with the responses of cloud ice, precipitating hydrometeors are enhanced by the ACI effect in the local afternoon and early night due to the invigorated convection. Generally, an overall reduction in precipitation is induced by the ACI, similar to previous WRF-Chem simulations of BB aerosol microphysical effects in the Amazon (Wu et al., 2011). The results of the ARI effect show an overall positive impact on precipitating hydrometeor concentrations (Fig. 8b) and consequent surface precipitation (Fig. 9a) at the EMIS1 scenario. With the influence of the ARI effect, significant enhancement appears in the precipitating hydrometeors above the freezing level beginning in the early morning, indicating cold rain processes. Specifically, the graupel concentration, which is mainly responsible for the cold rain response (Fig. S13) is promoted as more supercooled cloud droplets efficiently feed the growth of graupel. The increased supercooled cloud water concentration could be a result of the enhanced updraft promoted by the ARI (Fig. 7b). By 17:00–18:00 UTC, the precipitation reaching the surface is increased correspondingly. The increase in precipitation by the local ARI effect was also found in previous simulations of light-absorbing aerosols, including black carbon (Lin et al., 2016) and mineral dust (Dipu et al., 2013; Shi et al., 2014; Huang et al., 2018). Influenced by the overall effect of both the ACI and ARI mechanisms, a reduction of precipitating hydrometeors is prominent in the morning and afternoon, while enhanced precipitation hydrometeor abundance occurs in a narrow time span from local noon to early afternoon. The variation of convection response throughout the convective evolution cycle implies a possible dependence of aerosol-radiation-cloud interactions on environmental stabilization, which is also shown by the observation that BB aerosols tend to increase precipitation under unstable conditions (Goncalves et al., 2015).

The response of the precipitation rate to different emission intensities of BB aerosols (represented as AOD) is shown in Fig. 9a. The precipitation reduction by ACI is climatically significant in all emission scenarios, with a monthly mean change of –4% and –19% at EMIS1 and EMIS6, respectively. The precipitation rate is slightly increased by the ARI at low aerosol loading due to invigorated daytime precipitation as discussed above. However, at high emission intensity, the strong radiative dimming effect of BB aerosols dramatically reduces surface heating (Table 3), which damps the ARI-induced convection invigoration (Fig. S12b) and leads to an overall suppression of convection and a significant reduction of precipitation (Rosenfeld et al., 2008), as reflected by diminished liquid clouds (Fig. S14) and precipitating hydrometeors (Fig. S12b). This dimming effect is even more pronounced than the ACI effect in reducing precipitation for the EMIS6 scenario (Fig. 9). Taking the ACI and ARI effects together, the monthly mean precipitation rate is decreased by BB aerosols at all emission scenarios used in this study. A reduction of –5% and –23% is calculated for the EMIS1 and EMIS6 emission scenarios, respectively, aligning in magnitude with a precipitation change by –14.5% for the switch of aerosol loading from the low emission to the

Deleted: 4
Deleted: investigate
Deleted: 14
Deleted: the
Deleted: b
Deleted: 14
Deleted: 15
Deleted: 7
Deleted: are present due to the ARI and
Deleted: originating from
Deleted: 11
Deleted: ;
Deleted: lower concentration
Deleted: produced by BB aerosols (Fig. 14c)
Deleted: 15
Deleted: 5
Deleted: 6
Deleted: 8
Deleted: 6
Deleted: 15

high emission scenario in the Amazon found by Thornhill et al. (2018). To examine the precipitation responses at different precipitation intensities (Fig. 10), a threshold of daily maximum 3-hour accumulated precipitation exceeding 3 mm, the upper boundary of the domain averaged amount (Fig. S6), is used to distinguish the intensive precipitation grids from the light precipitation ones. High convective strength indicated by larger CAPE (Fig. 10) corresponds to intensive precipitation, whereas relatively weaker convection is associated with the light precipitation regime. Intensive precipitation shows a significant nonlinear ARI response, whereas light precipitation tends to be reduced monotonically by the ARI. The precipitation reduction by ACI at low aerosol concentration is less prominent in heavy than in light rainfall, due possibly to the dynamic feedbacks in deep convection (Rosenfeld et al., 2008). By contrast, a stronger ACI effect at larger aerosol amounts is shown in heavy precipitation as a result of the larger potential for CCN activation in strong convection (Reutter et al., 2009). The dependence of precipitation change on aerosol concentration is greater for the intensive precipitation than the light precipitation regime, given that the precipitation responses at the EMIS1 and EMIS6 scenarios are –1% and –27 % respectively for the intensive regime and –5% and –17% respectively for the light precipitation. This is consistent with the rainfall sensitivity to increasing aerosol concentration for strong and weak convection in Chang et al. (2015). The dominance role of ARI over ACI at high aerosol loadings is found at both regimes. The precipitation occurrence (calculated as the ratio of precipitating grid cells to the total domain grid cells over the simulation period), which is approximately 11% in the clean case, is reduced noticeably by both the ACI and ARI effects (Fig. 9). The more extensive dry area coverage due to the presence of BB aerosols may act to aggravate the precipitation shortage for the Amazon forest in the dry season (Cox et al., 2008).

Deleted: ,
Deleted: indicating
Deleted: and threatening an
Deleted: ion of

4 Conclusion

Deleted: 5

In this study, a comprehensive assessment of the impacts of BB aerosols on the regional radiation balance, cloud properties, and precipitation and their sensitivity to inter-annual variations of BB aerosol emissions was conducted using the fully coupled WRF-Chem model with a 3-km resolution domain in the central Amazon Basin for the dry season. Parallel numerical experiments were performed with different emission scenarios by scaling up and down the original emission rate of the year 2014. These experiments with varying emission scenarios, together with experiments switching off the aerosol-radiation interactions in the model were performed to separate the effects of ARI and ACI, which enables us to quantify each effect individually and compare their relative significance.

The results show that the shortwave RF by BB aerosols is the outcome of a competition between positive RF by the ARI effect and negative RF by the ACI effect, which is driven largely by the cloud response. The positive shortwave RF associated with cloud reduction due to the semi-direct effect of the BB aerosols counteracts the negative direct shortwave RF and constitutes the dominant component of ARI-induced effective shortwave RF. Contrarily, the ACI-induced more numerous, but smaller, cloud droplets increase cloud albedo and thereby exert a negative indirect shortwave RF. The relative significance of the ACI and ARI effects varies with aerosol loading, with a dominant role of the former at low aerosol emission rate while the

Deleted: radius

latter dominates at high emission intensity. The positive longwave RF by BB aerosols is driven by the ARI effect, through both aerosol direct radiative forcing and subsequent adjustment of enhanced ice cloud. The all-band aerosol RF is –0.2 W m^{-2} and 1.5 W m^{-2} for BB aerosols in the EMIS1 and EMIS6 scenarios, respectively. Surface shortwave radiation is reduced by BB aerosols, with an estimate of –17.1 W m^{-2} for a multi-year averaged emission intensity (EMIS3), which is compensated mostly by suppression of sensible and latent heat flux from ground to the atmosphere. The response of cloud LWP to BB aerosols is driven in opposite directions by the ARI and ACI effects. The surface cooling generated by radiation extinction together with the atmospheric heating from absorption of solar radiation stabilizes the atmosphere, inhibits convection development, and thereby decreases the cloud LWP. In contrast, higher cloud LWP is produced by the ACI through inhibited warm rain formation. The relative significance of the competing effects depends on the aerosol amount, consistent with the aerosol shortwave radiative forcing response, implying a crucial role of cloud adjustments in determining aerosol radiative forcing on the Earth-atmosphere system. Enhanced cloud IWP with the presence of BB aerosols is related to a stronger upward flux of water vapor induced by the ARI effect.

Lower precipitation occurrence is induced by both the ARI and ACI effects, which implies a larger fraction of dry areas in the Amazon Basin when affected by BB aerosols, threatening to exacerbate droughts during the dry season. The domain-averaged precipitation rate is diminished substantially by ACI consistently over all the emission scenarios used in this study, implying the importance of including ACI effects on the sub-grid cumulus convection when applying large-scale simulations at coarse grid resolution (Archer-Nicholls et al., 2016). Strong suppression of warm rain formation is responsible for the precipitation reduction caused by the ACI, but in the lower emission scenarios, an ACI-induced invigoration of deep convection occurs during a narrow time period, due to latent heat release from more abundant smaller droplets aloft (Rosenfeld et al., 2008). The precipitation response to the ARI effect is nonlinear due to the effects of mixed-phase precipitation. At low BB aerosol emission rates, enhanced mixed-phase precipitation is found as a result of higher graupel content with the enhanced supply of supercooled cloud droplets by the ARI, while the invigoration disappears in the high emission scenarios with reduced presence of supercooled cloud droplets due to overwhelming suppression of convection by BB aerosols. Reduction in monthly mean precipitation rate by the overall effects of BB aerosols is found for all emission scenarios, and intensifies with aerosol loading, which may imply a positive feedback between precipitation scavenging and aerosol concentration for intense BB events. A reduction of monthly mean precipitation rate by –5% and –23% is estimated for the EMIS1 and EMIS6 scenarios, respectively, suggesting a strong sensitivity of precipitation to aerosol concentration. The sensitivity of precipitation change to aerosol concentration is more prominent in the intensive precipitation regime than in the light precipitation case.

The high sensitivity and nonlinear relationship between regional radiation, liquid water content, precipitation, and BB aerosol abundance highlights the importance of comprehensive assessments of BB aerosol effects in the Amazon with multiannual aerosol emission scenarios. The variation of the ACI and ARI effects with increasing aerosol emission revealed a saturating tendency for the ACI, in contrast to a continuingly increasing effect of the ARI at high aerosol loadings. This may shed light on the climatic importance of the ARI at highly polluted regions and during episodes with severe combustion aerosol

Deleted: ed
Deleted:
Deleted: while
Deleted: role

emissions such as intensive wildfires, industrialization-related fossil fuel combustion, and agricultural crop waste burning. The key role of the ARI also highlights the importance of accurate representation of aerosols and their optical properties in models when addressing their climate effects.

It should be noted that this study only focuses on the local effects of BB aerosols for a typical region in the Amazon Basin. The large-scale response in the atmospheric field (Lee et al., 2014) caused by horizontally inhomogeneous responses to unevenly distributed aerosols is out of the scope of this study. The role of aerosols acting as IN has not been included in the WRF-Chem model used here. Parameterization of this mechanism is needed to better quantify aerosol effects on climate. In addition, further investigations on the formation mechanisms and light absorption associated with SOA are needed to better parameterize the physical and optical properties of organic aerosols in the model (Shrivastava et al., 2017, 2019), in order to better recognize the role of BB aerosols in the climate system. Furthermore, the sensitivity of the climate response to the concentration of BB aerosols may be influenced by the meteorological conditions, and as this study is based on September 2014, continuing model investigations based on varying and longer periods are needed to characterize the influence of variations in meteorology and to provide climatic assessments.

Deleted: continuing investigation is needed to characterize the influence of variations in meteorological factors

Author contributions

Y.C. and H.S. designed and led the study. L.L. performed the model simulation and analyzed the data. L.L., H.S. and Y.C. interpreted the results. M.O.A., M.S. and U.P. discussed the results. M.P. and C.P. contributed data for model validation. L.L. wrote the manuscript with input from all coauthors.

Competing interests

The authors declare that they have no conflict of interest.

Acknowledgements

We thank the Max Planck Society (MPG) for support and Minerva Program of MPG. We acknowledge the MODIS, TRMM, AERONET and IGRA teams for the data used in this study. Furthermore, we would like to thank for the support by the ATTO project and all the people involved in it. We would like to acknowledge the German Federal Ministry of Education and Research (BMBF contracts 01LB1001A and 01LK1602B), supporting this project as well as the construction and operation of the ATTO site. We also acknowledge the support of the Brazilian Ministério da Ciência, Tecnologia e Inovação (MCTI/FINEP contract 01.11.01248.00) as well as the Amazon State University (UEA), FAPEAM, LBA/INPA and SDS/CEUC/RDS-Uatumã for their support during construction and operation of the ATTO site. Dr. Shrivastava was supported

by the U.S. Department of Energy (DOE), Office of Science, Office of Biological and Environmental Research through the Atmospheric System Research (ASR) and Early Career Research Programs.

References

Abdul-Razzak, H., and Ghan, S. J.: A parameterization of aerosol activation - 3. Sectional representation, J. Geophys. Res.-Atmos., 107, doi: 10.1029/2001jd000483, 2002.

Ackerman, A. S., Toon, O. B., Stevens, D. E., Heymsfield, A. J., Ramanathan, V. V., and Welton, E. J.: Reduction of tropical cloudiness by soot, Science, 288, 1042–1047, 2000.

Albrecht, B. A.: Aerosols, cloud microphysics, and fractional cloudiness, Science, 245, 1227–1230, doi:10.1126/science.245.4923.1227, 1989.

Andreae, M. O., Artaxo, P., Brandao, C., Carswell, F. E., Ciccioli, P., da Costa, A. L., Culf, A. D., Esteves, J. L., Gash, J. H. C., Grace, J., Kabat, P., Lelieveld, J., Malhi, Y., Manzi, A. O., Meixner, F. X., Nobre, A. D., Nobre, C., Ruivo, M. D. L. P., Silva-Dias, M. A., Stefani, P., Valentini, R., von Jouanne, J., and Waterloo, M. J.: Biogeochemical cycling of carbon, water, energy, trace gases, and aerosols in Amazonia: The LBA-EUSTACH experiments, J. Geophys. Res.-Atmos., 107, 8066, doi:10.1029/2001jd000524, 2002.

Andreae, M. O., Rosenfeld, D., Artaxo, P., Costa, A. A., Frank, G. P., Longo, K. M., and Silva-Dias, M. A.: Smoking rain clouds over the Amazon, Science, 303, 1337–1342, doi:10.1126/science.1092779, 2004.

Andreae, M. O., Acevedo, O. C., Araujo, A., Artaxo, P., Barbosa, C. G. G., Barbosa, H. M. J., Brito, J., Carbone, S., Chi, X., Cintra, B. B. L., da Silva, N. F., Dias, N. L., Dias, C. Q., Ditas, F., Ditz, R., Godoi, A. F. L., Godoi, R. H. M., Heimann, M., Hoffmann, T., Kesselmeier, J., Konemann, T., Kruger, M. L., Lavric, J. V., Manzi, A. O., Lopes, A. P., Martins, D. L., Mikhailov, E. F., Moran-Zuloaga, D., Nelson, B. W., Nolscher, A. C., Nogueira, D. S., Piedade, M. T. F., Pöhlker, C., Pöschl, U., Quesada, C. A., Rizzo, L. V., Ro, C. U., Ruckteschler, N., Sa, L. D. A., Sa, M. D., Sales, C. B., dos Santos, R. M. N., Saturno, J., Schongart, J., Sorgel, M., de Souza, C. M., de Souza, R. A. F., Su, H., Targhetta, N., Tota, J., Trebs, I., Trumbore, S., van Eijck, A., Walter, D., Wang, Z., Weber, B., Williams, J., Winderlich, J., Wittmann, F., Wolff, S., and Yanez-Serrano, A. M.: The Amazon Tall Tower Observatory (ATTO): overview of pilot measurements on ecosystem ecology, meteorology, trace gases, and aerosols, Atmos. Chem. Phys., 15, 10723–10776, doi:10.5194/acp-15-10723-2015, 2015.

Andreae, M. O.: Emission of trace gases and aerosols from biomass burning – an updated assessment, Atmos. Chem. Phys., 19, 8523–8546, doi:10.5194/acp-19-8523-2019, 2019.

Archer-Nicholls, S., Lowe, D., Darbyshire, E., Morgan, W. T., Bela, M. M., Pereira, G., Trembath, J., Kaiser, J. W., Longo, K. M., Freitas, S. R., Coe, H., and McFiggans, G.: Characterising Brazilian biomass burning emissions using WRF-Chem with MOSAIC sectional aerosol, Geosci. Model Dev., 8, 549–577, doi:10.5194/gmd-8-549-2015, 2015.

Archer-Nicholls, S., Lowe, D., Schultz, D. M., and McFiggans, G.: Aerosol-radiation-cloud interactions in a regional coupled model: the effects of convective parameterisation and resolution, Atmos. Chem. Phys., 16, 5573–5594, doi:10.5194/acp-16-5573-2016, 2016.

Barnard, J. C., Fast, J. D., Paredes-Miranda, G., Arnott, W. P., and Laskin, A.: Technical Note: Evaluation of the WRF-Chem "Aerosol Chemical to Aerosol Optical Properties" Module using data from the MILAGRO campaign, Atmos. Chem. Phys., 10, 7325–7340, doi:10.5194/acp-10-7325-2010, 2010.

Bevan, S. L., North, P. R. J., Grey, W. M. F., Los, S. O., and Plummer, S. E.: Impact of atmospheric aerosol from biomass burning on Amazon dry-season drought, J. Geophys. Res.-Atmos., 114, doi:10.1029/2008jd011112, 2009.

Bond, T. C., and Bergstrom, R. W.: Light Absorption by Carbonaceous Particles: An Investigative Review, Aerosol Science and Technology, 40, 27–67, doi:10.1080/02786820500421521, 2006.

Bony, S., Colman, R., Kattsov, V. M., Allan, R. P., Bretherton, C. S., Dufresne, J. L., Hall, A., Hallegatte, S., Holland, M. M., Ingram, W., Randall, D. A., Soden, B. J., Tselioudis, G., and Webb, M. J.: How well do we understand and evaluate climate change feedback processes?, J. Climate, 19, 3445–3482, doi:10.1175/Jcli3819.1, 2006.

Braga, R. C., Rosenfeld, D., Weigel, R., Jurkat, T., Andreae, M. O., Wendisch, M., Pöschl, U., Voigt, C., Mahnke, C., Borrmann, S., Albrecht, R. I., Molleker, S., Vila, D. A., Machado, L. A. T., and Grulich, L.: Further evidence for CCN aerosol concentrations determining the height of warm rain and ice initiation in convective clouds over the Amazon basin, Atmos. Chem. Phys., 17, 14433–14456, doi:10.5194/acp-17-14433-2017, 2017.

Breon, F. M., Tanre, D., and Generoso, S.: Aerosol effect on cloud droplet size monitored from satellite, Science, 295, 834–838, doi:10.1126/science.1066434, 2002.

Brito, J., Rizzo, L. V., Morgan, W. T., Coe, H., Johnson, B., Haywood, J., Longo, K., Freitas, S., Andreae, M. O., and Artaxo, P.: Ground-based aerosol characterization during the South American Biomass Burning Analysis (SAMBBA) field experiment, Atmos. Chem. Phys., 14, 12069–12083, doi:10.5194/acp-14-12069-2014, 2014.

Carslaw, K. S., Lee, L. A., Reddington, C. L., Pringle, K. J., Rap, A., Forster, P. M., Mann, G. W., Spracklen, D. V., Woodhouse, M. T., Regayre, L. A., and Pierce, J. R.: Large contribution of natural aerosols to uncertainty in indirect forcing, Nature, 503, 67–71, doi:10.1038/nature12674, 2013.

Cecchini, M. A., Machado, L. A. T., Andreae, M. O., Martin, S. T., Albrecht, R. I., Artaxo, P., Barbosa, H. M. J., Borrmann, S., Futterer, D., Jurkat, T., Mahnke, C., Minikin, A., Molleker, S., Pöhlker, M. L., Pöschl, U., Rosenfeld, D., Voigt, C., Weinzierl, B., and Wendisch, M.: Sensitivities of Amazonian clouds to aerosols and updraft speed, Atmos. Chem. Phys., 17, 10037–10050, doi:10.5194/acp-17-10037-2017, 2017.

Chang, D., Cheng, Y., Reutter, P., Trentmann, J., Burrows, S. M., Spichtinger, P., Nordmann, S., Andreae, M. O., Pöschl, U., and Su, H.: Comprehensive mapping and characteristic regimes of aerosol effects on the formation and evolution of pyro-convective clouds, Atmos. Chem. Phys., 15, 10325–10348, doi:10.5194/acp-15-10325-2015, 2015.

Deleted: Baro, R., Jimenez-Guerrero, P., Stengel, M., Brunner, D., Curci, G., Forkel, R., Nea, L., Palacios-Pena, L., Savage, N., Schaap, M., Tuccella, P., van der Gon, H. D., and Galmarini, S.: Evaluating cloud properties in an ensemble of regional online coupled models against satellite observations, Atmos. Chem. Phys., 18, 15183–15199, doi:10.5194/acp-18-15183-2018, 2018.¶

Chapman, E. G., Gustafson, W. I., Easter, R. C., Barnard, J. C., Ghan, S. J., Pekour, M. S., and Fast, J. D.: Coupling aerosol-cloud-radiative processes in the WRF-Chem model: Investigating the radiative impact of elevated point sources, Atmos. Chem. Phys., 9, 945–964, doi:10.5194/acp-9-945-2009, 2009.

Charlson, R. J., Schwartz, S. E., Hales, J. M., Cess, R. D., Coakley, J. A., Jr., Hansen, J. E., and Hofmann, D. J.: Climate forcing by anthropogenic aerosols, Science, 255, 423–430, doi:10.1126/science.255.5043.423, 1992.

Cheng, Y. F., Wiedensohler, A., Eichler, H., Su, H., Gnauk, T., Brueggemann, E., Herrmann, H., Heintzenberg, J., Slanina, J., Tuch, T., Hu, M., and Zhang, Y. H.: Aerosol optical properties and related chemical apportionment at Xinken in Pearl River Delta of China, Atmos. Environ., 42, 6351–6372, doi:10.1016/j.atmosenv.2008.02.034, 2008a.

Cheng, Y. F., Wiedensohler, A., Eichler, H., Heintzenberg, J., Tesche, M., Ansmann, A., Wendisch, M., Su, H., Althausen, D., Herrmann, H., Gnauk, T., Bruggemann, E., Hu, M., and Zhang, Y. H.: Relative humidity dependence of aerosol optical properties and direct radiative forcing in the surface boundary layer at Xinken in Pearl River Delta of China: An observation based numerical study, Atmos. Environ., 42, 6373–6397, doi:10.1016/j.atmosenv.2008.04.009, 2008b.

Collier, S., Zhou, S., Onasch, T. B., Jaffe, D. A., Kleinman, L., Sedlacek, A. J., 3rd, Briggs, N. L., Hee, J., Fortner, E., Shilling, J. E., Worsnop, D., Yokelson, R. J., Parworth, C., Ge, X., Xu, J., Butterfield, Z., Chand, D., Dubey, M. K., Pekour, M. S., Springston, S., and Zhang, Q.: Regional Influence of Aerosol Emissions from Wildfires Driven by Combustion Efficiency: Insights from the BBOP Campaign, Environ. Sci. Technol., 50, 8613–8622, doi:10.1021/acs.est.6b01617, 2016.

Cox, P. M., Harris, P. P., Huntingford, C., Betts, R. A., Collins, M., Jones, C. D., Jupp, T. E., Marengo, J. A., and Nobre, C. A.: Increasing risk of Amazonian drought due to decreasing aerosol pollution, Nature, 453, 212–217, doi:10.1038/nature06960, 2008.

Crutzen, P. J., and Andreae, M. O.: Biomass burning in the tropics: impact on atmospheric chemistry and biogeochemical cycles, Science, 250, 1669–1678, doi:10.1126/science.250.4988.1669, 1990.

Ding, A. J., Fu, C. B., Yang, X. Q., Sun, J. N., Petaja, T., Kerminen, V. M., Wang, T., Xie, Y., Herrmann, E., Zheng, L. F., Nie, W., Liu, Q., Wei, X. L., and Kulmala, M.: Intense atmospheric pollution modifies weather: a case of mixed biomass burning with fossil fuel combustion pollution in eastern China, Atmos. Chem. Phys., 13, 10545–10554, doi:10.5194/acp-13-10545-2013, 2013.

Dipu, S., Prabha, T. V., Pandithurai, G., Dudhia, J., Pfister, G., Rajesh, K., and Goswami, B. N.: Impact of elevated aerosol layer on the cloud macrophysical properties prior to monsoon onset, Atmos Environ, 70, 454-467, 10.1016/j.atmosenv.2012.12.036, 2013.

Ditas, J., Ma, N., Zhang, Y., Assmann, D., Neumaier, M., Riede, H., Karu, E., Williams, J., Scharffe, D., Wang, Q., Saturno, J., Schwarz, J. P., Katich, J. M., McMeeking, G. R., Zahn, A., Hermann, M., Brenninkmeijer, C. A. M., Andreae, M. O., Pöschl, U., Su, H., and Cheng, Y.: Strong impact of wildfires on the abundance and aging of black carbon in the lowermost stratosphere, P. Natl. Acad. Sci. USA, 115, E11595–E11603, doi:10.1073/pnas.1806868115, 2018.

Easter, R. C., Ghan, S. J., Zhang, Y., Saylor, R. D., Chapman, E. G., Laulainen, N. S., Abdul-Razzak, H., Leung, L. R., Bian, X. D., and Zaveri, R. A.: MIRAGE: Model description and evaluation of aerosols and trace gases, J. Geophys. Res.-Atmos., 109, doi:10.1029/2004jd004571, 2004.

Echalar, F., Artaxo, P., Martins, J. V., Yamasoe, M., Gerab, F., Maenhaut, W., and Holben, B.: Long-term monitoring of atmospheric aerosols in the Amazon Basin: Source identification and apportionment, J. Geophys. Res.-Atmos., 103, 31849–31864, doi:10.1029/98jd01749, 1998.

Emmons, L. K., Walters, S., Hess, P. G., Lamarque, J. F., Pfister, G. G., Fillmore, D., Granier, C., Guenther, A., Kinnison, D., Laepple, T., Orlando, J., Tie, X., Tyndall, G., Wiedinmyer, C., Baughcum, S. L., and Kloster, S.: Description and evaluation of the Model for Ozone and Related chemical Tracers, version 4 (MOZART-4), Geosci. Model Dev., 3, 43–67, doi:10.5194/gmd-3-43-2010, 2010.

Fahey, K. M., and Pandis, S. N.: Optimizing model performance: variable size resolution in cloud chemistry modeling, Atmos. Environ., 35, 4471–4478, doi:10.1016/S1352-2310(01)00224-2, 2001.

Fan, J., Yuan, T., Comstock, J. M., Ghan, S., Khain, A., Leung, L. R., Li, Z., Martins, V. J., and Ovchinnikov, M.: Dominant role by vertical wind shear in regulating aerosol effects on deep convective clouds, J. Geophys. Res., 114, doi:10.1029/2009jd012352, 2009.

Fan, J., Rosenfeld, D., Zhang, Y., Giangrande, S. E., Li, Z., Machado, L. A. T., Martin, S. T., Yang, Y., Wang, J., Artaxo, P., Barbosa, H. M. J., Braga, R. C., Comstock, J. M., Feng, Z., Gao, W., Gomes, H. B., Mei, F., Pöhlker, C., Pöhlker, M. L., Pöschl, U., and de Souza, R. A. F.: Substantial convection and precipitation enhancements by ultrafine aerosol particles, Science, 359, 411–418, doi:10.1126/science.aan8461, 2018.

Fast, J. D., Gustafson, W. I., Easter, R. C., Zaveri, R. A., Barnard, J. C., Chapman, E. G., Grell, G. A., and Peckham, S. E.: Evolution of ozone, particulates, and aerosol direct radiative forcing in the vicinity of Houston using a fully coupled meteorology-chemistry-aerosol model, J. Geophys. Res., 111, doi:10.1029/2005jd006721, 2006.

Feingold, G., Jiang, H. L., and Harrington, J. Y.: On smoke suppression of clouds in Amazonia, Geophys. Res. Lett., 32, L02804, doi:10.1029/2004gl021369, 2005.

Fiedler, S., Stevens, B., and Mauritsen, T.: On the sensitivity of anthropogenic aerosol forcing to model-internal variability and parameterizing a Twomey effect, J. Adv. Model Earth. Sy., 9, 1325–1341, doi:10.1002/2017ms000932, 2017.

Freitas, S. R., Longo, K. M., Diasb, M. A. F. S., Diasb, P. L. S., Chatfield, R., Prins, E., Artaxo, P., Grell, G. A., and Recuero, F. S.: Monitoring the transport of biomass burning emissions in South America, Environ. Fluid Mech., 5, 135–167, doi:10.1007/s10652-005-0243-7, 2005.

Freitas, S. R., Longo, K. M., Chatfield, R., Latham, D., Dias, M. A. F. S., Andreae, M. O., Prins, E., Santos, J. C., Gielow, R., and Carvalho, J. A.: Including the sub-grid scale plume rise of vegetation fires in low resolution atmospheric transport models, Atmos. Chem. Phys., 7, 3385–3398, doi:10.5194/acp-7-3385-2007, 2007.

Gan, M. A., Kousky, V. E., and Ropelewski, C. F.: The South America monsoon circulation and its relationship to rainfall over west-central Brazil, J. Climate, 17, 47–66, doi:10.1175/1520-0442(2004)017<0047:Tsamca>2.0.Co;2, 2004.

Deleted: Durre, I., Vose, R. S., and Wuertz, D. B.: Overview of the Integrated Global Radiosonde Archive, J. Climate, 19, 53–68, doi:10.1175/Jcli3594.1, 2006.¶

Ge, C., Wang, J., and Reid, J. S.: Mesoscale modeling of smoke transport over the Southeast Asian Maritime Continent: coupling of smoke direct radiative effect below and above the low-level clouds, Atmos. Chem. Phys., 14, 159–174, doi:10.5194/acp-14-159-2014, 2014.

Ghan, S. J., Leung, L. R., Easter, R. C., and AbdulRazzak, K.: Prediction of cloud droplet number in a general circulation model, J. Geophys. Res.-Atmos., 102, 21777–21794, doi:10.1029/97jd01810, 1997.

Ghan, S. J., Liu, X., Easter, R. C., Zaveri, R., Rasch, P. J., Yoon, J. H., and Eaton, B.: Toward a Minimal Representation of Aerosols in Climate Models: Comparative Decomposition of Aerosol Direct, Semidirect, and Indirect Radiative Forcing, J Climate, 25, 6461-6476, 10.1175/Jcli-D-11-00650.1, 2012.

Goncalves, W. A., Machado, L. A. T., and Kirstetter, P. E.: Influence of biomass aerosol on precipitation over the Central Amazon: an observational study, Atmos. Chem. Phys., 15, 6789–6800, doi:10.5194/acp-15-6789-2015, 2015.

Grell, G., Freitas, S. R., Stuefer, M., and Fast, J.: Inclusion of biomass burning in WRF-Chem: impact of wildfires on weather forecasts, Atmos. Chem. Phys., 11, 5289–5303, doi:10.5194/acp-11-5289-2011, 2011.

Grell, G. A., and Devenyi, D.: A generalized approach to parameterizing convection combining ensemble and data assimilation techniques, Geophys. Res. Lett., 29, 1693, doi:10.1029/2002gl015311, 2002.

Grell, G. A., Peckham, S. E., Schmitz, R., McKeen, S. A., Frost, G., Skamarock, W. C., and Eder, B.: Fully coupled "online" chemistry within the WRF model, Atmos. Environ., 39, 6957–6975, doi:10.1016/j.atmosenv.2005.04.027, 2005.

Guenther, A., Karl, T., Harley, P., Wiedinmyer, C., Palmer, P. I., and Geron, C.: Estimates of global terrestrial isoprene emissions using MEGAN (Model of Emissions of Gases and Aerosols from Nature), Atmos. Chem. Phys., 6, 3181–3210, doi:10.5194/acp-6-3181-2006, 2006.

Hansen, J., Sato, M., and Ruedy, R.: Radiative forcing and climate response, J. Geophys. Res.-Atmos., 102, 6831–6864, doi:10.1029/96jd03436, 1997.

Hartmann, D. L., Ockert-Bell, M. E., and Michelsen, M. L.: The Effect of Cloud Type on Earth's Energy Balance: Global Analysis, J. Climate, 5, 1281–1304, doi:10.1175/1520-0442(1992)005<1281:teocto>2.0.co;2, 1992.

Holanda, B. A., Pöhlker, M. L., Walter, D., Saturno, J., Sörgel, M., Ditas, J., Ditas, F., Schulz, C., Franco, M. A., Wang, Q., Donth, T., Artaxo, P., Barbosa, H. M. J., Borrmann, S., Braga, R., Brito, J., Cheng, Y., Dollner, M., Kaiser, J. W., Klimach, T., Knote, C., Krüger, O. O., Fütterer, D., Lavrič, J. V., Ma, N., Machado, L. A. T., Ming, J., Morais, F. G., Paulsen, H., Sauer, D., Schlager, H., Schneider, J., Su, H., Weinzierl, B., Walser, A., Wendisch, M., Ziereis, H., Zöger, M., Pöschl, U., Andreae, M. O., and Pöhlker, C.: Influx of African biomass burning aerosol during the Amazonian dry season through layered transatlantic transport of black carbon-rich smoke, Atmos. Chem. Phys., 20, 4757–4785, doi:10.5194/acp-20-4757-2020, 2020.

Hong, S. Y.: A new stable boundary-layer mixing scheme and its impact on the simulated East Asian summer monsoon, Q. J. Roy. Meteor. Soc., 136, 1481–1496, doi:10.1002/qj.665, 2010.

Deleted: Holben, B. N., Tanré, D., Smirnov, A., Eck, T. F., Slutsker, I., Abuhassan, N., Newcomb, W. W., Schafer, J. S., Chatenet, B., Lavenu, F., Kaufman, Y. J., Castle, J. V., Setzer, A., Markham, B., Clark, D., Frouin, R., Halthore, R., Karneli, A., O'Neill, N. T., Pietras, C., Pinker, R. T., Voss, K., and Zibordi, G.: An emerging ground-based aerosol climatology: Aerosol optical depth from AERONET, J. Geophys. Res.-Atmos., 106, 12067–12097, doi:10.1029/2001jd900014, 2001.¶

Huang, X., Ding, A. J., Liu, L. X., Liu, Q., Ding, K., Niu, X. R., Nie, W., Xu, Z., Chi, X. G., Wang, M. H., Sun, J. N., Guo, W. D., and Fu, C. B.: Effects of aerosol-radiation interaction on precipitation during biomass-burning season in East China, Atmos. Chem. Phys., 16, 10063–10082, doi:10.5194/acp-16-10063-2016, 2016.

Huang, C.-C., Chen, S.-H., Lin, Y.-C., Earl, K., Matsui, T., Lee, H.-H., Tsai, I. C., Chen, J.-P., and Cheng, C.-T.: Impacts of Dust–Radiation versus Dust–Cloud Interactions on the Development of a Modeled Mesoscale Convective System over North Africa, Mon. Weather Rev., 147, 3301–3326, doi:10.1175/mwr-d-18-0459.1, 2019.

IPCC: Climate Change 2013: The Physical Science Basis. Contribution of Working Group I to the Fifth Assessment Report of the Intergovernmental Panel on Climate Change [Stocker, T.F., D. Qin, G.-K. Plattner, M. Tignor, S.K. Allen, J. Boschung, A. Nauels, Y. Xia, V. Bex and P.M. Midgley (eds.)]. Cambridge University Press, Cambridge, United Kingdom and New York, NY, USA, 1535 pp, doi:10.1017/CBO9781107415324, 2013.

Janssens-Maenhout, G., Crippa, M., Guizzardi, D., Dentener, F., Muntean, M., Pouliot, G., Keating, T., Zhang, Q., Kurokawa, J., Wankmüller, R., Denier van der Gon, H., Kuenen, J. J. P., Klimont, Z., Frost, G., Darras, S., Koffi, B., and Li, M.: HTAP_v2.2: a mosaic of regional and global emission grid maps for 2008 and 2010 to study hemispheric transport of air pollution, Atmos. Chem. Phys., 15, 11411–11432, https://doi.org/10.5194/acp-15-11411-2015, 2015.

Jiang, H. L., and Feingold, G.: Effect of aerosol on warm convective clouds: Aerosol-cloud-surface flux feedbacks in a new coupled large eddy model, J. Geophys. Res.-Atmos., 111, D01202, doi:10.1029/2005jd006138, 2006.

Jiang, J. H., Su, H., Huang, L., Wang, Y., Massie, S., Zhao, B., Omar, A., and Wang, Z.: Contrasting effects on deep convective clouds by different types of aerosols, Nat. Commun., 9, 3874, doi:10.1038/s41467-018-06280-4, 2018.

Johnson, B. T., Shine, K. P., and Forster, P. M.: The semi-direct aerosol effect: Impact of absorbing aerosols on marine stratocumulus, Q. J. Roy. Meteor. Soc., 130, 1407–1422, doi:10.1256/qj.03.61, 2004.

Kaufman, Y. J., and Fraser, R. S.: The effect of smoke particles on clouds and climate forcing, Science, 277, 1636–1639, doi:10.1126/science.277.5332.1636, 1997.

Kaufman, Y. J., and Koren, I.: Smoke and pollution aerosol effect on cloud cover, Science, 313, 655–658, doi:10.1126/science.1126232, 2006.

Khain, A., Rosenfeld, D., and Pokrovsky, A.: Aerosol impact on the dynamics and microphysics of deep convective clouds, Q. J. Roy. Meteor. Soc., 131, 2639–2663, doi:10.1256/qj.04.62, 2005.

Koch, D., and Del Genio, A. D.: Black carbon semi-direct effects on cloud cover: review and synthesis, Atmos. Chem. Phys., 10, 7685–7696, doi:10.5194/acp-10-7685-2010, 2010.

Kolusu, S. R., Marsham, J. H., Mulcahy, J., Johnson, B., Dunning, C., Bush, M., and Spracklen, D. V.: Impacts of Amazonia biomass burning aerosols assessed from short-range weather forecasts, Atmos. Chem. Phys., 15, 12251–12266, doi:10.5194/acp-15-12251-2015, 2015.

Koren, I., Kaufman, Y. J., Remer, L. A., and Martins, J. V.: Measurement of the effect of Amazon smoke on inhibition of cloud formation, Science, 303, 1342–1345, doi:10.1126/science.1089424, 2004.

Deleted: Huffman, G. J., Adler, R. F., Bolvin, D. T., Gu, G. J., Nelkin, E. J., Bowman, K. P., Hong, Y., Stocker, E. F., and Wolff, D. B.: The TRMM multisatellite precipitation analysis (TMPA): Quasi-global, multiyear, combined-sensor precipitation estimates at fine scales, J. Hydrometeorol., 8, 38–55, doi:10.1175/Jhm560.1, 2007.¶

Koren, I., Martins, J. V., Remer, L. A., and Afargan, H.: Smoke invigoration versus inhibition of clouds over the Amazon, Science, 321, 946–949, doi:10.1126/science.1159185, 2008.

Koren, I., Remer, L. A., Altaratz, O., Martins, J. V., and Davidi, A.: Aerosol-induced changes of convective cloud anvils produce strong climate warming, Atmos. Chem. Phys., 10, 5001–5010, doi:10.5194/acp-10-5001-2010, 2010.

Lee, H. H., Chen, S. H., Kleeman, M. J., Zhang, H. L., DeNero, S. P., and Joe, D. K.: Implementation of warm-cloud processes in a source- oriented WRF/Chem model to study the effect of aerosol mixing state on fog formation in the Central Valley of California, Atmos. Chem. Phys., 16, 8353–8374, doi:10.5194/acp-16-8353-2016, 2016.

Lee, S. S., Kim, B. G., Lee, C., Yum, S. S., and Posselt, D.: Effect of aerosol pollution on clouds and its dependence on precipitation intensity, Clim. Dynam., 42, 557–577, doi:10.1007/s00382-013-1898-2, 2014.

Lee, S. S., Li, Z., Mok, J., Ahn, M.-H., Kim, B.-G., Choi, Y.-S., Jung, C.-H., and Yoo, H. L.: Interactions between aerosol absorption, thermodynamics, dynamics, and microphysics and their impacts on a multiple-cloud system, Clim. Dynam., 49, 3905–3921, doi:10.1007/s00382-017-3552-x, 2017.

Li, Z. Q.: Influence of absorbing aerosols on the inference of solar surface radiation budget and cloud absorption, J. Climate, 11, 5–17, doi:10.1175/1520-0442(1998)011<0005:Ioaaot>2.0.Co;2, 1998.

Lin, J. C., Matsui, T., Pielke, R. A., and Kummerow, C.: Effects of biomass-burning-derived aerosols on precipitation and clouds in the Amazon Basin: a satellite-based empirical study, J. Geophys. Res.-Atmos., 111, D19204, doi:10.1029/2005jd006884, 2006.

Lin, Y., Wang, Y., Pan, B. W., Hu, J. X., Liu, Y. G., and Zhang, R. Y.: Distinct Impacts of Aerosols on an Evolving Continental Cloud Complex during the RACORO Field Campaign, J. Atmos. Sci., 73, 3681–3700, doi:10.1175/Jas-D-15-0361.1, 2016.

Lin, Y. L., Farley, R. D., and Orville, H. D.: Bulk Parameterization of the Snow Field in a Cloud Model, J. Clim. Appl. Meteorol., 22, 1065–1092, doi:10.1175/1520-0450(1983)022<1065:Bpotsf>2.0.Co;2, 1983.

Liu, Y. G., Daum, P. H., and McGraw, R. L.: Size truncation effect, threshold behavior, and a new type of autoconversion parameterization, Geophys. Res. Lett., 32, L11811, doi:10.1029/2005gl022636, 2005.

Martin, S. T., Andreae, M. O., Artaxo, P., Baumgardner, D., Chen, Q., Goldstein, A. H., Guenther, A., Heald, C. L., Mayol-Bracero, O. L., McMurry, P. H., Pauliquevis, T., Pöschl, U., Prather, K. A., Roberts, G. C., Saleska, S. R., Dias, M. A. S., Spracklen, D. V., Swietlicki, E., and Trebs, I.: Sources and Properties of Amazonian Aerosol Particles, Rev. Geophys., 48, doi:10.1029/2008rg000280, 2010.

Martins, J. A., Dias, M. A. F. S., and Goncalves, F. L. T.: Impact of biomass burning aerosols on precipitation in the Amazon: A modeling case study, J. Geophys. Res.-Atmos., 114, D02207, doi:10.1029/2007jd009587, 2009.

Martins, J. V., Artaxo, P., Liousse, C., Reid, J. S., Hobbs, P. V., and Kaufman, Y. J.: Effects of black carbon content, particle size, and mixing on light absorption by aerosols from biomass burning in Brazil, J. Geophys. Res.-Atmos., 103, 32041–32050, doi:10.1029/98jd02593, 1998.

Deleted: Lee, C. B., Kim, J. C., Belorid, M., and Zhao, P.: Performance Evaluation of Four Different Land Surface Models in WRF, Asian J. Atmos. Enviro., 10, 42–50, doi:10.5572/ajae.2016.10.1.042, 2016a.¶

Deleted: b

McCluskey, C. S., DeMott, P. J., Prenni, A. J., Levin, E. J. T., McMeeking, G. R., Sullivan, A. P., Hill, T. C. J., Nakao, S., Carrico, C. M., and Kreidenweis, S. M.: Characteristics of atmospheric ice nucleating particles associated with biomass burning in the US: Prescribed burns and wildfires, J. Geophys. Res.-Atmos., 119, doi:10.1002/2014jd021980, 2014.

Mlawer, E. J., Taubman, S. J., Brown, P. D., Iacono, M. J., and Clough, S. A.: Radiative transfer for inhomogeneous atmospheres: RRTM, a validated correlated-k model for the longwave, J. Geophys. Res.-Atmos., 102, 16663–16682, doi:10.1029/97jd00237, 1997.

Otte, T. L., Nolte, C. G., Otte, M. J., and Bowden, J. H.: Does Nudging Squelch the Extremes in Regional Climate Modeling?, J. Climate, 25, 7046–7066, doi:10.1175/Jcli-D-12-00048.1, 2012.

Peng, J., Hu, M., Guo, S., Du, Z., Zheng, J., Shang, D., Levy Zamora, M., Zeng, L., Shao, M., Wu, Y. S., Zheng, J., Wang, Y., Glen, C. R., Collins, D. R., Molina, M. J., and Zhang, R.: Markedly enhanced absorption and direct radiative forcing of black carbon under polluted urban environments, P. Natl. Acad. Sci. USA, 113, 4266–4271, doi:10.1073/pnas.1602310113, 2016

Pincus, R., Barker, H. W., and Morcrette, J. J.: A fast, flexible, approximate technique for computing radiative transfer in inhomogeneous cloud fields, J. Geophys. Res.-Atmos., 108, 4376, doi:10.1029/2002jd003322, 2003.

Pöhlker, C., Walter, D., Paulsen, H., Konemann, T., Rodriguez-Caballero, E., Moran-Zuloaga, D., Brito, J., Carbone, S., Degrendele, C., Despres, V. R., Ditas, F., Holanda, B. A., Kaiser, J. W., Lammel, G., Lavric, J. V., Ming, J., Pickersgill, D., Pöhlker, M. L., Prass, M., Lobs, N., Saturno, J., Sorgel, M., Wang, Q. Q., Weber, B., Wolff, S., Artaxo, P., Pöschl, U., and Andreae, M. O.: Land cover and its transformation in the backward trajectory footprint region of the Amazon Tall Tower Observatory, Atmos. Chem. Phys., 19, 8425–8470, doi:10.5194/acp-19-8425-2019, 2019.

Pöhlker, M. L., Pöhlker, C., Ditas, F., Klimach, T., de Angelis, I. H., Araujo, A., Brito, J., Carbone, S., Cheng, Y. F., Chi, X. G., Ditz, R., Gunthe, S. S., Kesselmeier, J., Konemann, T., Lavric, J. V., Martin, S. T., Mikhailov, E., Moran-Zuloaga, D., Rose, D., Saturno, J., Su, H., Thalman, R., Walter, D., Wang, J., Wolff, S., Barbosa, H. M. J., Artaxo, P., Andreae, M. O., and Pöschl, U.: Long-term observations of cloud condensation nuclei in the Amazon rain forest - Part 1: Aerosol size distribution, hygroscopicity, and new model parametrizations for CCN prediction, Atmos. Chem. Phys., 16, 15709–15740, doi:10.5194/acp-16-15709-2016, 2016.

Pöhlker, M. L., Ditas, F., Saturno, J., Klimach, T., de Angelis, I. H., Araujo, A. C., Brito, J., Carbone, S., Cheng, Y. F., Chi, X. G., Ditz, R., Gunthe, S. S., Holanda, B. A., Kandler, K., Kesselmeier, J., Konemann, T., Kruger, O. O., Lavric, J. V., Martin, S. T., Mikhailov, E., Moran-Zuloaga, D., Rizzo, L. V., Rose, D., Su, H., Thalman, R., Walter, D., Wang, J., Wolff, S., Barbosa, H. M. J., Artaxo, P., Andreae, M. O., Pöschl, U., and Pöhlker, C.: Long-term observations of cloud condensation nuclei over the Amazon rain forest - Part 2: Variability and characteristics of biomass burning, long-range transport, and pristine rain forest aerosols, Atmos. Chem. Phys., 18, 10289–10331, doi:10.5194/acp-18-10289-2018, 2018.

Procopio, A. S., Artaxo, P., Kaufman, Y. J., Remer, L. A., Schafer, J. S., and Holben, B. N.: Multiyear analysis of amazonian biomass burning smoke radiative forcing of climate, Geophys. Res. Lett., 31, L03108, doi:10.1029/2003gl018646, 2004.

Ramachandran, S., and Kedia, S.: Black carbon aerosols over an urban region: Radiative forcing and climate impact, J. Geophys. Res., 115, doi:10.1029/2009jd013560, 2010.

Ramanathan, V., Crutzen, P. J., Kiehl, J. T., and Rosenfeld, D.: Aerosols, climate, and the hydrological cycle, Science, 294, 2119–2124, doi:10.1126/science.1064034, 2001.

Reddington, C. L., Butt, E. W., Ridley, D. A., Artaxo, P., Morgan, W. T., Coe, H., and Spracklen, D. V.: Air quality and human health improvements from reductions in deforestation-related fire in Brazil, Nat. Geosci., 8, doi:10.1038/Ngeo2535, 2015.

Reid, J. S., Koppmann, R., Eck, T. F., and Eleuterio, D. P.: A review of biomass burning emissions part II: intensive physical properties of biomass burning particles, Atmos. Chem. Phys., 5, 799–825, doi:10.5194/acp-5-799-2005, 2005.

Reutter, P., Su, H., Trentmann, J., Simmel, M., Rose, D., Gunthe, S. S., Wernli, H., Andreae, M. O., and Pöschl, U.: Aerosol- and updraft-limited regimes of cloud droplet formation: influence of particle number, size and hygroscopicity on the activation of cloud condensation nuclei (CCN), Atmos. Chem. Phys., 9, 7067–7080, doi:10.5194/acp-9-7067-2009, 2009.

Reutter, P., Trentmann, J., Seifert, A., Neis, P., Su, H., Chang, D., Herzog, M., Wernli, H., Andreae, M. O., and Pöschl, U.: 3-D model simulations of dynamical and microphysical interactions in pyroconvective clouds under idealized conditions, Atmos. Chem. Phys., 14, 7573–7583, doi:10.5194/acp-14-7573-2014, 2014.

Roberts, G. C., Nenes, A., Seinfeld, J. H., and Andreae, M. O.: Impact of biomass burning on cloud properties in the Amazon Basin, J. Geophys. Res.-Atmos., 108, 4062, doi:10.1029/2001jd000985, 2003.

Roberts, M. C., Andreae, M. O., Zhou, J. C., and Artaxo, P.: Cloud condensation nuclei in the Amazon Basin: "Marine" conditions over a continent?, Geophys. Res. Lett., 28, 2807–2810, doi:10.1029/2000gl012585, 2001.

Rosenfeld, D.: Suppression of rain and snow by urban and industrial air pollution, Science, 287, 1793–1796, 2000.

Rosenfeld, D., Lohmann, U., Raga, G. B., O'Dowd, C. D., Kulmala, M., Fuzzi, S., Reissell, A., and Andreae, M. O.: Flood or drought: How do aerosols affect precipitation?, Science, 321, 1309–1313, doi:10.1126/science.1160606, 2008.

Rutledge, S. A. H., P. V: The Mesoscale and Microscale Structure and Organization of Clouds and Precipitation in Midlatitude Cyclones. XII: A Diagnostic Modeling Study of Precipitation Development in Narrow Cold-Frontal Rainbands, J. Atmos. Sci., 20, 2949–2972, 1984.

Samset, B. H., and Myhre, G.: Vertical dependence of black carbon, sulphate and biomass burning aerosol radiative forcing, Geophys. Res. Lett., 38, L24802, doi:10.1029/2011gl049697, 2011.

Sena, E. T., Artaxo, P., and Correia, A. L.: Spatial variability of the direct radiative forcing of biomass burning aerosols and the effects of land use change in Amazonia, Atmos. Chem. Phys., 13, 1261–1275, doi:10.5194/acp-13-1261-2013, 2013.

Sengupta, S. K., Welch, R. M., Navar, M. S., Berendes, T. A., and Chen, D. W.: Cumulus Cloud Field Morphology and Spatial Patterns Derived from High Spatial-Resolution Landsat Imagery, J. Appl. Meteorol., 29, 1245–1267, doi:10.1175/1520-0450(1990)029<1245:Ccfmas>2.0.Co;2, 1990.

Setzer, A. W., and Pereira, M. C.: Amazonia Biomass Burnings in 1987 and an Estimate of Their Tropospheric Emissions, Ambio., 20, 19–22, 1991.

Deleted: Reid, J. S., Hobbs, P. V., Ferek, R. J., Blake, D. R., Martins, J. V., Dunlap, M. R., and Liousse, C.: Physical, chemical, and optical properties of regional hazes dominated by smoke in Brazil, J. Geophys. Res.-Atmos., 103, 32059–32080, doi:10.1029/98jd00458, 1998.¶

Deleted: Remer, L. A., Kaufman, Y. J., Tanre, D., Mattoo, S., Chu, D. A., Martins, J. V., Li, R. R., Ichoku, C., Levy, R. C., Kleidman, R. G., Eck, T. F., Vermote, E., and Holben, B. N.: The MODIS aerosol algorithm, products, and validation, J. Atmos. Sci., 62, 947–973, doi:10.1175/Jas3385.1, 2005.¶

Deleted: Rizzo, L. V., Artaxo, P., Muller, T., Wiedensohler, A., Paixao, M., Cirino, G. G., Arana, A., Swietlicki, E., Roldin, P., Fors, E. O., Wiedemann, K. T., Leal, L. S. M., and Kulmala, M.: Long term measurements of aerosol optical properties at a primary forest site in Amazonia, Atmos. Chem. Phys., 13, 2391–2413, doi:10.5194/acp-13-2391-2013, 2013.¶

Deleted: Rosario, N. E., Longo, K. M., Freitas, S. R., Yamasoe, M. A., and Fonseca, R. M.: Modeling the South American regional smoke plume: aerosol optical depth variability and surface shortwave flux perturbation, Atmos. Chem. Phys., 13, 2923–2938, doi:10.5194/acp-13-2923-2013, 2013.¶

Deleted: Saturno, J., Ditas, F., Penning de Vries, M., Holanda, B. A., Pöhlker, M. L., Carbone, S., Walter, D., Bobrowski, N., Brito, J., Chi, X., Gutmann, A., Hrabe de Angelis, I., Machado, L. A. T., Moran-Zuloaga, D., Rüdiger, J., Schneider, J., Schulz, C., Wang, Q., Wendisch, M., Artaxo, P., Wagner, T., Pöschl, U., Andreae, M. O., and Pöhlker, C.: African volcanic emissions influencing atmospheric aerosols over the Amazon rain forest, Atmos. Chem. Phys., 18, 10391–10405, doi:10.5194/acp-18-10391-2018, 2018a.¶ Saturno, J., Holanda, B. A., Pöhlker, C., Ditas, F., Wang, Q. Q., Moran-Zuloaga, D., Brito, J., Carbone, S., Cheng, Y. F., Chi, X. G., Ditas, J., Hoffmann, T., de Angelis, I. H., Konemann, T., Lavric, J. V., Ma, N., Ming, J., Paulsen, H., Pöhlker, M. L., Rizzo, L. V., Schlag, P., Su, H., Walter, D., Wolff, S., Zhang, Y. X., Artaxo, P., Pöschl, U., and Andreae, M. O.: Black and brown carbon over central Amazonia: long-term aerosol measurements at the ATTO site, Atmos. Chem. Phys., 18, 12817–12843, doi:10.5194/acp-18-12817-2018, 2018b.¶

Shi, J. J., Matsui, T., Tao, W. K., Tan, Q., Peters-Lidard, C., Chin, M., Pickering, K., Guy, N., Lang, S., and Kemp, E. M.: Implementation of an aerosol-cloud-microphysics-radiation coupling into the NASA unified WRF: Simulation results for the 6-7 August 2006 AMMA special observing period, Q. J. Roy. Meteor. Soc., 140, 2158–2175, doi:10.1002/qj.2286, 2014.

Shrivastava, M., Cappa, C. D., Fan, J. W., Goldstein, A. H., Guenther, A. B., Jimenez, J. L., Kuang, C., Laskin, A., Martin, S. T., Ng, N. L., Petaja, T., Pierce, J. R., Rasch, P. J., Roldin, P., Seinfeld, J. H., Shilling, J., Smith, J. N., Thornton, J. A., Volkamer, R., Wang, J., Worsnop, D. R., Zaveri, R. A., Zelenyuk, A., and Zhang, Q.: Recent advances in understanding secondary organic aerosol: Implications for global climate forcing, Rev. Geophys., 55, 509–559, doi:10.1002/2016rg000540, 2017.

Shrivastava, M., Andreae, M. O., Artaxo, P., Barbosa, H. M. J., Berg, L. K., Brito, J., Ching, J., Easter, R. C., Fan, J., Fast, J. D., Feng, Z., Fuentes, J. D., Glasius, M., Goldstein, A. H., Alves, E. G., Gomes, H., Gu, D., Guenther, A., Jathar, S. H., Kim, S., Liu, Y., Lou, S., Martin, S. T., McNeill, V. F., Medeiros, A., de Sa, S. S., Shilling, J. E., Springston, S. R., Souza, R. A. F., Thornton, J. A., Isaacman-VanWertz, G., Yee, L. D., Ynoue, R., Zaveri, R. A., Zelenyuk, A., and Zhao, C.: Urban pollution greatly enhances formation of natural aerosols over the Amazon rainforest, Nat. Commun., 10, 1046, doi:10.1038/s41467-019-08909-4, 2019.

Smirnova, T. G., Brown, J. M., and Benjamin, S. G.: Performance of different soil model configurations in simulating ground surface temperature and surface fluxes, Mon. Weather Rev., 125, 1870–1884, doi:10.1175/1520-0493(1997)125<1870:Podsmc>2.0.Co;2, 1997.

Smirnova, T. G., Brown, J. M., Benjamin, S. G., and Kim, D.: Parameterization of cold-season processes in the MAPS land-surface scheme, J. Geophys. Res.-Atmos., 105, 4077–4086, doi:10.1029/1999jd901047, 2000.

Spracklen, D. V., Carslaw, K. S., Pöschl, U., Rap, A., and Forster, P. M.: Global cloud condensation nuclei influenced by carbonaceous combustion aerosol, Atmos. Chem. Phys., 11, 9067–9087, doi:10.5194/acp-11-9067-2011, 2011.

Stevens, B., and Feingold, G.: Untangling aerosol effects on clouds and precipitation in a buffered system, Nature, 461, 607–613, doi:10.1038/nature08281, 2009.

Streets, D. G.: Dissecting future aerosol emissions: Warming tendencies and mitigation opportunities, Climatic Change, 81, 313–330, doi:10.1007/s10584-006-9112-8, 2007.

Su, H., Jiang, J. H., Lu, X. H., Penner, J. E., Read, W. G., Massie, S., Schoeberl, M. R., Colarco, P., Livesey, N. J., and Santee, M. L.: Observed Increase of TTL Temperature and Water Vapor in Polluted Clouds over Asia, J. Climate, 24, 2728–2736, doi:10.1175/2010jcli3749.1, 2011.

Takahama, S., Schwartz, R. E., Russell, L. M., Macdonald, A. M., Sharma, S., and Leaitch, W. R.: Organic functional groups in aerosol particles from burning and non-burning forest emissions at a high-elevation mountain site, Atmos. Chem. Phys., 11, 6367–6386, doi:10.5194/acp-11-6367-2011, 2011.

Deleted: Su, H., Rose, D., Cheng, Y. F., Gunthe, S. S., Massling, A., Stock, M., Wiedensohler, A., Andreae, M. O., and Pöschl, U.: Hygroscopicity distribution concept for measurement data analysis and modeling of aerosol particle mixing state with regard to hygroscopic growth and CCN activation, Atmos. Chem. Phys., 10, 7489–7503, doi:10.5194/acp-10-7489-2010, 2010.¶
Su, L., and Fung, J. C. H.: Investigating the role of dust in ice nucleation within clouds and further effects on the regional weather system over East Asia – Part 1: model development and validation, Atmos. Chem. Phys., 18, 8707–8725, doi:10.5194/acp-18-8707-2018, 2018.¶

Tao, W. K., Li, X. W., Khain, A., Matsui, T., Lang, S., and Simpson, J.: Role of atmospheric aerosol concentration on deep convective precipitation: Cloud-resolving model simulations, J. Geophys. Res.-Atmos., 112, D24s18, doi:10.1029/2007jd008728, 2007.

Ten Hoeve, J. E., Jacobson, M. Z., and Remer, L. A.: Comparing results from a physical model with satellite and in situ observations to determine whether biomass burning aerosols over the Amazon brighten or burn off clouds, J. Geophys. Res.-Atmos., 117, D08203, doi:10.1029/2011jd016856, 2012.

Thornhill, G. D., Ryder, C. L., Highwood, E. J., Shaffrey, L. C., and Johnson, B. T.: The effect of South American biomass burning aerosol emissions on the regional climate, Atmos. Chem. Phys., 18, 5321–5342, doi:10.5194/acp-18-5321-2018, 2018.

Twomey, S.: Influence of Pollution on Shortwave Albedo of Clouds, J. Atmos. Sci., 34, 1149–1152, doi:10.1175/1520-0469(1977)034<1149:Tiopot>2.0.Co;2, 1977.

Wang, Y., Khalizov, A., Levy, M., and Zhang, R. Y.: New Directions: Light absorbing aerosols and their atmospheric impacts, Atmos. Environ., 81, 713–715, doi:10.1016/j.atmosenv.2013.09.034, 2013.

Wang, Y., Ma, P. L., Peng, J. F., Zhang, R. Y., Jiang, J. H., Easter, R. C., and Yung, Y. L.: Constraining Aging Processes of Black Carbon in the Community Atmosphere Model Using Environmental Chamber Measurements, J. Adv. Model Earth Sy., 10, 2514–2526, doi:10.1029/2018ms001387, 2018

Wiedinmyer, C., Akagi, S. K., Yokelson, R. J., Emmons, L. K., Al-Saadi, J. A., Orlando, J. J., and Soja, A. J.: The Fire INventory from NCAR (FINN): a high resolution global model to estimate the emissions from open burning, Geosci. Model Dev., 4, 625–641, doi:10.5194/gmd-4-625-2011, 2011.

Wild, O., Zhu, X., and Prather, M. J.: Fast-j: Accurate simulation of in- and below-cloud photolysis in tropospheric chemical models, J. Atmos. Chem., 37, 245–282, doi:10.1023/A:1006415919030, 2000.

Williams, E., Rosenfeld, D., Madden, N., Gerlach, J., Gears, N., Atkinson, L., Dunnemann, N., Frostrom, G., Antonio, M., Biazon, B., Camargo, R., Franca, H., Gomes, A., Lima, M., Machado, R., Manhaes, S., Nachtigall, L., Piva, H., Quintiliano, W., Machado, L., Artaxo, P., Roberts, G., Renno, N., Blakeslee, R., Bailey, J., Boccippio, D., Betts, A., Wolff, D., Roy, B., Halverson, J., Rickenbach, T., Fuentes, J., and Avelino, E.: Contrasting convective regimes over the Amazon: Implications for cloud electrification, J. Geophys. Res.-Atmos., 107, 8082, doi:10.1029/2001jd000380, 2002.

Wu, L., Su, H., and Jiang, J. H.: Regional simulations of deep convection and biomass burning over South America: 2. Biomass burning aerosol effects on clouds and precipitation, J. Geophys. Res., 116, doi:10.1029/2011jd016106, 2011.

Ye, X. Y., Cao, Q. M., Jiang, B. L., and Lin, W. S.: Numerical Simulation of the Effect of Cloud Condensation Nuclei Concentration on the Microphysical Processes in Typhoon Usagi, Adv. Meteorol., 8293062, doi:10.1155/2019/8293062, 2019.

Yokelson, R. J., Crounse, J. D., DeCarlo, P. F., Karl, T., Urbanski, S., Atlas, E., Campos, T., Shinozuka, Y., Kapustin, V., Clarke, A. D., Weinheimer, A., Knapp, D. J., Montzka, D. D., Holloway, J., Weibring, P., Flocke, F., Zheng, W., Toohey, D., Wennberg, P. O., Wiedinmyer, C., Mauldin, L., Fried, A., Richter, D., Walega, J., Jimenez, J. L., Adachi, K., Buseck,

Deleted: Tuccella, P., Curci, G., Visconti, G., Bessagnet, B., Menut, L., and Park, R. J.: Modeling of gas and aerosol with WRF/Chem over Europe: Evaluation and sensitivity study, J. Geophys. Res.-Atmos., 117, doi:10.1029/2011jd016302, 2012.¶

Deleted: Ward, D. S., Kloster, S., Mahowald, N. M., Rogers, B. M., Randerson, J. T., and Hess, P. G.: The changing radiative forcing of fires: global model estimates for past, present and future, Atmos. Chem. Phys., 12, 10857–10886, doi:10.5194/acp-12-10857-2012, 2012.¶

Deleted: Wu, L., Su, H., and Jiang, J. H.: Regional simulations of deep convection and biomass burning over South America: 1. Model evaluations using multiple satellite data sets, J. Geophys. Res., 116, doi:10.1029/2011jd016105, 2011a.¶

Deleted: b

P. R., Hall, S. R., and Shetter, R.: Emissions from biomass burning in the Yucatan, Atmos. Chem. Phys., 9, 5785–5812, doi:10.5194/acp-9-5785-2009, 2009.

Yu, H. B., Liu, S. C., and Dickinson, R. E.: Radiative effects of aerosols on the evolution of the atmospheric boundary layer, J. Geophys. Res.-Atmos., 107, 4142, doi:10.1029/2001jd000754, 2002.

Zaveri, R. A., and Peters, L. K.: A new lumped structure photochemical mechanism for large-scale applications, J. Geophys. Res.-Atmos., 104, 30387–30415, doi:10.1029/1999jd900876, 1999.

Zaveri, R. A., Easter, R. C., Fast, J. D., and Peters, L. K.: Model for Simulating Aerosol Interactions and Chemistry (MOSAIC), J. Geophys. Res.-Atmos., 113, D13204, doi:10.1029/2007jd008782, 2008.

Zhang, Y., Fu, R., Yu, H. B., Dickinson, R. E., Juarez, R. N., Chin, M., and Wang, H.: A regional climate model study of how biomass burning aerosol impacts land-atmosphere interactions over the Amazon, J. Geophys. Res.-Atmos., 113, D14s15, doi:10.1029/2007jd009449, 2008.

Zhang, Y., Fu, R., Yu, H. B., Qian, Y., Dickinson, R., Dias, M. A. F. S., Dias, P. L. D., and Fernandes, K.: Impact of biomass burning aerosol on the monsoon circulation transition over Amazonia, Geophys. Res. Lett., 36, L10814, doi:10.1029/2009gl037180, 2009.

Zhao, C., Leung, L. R., Easter, R., Hand, J., and Avise, J.: Characterization of speciated aerosol direct radiative forcing over California, J. Geophys. Res.-Atmos., 118, 2372–2388, doi:10.1029/2012jd018364, 2013.

Deleted: Zhang, Y., Zhang, X., Wang, K., He, J., Leung, L. R., Fan, J., and Nenes, A.: Incorporating an advanced aerosol activation parameterization into WRF-CAM5: Model evaluation and parameterization intercomparison, J. Geophys. Res.-Atmos., 120, 6952–6979, doi:10.1002/2014jd023051, 2015.¶

Table 1. WRF-Chem configuration.

Atmospheric Process	WRF-Chem Option
Longwave radiation	RRTMG
Shortwave radiation	RRTMG
Surface layer	Monin-Obukov
Land surface	RUC
Boundary layer	YSU
Microphysics	Lin et al.
Cumulus	Grell-Devenyi ensemble scheme in the 75 km and 15 km simulations; no cumulus scheme in the 3 km simulation
Gas-phase chemistry	CBMZ
Aerosol chemistry	MOSAIC
Aqueous-phase chemistry	Fahey and Pandis
Photolysis	Fast-J
Anthropogenic emissions	EDGAR-HTAPv2
Biogenic emissions	MEGAN
Biomass burning emissions	FINNv1.5

Table 2. Experiment design description.

Experiment identification	Experiment description
CC3	Clean case at 3 km resolution without BB emission.
CCNR3	Clean case at 3 km resolution without BB emission. The aerosol radiation feedback is turned off.
PC3_EMISX	Polluted case at 3 km resolution with BB emission scenario EMISX. EMISX represents scenario with BB aerosol emission rate scaled by a factor of X based on original BB emission.
PCNR3_EMISX	Polluted case at 3 km resolution with BB emission scenario EMISX. The aerosol radiation feedback is turned off.

Table 3. Summary of monthly mean perturbations caused by the ARI and ACI of BB aerosols in the EMIS1 and EMIS6 emission scenarios.

Variable	ARI		ACI	
	EMIS1	EMIS6	EMIS1	EMIS6
TOA solar radiation (W m^{-2})	0.4	2.0	–0.7	–1.4
TOA solar + IR radiation (W m^{-2})	0.5	3.0	–0.7	–1.5
Surface solar radiation (W m^{-2})	–5.7	–30.5	–0.6	–1.3
Sensible heat flux (W m^{-2})	–2.3	–14.4	–0.1	–0.2
Latent heat flux (W m^{-2})	–2.0	–11.8	–0.5	–1.1
Surface temperature (°C)	–0.03	–0.20	0.00	0.01
PBL height (m)	–8	–58	0	2
Cloud droplets number (cm^{-2})	$–0.7\times10^5$	$–6.0\times10^5$	4.0×10^5	14.5×10^5
Cloud droplets radius (μm)	–0.7	–0.5	–1.0	–2.6
Cloud base height (m)	–6	–40	1	5
LWP (g m^{-2})	–0.6	–3.8	0.7	1.7
LWP in PBL (g m^{-2})	0.03	0.14	–0.01	–0.04
LWP in FT (g m^{-2})	–0.6	–3.9	0.7	1.7
IWP (g m^{-2})	0.04	0.26	–0.02	–0.07
Precipitation (mm day^{-1})	0.01	–0.11	–0.06	–0.10

Deleted: **Table 3.** Statistical indexes of the comparisons between modeled and observed surface air temperature (T), relative humidity (RH) and wind speed (WS) at the ATTO site over September 2014 ...

Deleted: 5

Deleted: ,

Deleted: and the overall effect from

Deleted: averaged over domain3 for

Formatted: Centered

Deleted: +

Deleted: +

Deleted: +

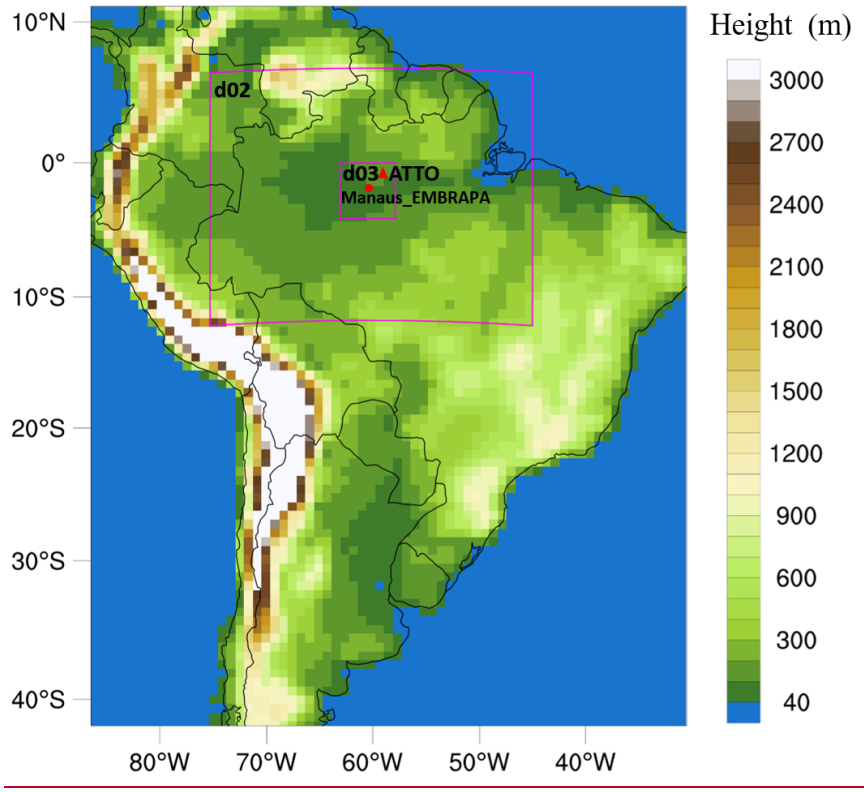

Figure 1. Model domain and orography. The outer map represents the parent domain with 75 km horizontal grid spacing, and the embedded squares show the extents of the 15-km (d02) and 3-km (d03) nested domains. The red dot denotes the AERONET monitoring station; the triangle represents the ATTO site.

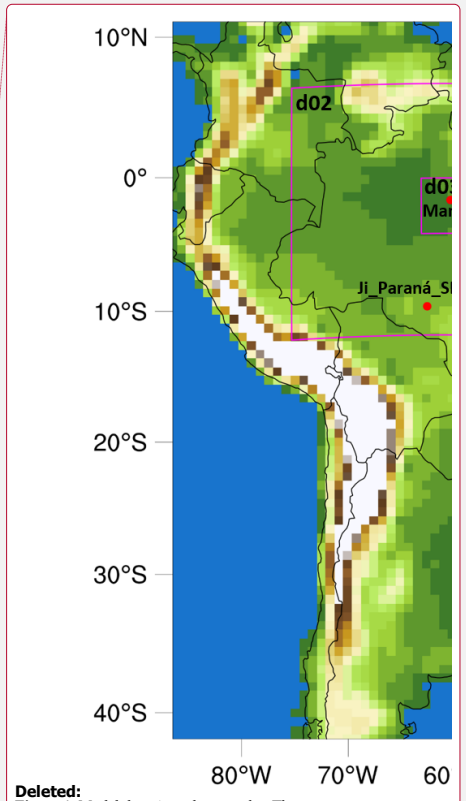

Deleted:
Figure 1. Model domain and orography. The outer map represents the parent domain with 75 km horizontal grid spacing, and the embedded squares show the extents of the 15-km (d02) and 3-km (d03) nested domains. Red dots denote AERONET monitoring stations; the triangle represents the ATTO site.¶

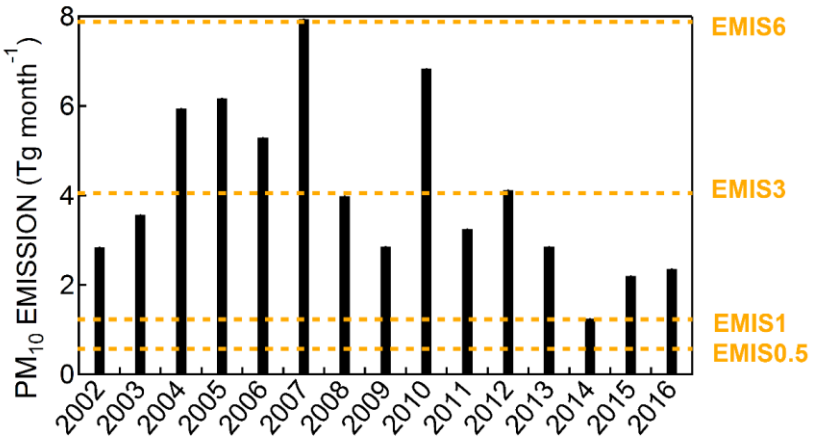

Figure 2. Annual variation of PM_{10} emission during September over domain1 based on FINNv1.5.

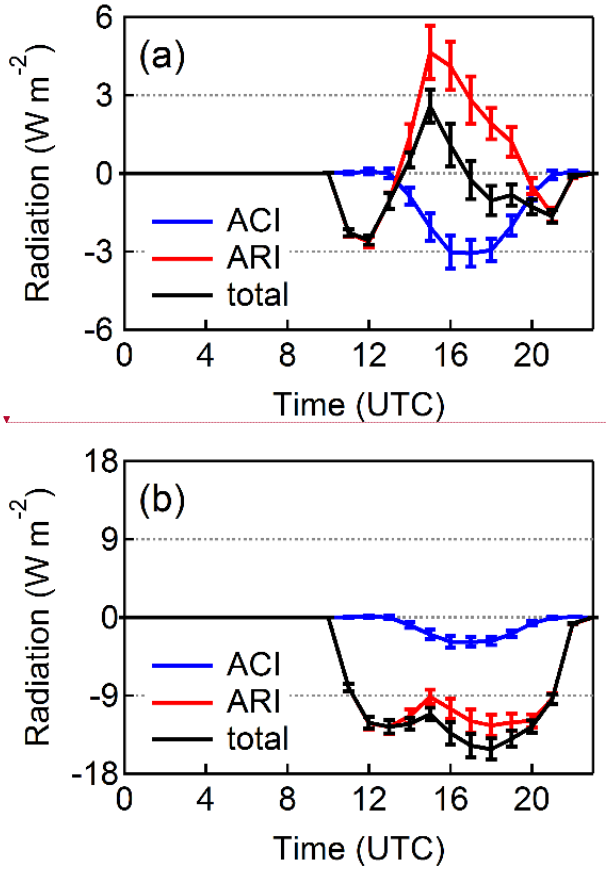

Figure 3. Diurnal variation of changes in all-sky shortwave radiation at TOA (a) and surface (b) in the EMIS1 emission scenario. Error bars denote the standard error.

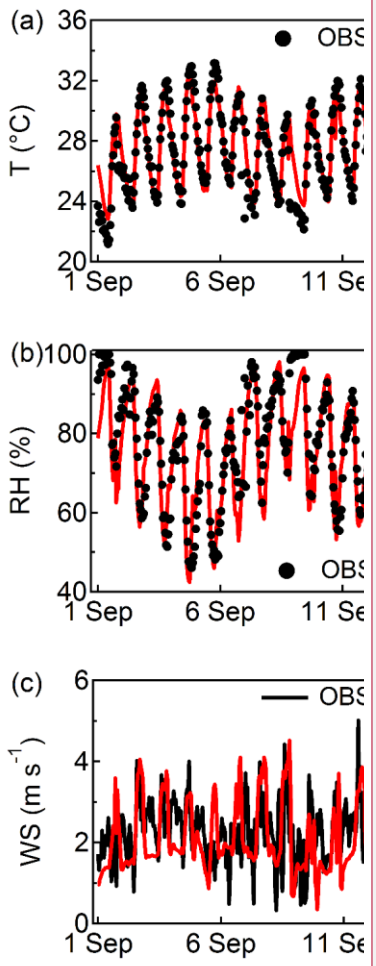

Deleted:
Figure 3. Time series of surface air temperature (a), relative humidity (b) and wind speed (c) from the domain3 simulation and the observations at ATTO during September 2014.¶

Deleted: 9

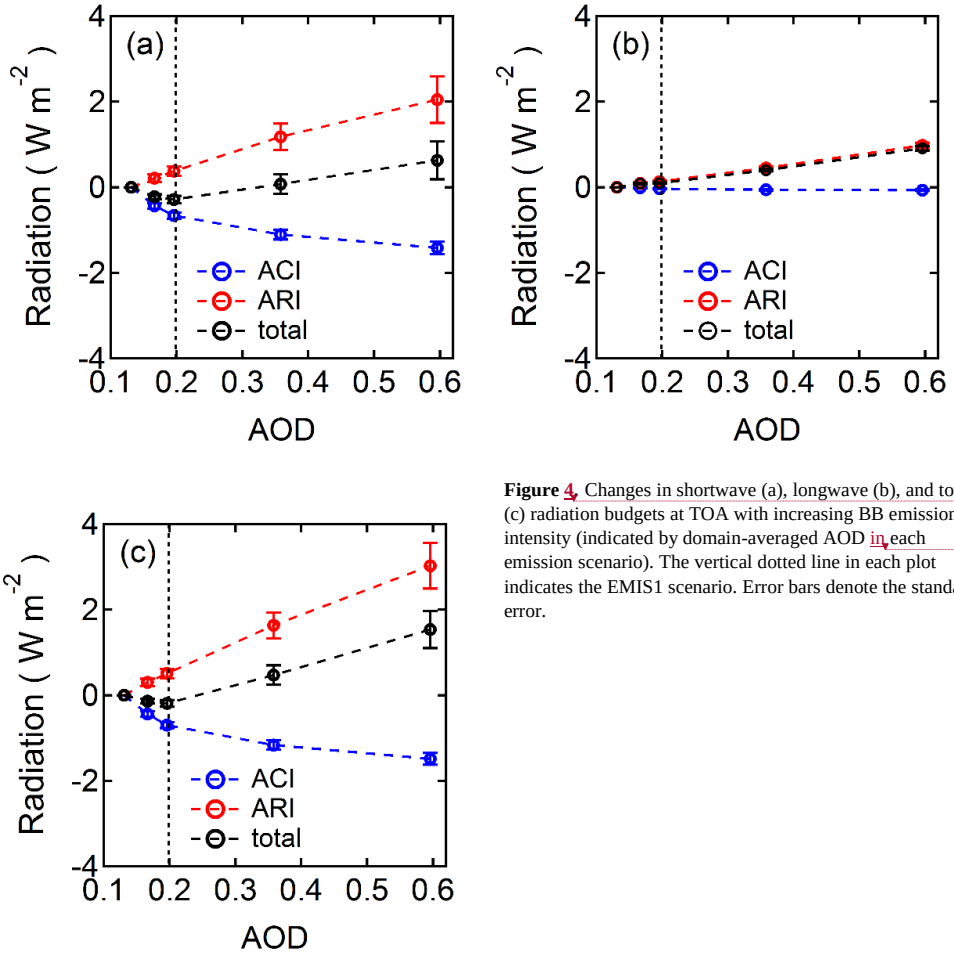

Figure 4. Changes in shortwave (a), longwave (b), and total (c) radiation budgets at TOA with increasing BB emission intensity (indicated by domain-averaged AOD in each emission scenario). The vertical dotted line in each plot indicates the EMIS1 scenario. Error bars denote the standard error.

Deleted: 10

Deleted: for

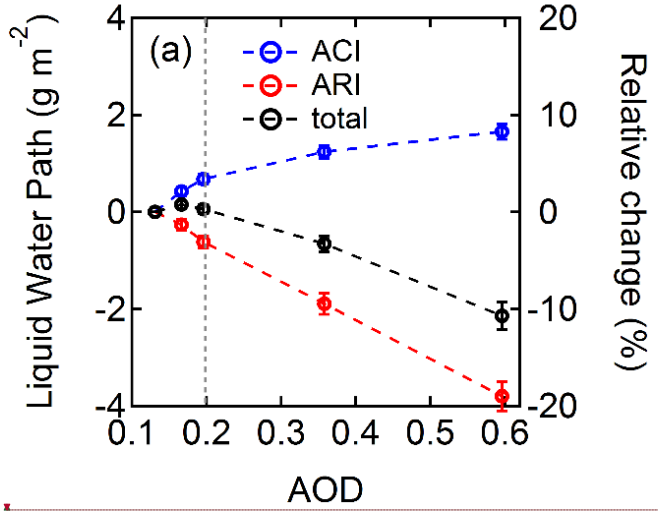

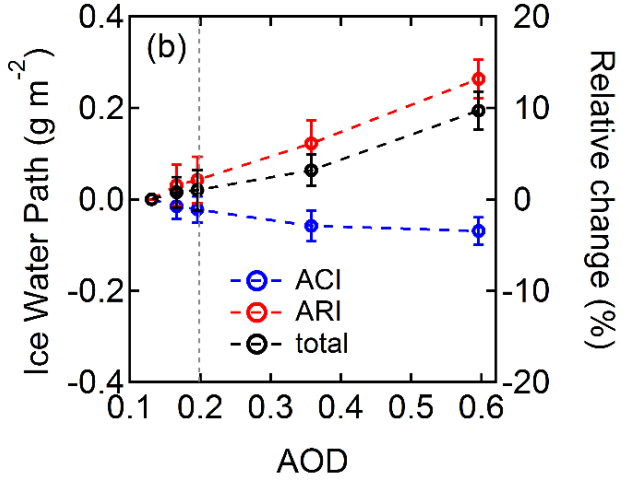

Figure 5. Changes in cloud LWP (a) and cloud IWP (b) with increasing BB emission intensity (indicated by domain-averaged AOD in each emission scenario). The vertical dotted line in each plot indicates the EMIS1 scenario. Error bars denote the standard error.

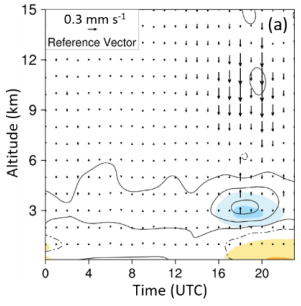

Moved down [1]:
Figure 11. Domain-averaged difference in air temperature (shaded, in intervals of 0.01°C), relative humidity (contour lines, in intervals of 0.1%), and updraft velocity (arrows) caused by BB aerosols' ACI (a), ARI (b), and total effect (c) in the EMIS1 emission scenario.¶

Deleted: Section Break (Next Page)

Deleted: 12

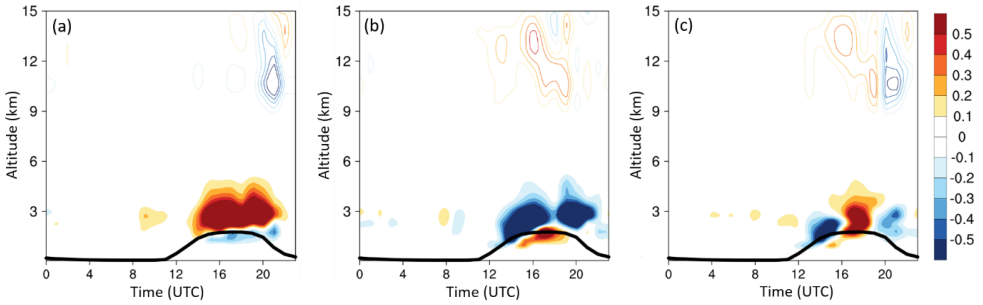

Figure 6. Diurnal variation of the vertical distribution of the domain-averaged difference in cloud water (shaded, in mg kg^{-1}) and cloud ice (contour lines, in 0.1 mg kg^{-1}) caused by BB aerosols' ACI (a), ARI (b), and total effect (c) in the EMIS1 emission scenario. The thick black line represents the PBL height.

Deleted: 13

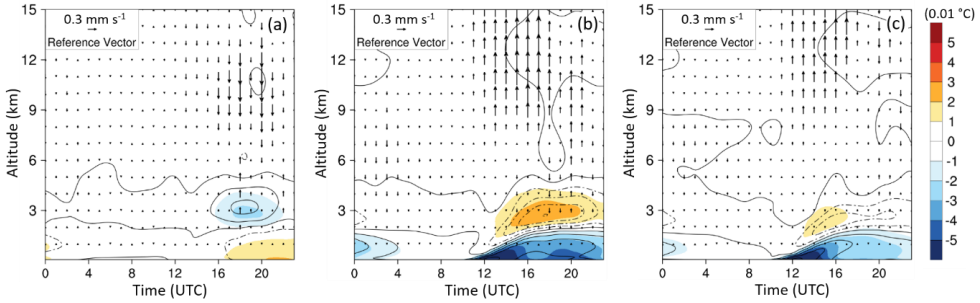

Figure 7. Domain-averaged difference in air temperature (shaded, in intervals of 0.01°C), relative humidity (contour lines, in intervals of 0.1%), and updraft velocity (arrows) caused by BB aerosols' ACI (a), ARI (b), and total effect (c) in the EMIS1 emission scenario.

Moved (insertion) [1]

Deleted: 11

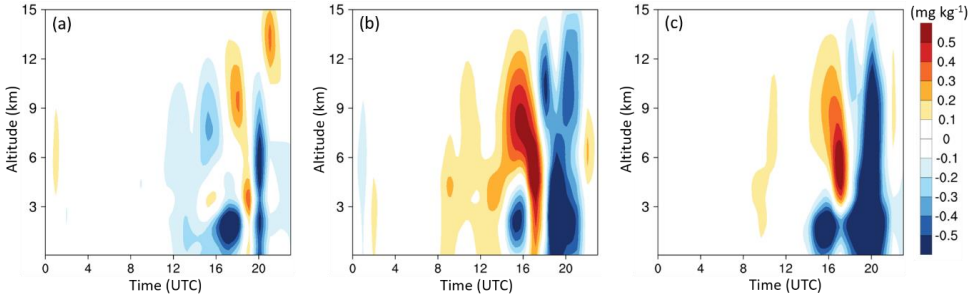

Figure 8. Diurnal variation of the vertical distribution of the domain-averaged difference in precipitating hydrometeor (QRAIN+QSNOW+QGRAUP) concentrations caused by BB aerosols' ACI (a), ARI (b), and total effect (c) in the EMIS1 emission scenario.

Deleted: 14

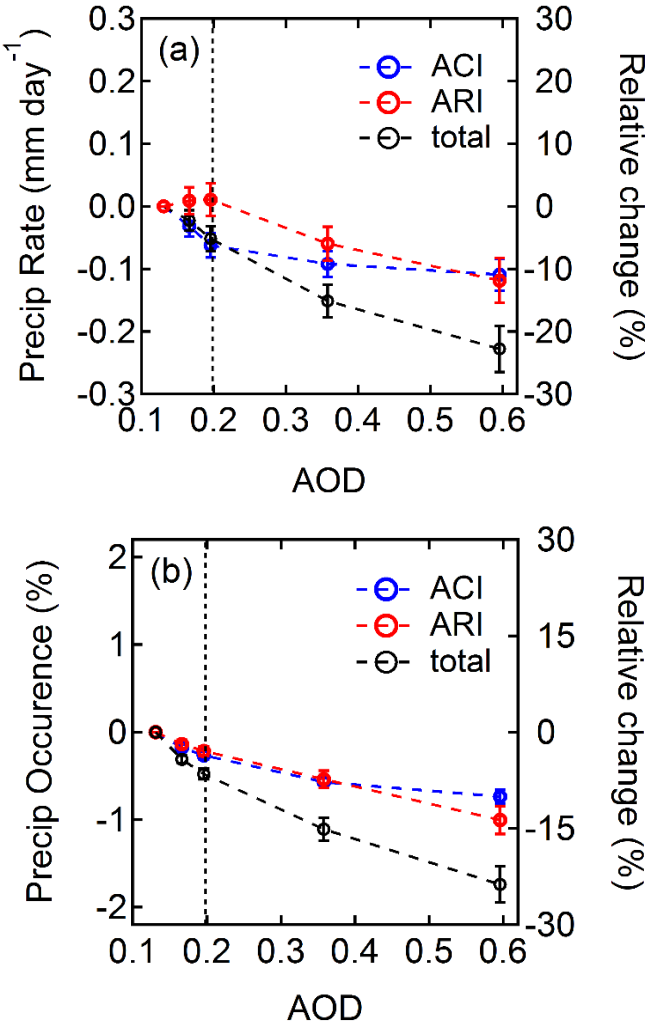

Figure 9. Changes in domain-averaged precipitation rate (a) and precipitation occurrence (b) with increasing BB emission intensity (indicated by domain-averaged AOD in each emission scenario). The vertical dotted line in each plot indicates the EMIS1 scenario. Error bars denote the standard error.

Deleted: 15

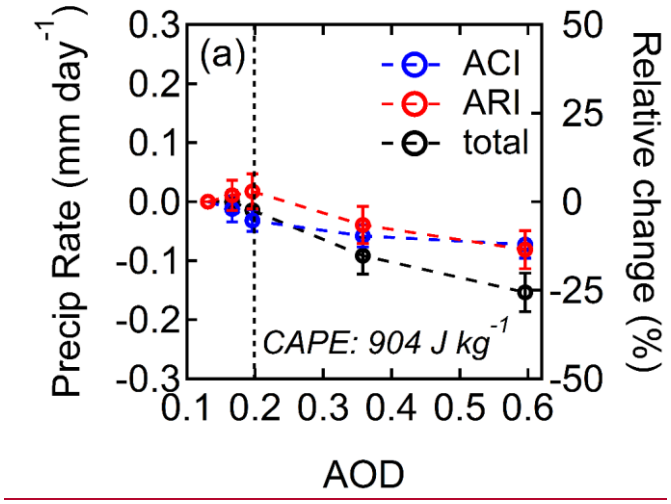

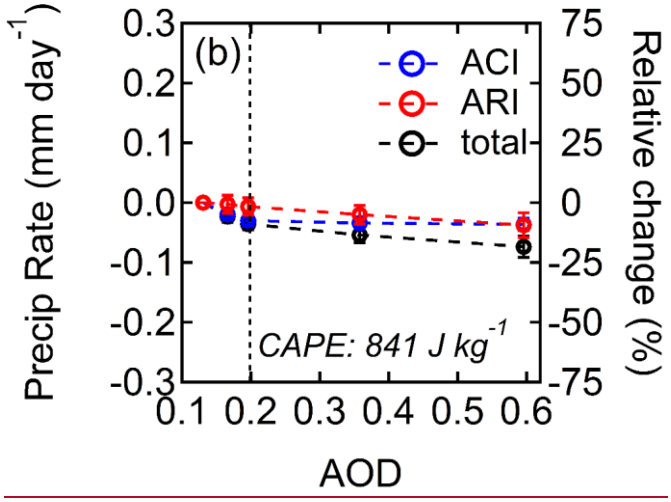

Figure 10. Changes in domain-averaged precipitation rate with increasing BB emission intensity (indicated by domain-averaged AOD in each emission scenario) at intensive precipitation regime (a) and light precipitation regime (b). The vertical dotted line in each plot indicates the EMIS1 scenario. Error bars denote the standard error.

Supplementary of

Impact of biomass burning aerosols on radiation, clouds, and precipitation over the Amazon: relative importance of aerosol-cloud and aerosol-radiation interactions

Deleted: during the dry season

Deleted: dependence of aerosol-cloud and aerosol-radiation interactions on aerosol loading

Lixia Liu[1], Yafang Cheng[1], Siwen Wang[1], Chao Wei[1], Mira Pöhlker[1], Christopher Pöhlker[1], Paulo Artaxo[2], Manish Shrivastava[3], Meinrat O. Andreae[1,4], Ulrich Pöschl[1] and Hang Su[1]

[1] Max Planck Institute for Chemistry, Mainz, Germany

[2] Institute of Physics, University of São Paulo, São Paulo 05508-900, Brazil

[3] Pacific Northwest National Laboratory, Richland, Washington, USA

[4] Scripps Institution of Oceanography, University of California at San Diego, La Jolla, California, USA

Correspondence to: *yafang.cheng@mpic.de & h.su@mpic.de*

Contents of this file

Introduction

Text S1 includes the observation data used in the model evaluation. Text S2, Table S2 and Figures S2–S6 include the model evaluation of the meteorological conditions. Text S3, Table S3 and Figures S7–S9 include the model evaluation of the aerosol field. Descriptions of Tables S1, Table S4, Figures S1 and Figures S10–S14 are shown in the corresponding caption.

Text S1

Observation data

1 Ground based measurements at ATTO

The Amazon Tall Tower Observatory (ATTO) site is located in the central Amazon, about 150 km northeast of Manaus, Brazil (Fig. 1), and represents a relatively clean rainforest background environment (Andreae et al., 2015). An 80-m tower, embedded within the canopy of about 35 m height, provides continuous measurements related to the research fields of meteorology, atmospheric trace gases, and aerosols (Andreae et al., 2015). Observational datasets used in this paper include meteorological variables, cloud condensation nuclei (CCN) number concentrations, and black carbon (BC) mass. Meteorology observations were obtained from a thermohygrometer and a 2-D sonic anemometer installed at 55 m on the tower. The data was averaged at 10-min resolution from raw observations taken at 1-min resolution. Air temperature and relative humidity (RH) measurements are only available from 1 Sep to 23 Sep 2014, while wind speed was observed over the complete simulation period. Aerosols were sampled at 60 m height. The CCN number concentration measurements by a CCN counter with supersaturation cycling through a set of levels ranging from 0.11% to 1.1% were used in this study. Detailed information on the CCN dataset can be found in Pöhlker et al. (Pöhlker et al., 2016, 2018). Equivalent black carbon (BCe) mass concentrations, M_{BCe}, were obtained from a multi-angle absorption photometer (MAAP; $\mu g\ m^{-3}$). The mass concentration was calculated by dividing the absorption coefficients at 637 nm by the dry season mass absorption cross-section of 12.3 $m^2\ g^{-1}$ according to Saturno et al. (2018a). Specific details about the MAAP measurements of M_{BCe} can be found in Saturno et al. (2018a).

2 Radiosonde measurements

Radiosonde observations from the Integrated Global Radiosonde Archive (IGRA; Durre et al., 2006) at the site Manaus (3.15 °S, 59.98 °W) were used to evaluate the vertical profile of meteorological elements. The IGRA sounding observations were conducted at 00:00 and 12:00 Universal Standard Time (UTC, which is 4 hours before local time). Note that throughout this paper the time referred to is UTC, unless Local Time (LT) is specifically mentioned. Radiosonde measurements at standard pressure levels within the troposphere (100, 150, 200, 250, 300, 400, 500, 700, 850 and 1000 hPa), as well as derived characteristic indices for convection, e.g., Convective Available Potential Energy (CAPE) and Lifting Condensation Level (LCL), were compared with simulation outputs.

3 TRMM

The Tropical Rainfall Measuring Mission (TRMM) 3B42 (Huffman et al., 2007) product was employed to evaluate the precipitation simulation performance. TRMM provides satellite observations of tropical and subtropical (50 °S–50 °N)

Deleted:) (

Deleted:)

Deleted: (

precipitation globally. The 3B42 rainfall dataset produces 3-hour averaged high-quality, infrared and microwave precipitation estimates at a resolution of 0.25° × 0.25° (Huffman et al., 2007).

4 MODIS

The Moderate Resolution Imaging Spectroradiometer (MODIS) Level 3 products provide satellite-derived daily estimates of cloud properties at a resolution of 1° × 1° (Platnick, S., et al., 2015). The measurements by MODIS onboard Aqua were used in this study, as the passing time of Aqua is approximately at 13:30 LT, when the local convective system is highly developed (Koren et al., 2004). The retrieval of cloud fraction, total liquid water path (LWP), and total ice water path (IWP) were compared with the corresponding modelling results. Model outputs at the satellite detection time were used when comparing against MODIS data.

5 AERONET

The Aerosol Robotic Network (AERONET) is an observation network of about 100 sites distributed globally, providing continuous measurements of aerosol optical properties (Holben et al., 2001). The observations are made by sun- and sky-scanning ground-based automated radiometers at various wavelengths. The aerosol optical depth (AOD) at 550 nm was interpolated using corresponding measurements at 675 nm and 440 nm. The level 2.0 cloud-screened product was used in this study. The observation data was retrieved for the site Manaus_EMBRAPA (2.9 °S, 60.0 °W) over September 2014.

6 CALIPSO

The Cloud-Aerosol Lidar and Infrared Pathfinder Satellite Observations (CALIPSO) Level 3 aerosol product (Tackett et al., 2018) is a global gridded dataset with a horizontal resolution of 2° × 5°, which provides monthly mean layered aerosol optical properties with a vertical resolution of 60 m for the troposphere below 12 km. The clear-sky retrieval of aerosol extinction at 532 nm was used to evaluate the vertical profile of the simulated aerosol. Both daytime and nighttime measurements over the studied region were utilized to provide the general vertical characteristics of aerosols.

Text S2

Evaluation of meteorological condition

Figure S2 shows the time series of hourly surface meteorological variables observed at the ATTO site and corresponding simulated results from domain3 in September 2014. As the canopy effect is integrated in the land surface model (Lee et al.,

Deleted: AOD and

Deleted: Remer et al., 2005

Deleted: AOD at 550 nm was used to validate the simulated aerosol concentration, and observations of

Deleted: and single scattering albedo (SSA)

Deleted: ere

Deleted: i

Deleted: Data is

Deleted: three sites during September 2014 within the Amazon Basin: Ji_Paraná_SE (10.9 °S, 61.9 °W),

Deleted: and Alta_Floresta (9.9 °S, 56.1 °W)

Deleted: 3

2016), the simulated meteorological variables are characterized by above-canopy properties. The variation patterns of the air temperature and RH are well captured by the model, with correlation coefficients of 0.86 and 0.78, respectively (Table S2). The surface air temperature is reproduced with a moderate overestimation of 0.2 °C (Table S2), which mainly occurs on 6 Sep, 8 Sep, and 17–18 Sep, whereas the RH exhibits an opposite bias. These significant biases occur corresponding to the missing prediction of rainfall on 6 and 18 Sep and underprediction of precipitation on 8 and 17 Sep by the model at this site (Fig. S3). This is expected since precipitation enhances surface evaporation and latent heat flux, leaves less net energy in the ground to heat the surface air (Zhuang et al., 2017), and therefore corresponds to a cool and moistened near-surface atmospheric state as can be found in the ATTO observation (Fig. S2). Consequently, the precipitation underestimation in the model was accompanied by higher biased simulated temperature and lower biased RH. This discrepancy between simulated and observed precipitation at the ATTO site could be associated with a bias of rainfall location and existence of unresolved subgrid-scale (<3 km), which will be further discussed later by comparing with the regional rainfall prediction. The wind speed from the simulation is generally lower than the observations with an average bias of –0.2 m s^{-1} (Table S2). The underestimation of the surface wind speed by the model also existed extensively in previous WRF-Chem simulations, and was ascribed to uncertainties in surface drag parameterization (Tuccella et al., 2012; Zhang et al., 2015).

The vertical distribution of the meteorological variables at the Manaus site over the 30-day simulation period is compared in Fig. S4. To keep consistency, simulation outputs of temperature and RH from domain3 were interpolated to the standard levels of the radiosonde data. The CAPE and LCL inferred from the temperature and humidity profiles from modeling and observations, are also shown. The model reproduces the air temperature profiles well. The RH generally follows the observed results below 300 hPa, while in the upper troposphere above 300 hPa a large overestimation occurs at 12:00 UTC. Similarly, an overestimation of simulated water vapor compared with MLS retrievals in the upper troposphere was found in WRF-Chem simulations of the Amazon Basin (Wu et al., 2011). The CAPE and LCL values estimated from the model agree well with that from the observations at 00:00 UTC. Noticeable differences of CAPE and LCL between model and observation of 240 J kg^{-1} and 266 m, respectively, are seen at 12:00 UTC, implying a possible earlier development of the simulated planetary boundary layer (PBL) ahead of observations.

The daily retrievals of cloud fraction, total LWP, and total IWP from the MODIS Aqua measurements are used to evaluate the simulation performance for cloud properties by WRF-Chem. The domain3 simulation results are averaged over the domain area to compare with the corresponding variables from the satellite measurements, as shown in Fig. S5. The simulated total LWP, calculated as the sum of liquid cloud and rainwater, correlates well with observations with a moderate underestimation. The total IWP from the model, as the sum of cloud ice, snow, and graupel, basically shows a positive correlation with the observations. However, a large underestimation of the total IWP from the model exists compared to the remote-sensed data. The model performs relatively well for the extreme low and high IWP regimes, with values being approximately 25% of the observations. The simulation of the total IWP by the WRF model has been found to produce a seasonally averaged underestimation by up to 80% compared with satellite measurements (Baro et al., 2018). The uncertainties inherent in the satellite dataset, e.g., eliminating data points with unrecognized cloud ice, would bias the observation results towards higher

Deleted: a
Deleted: 3
Deleted: 3
Deleted: 1
Deleted: Hence, a bias of rainfall location and existence of unresolved subgrid-scale (<3 km) convective precipitation may account for the discrepancy between simulated and observed surface temperature and RH.
Deleted: 3
Deleted: convective available potential energy (
Deleted:)
Deleted: lifted condensation level (
Deleted:)
Deleted: a

values and thus to some extent account for the discrepancy between model and observation. Besides, uncertainties associated with the ice-phase microphysical processes, e.g., the lack of IN parameterization, may also be a potential reason for this discrepancy (Su et al., 2018). Generally, the total cloud fraction from the model shows a linear correlation with the observations, falling between 25%–75% of the observed values.

Figure S6 shows the time series of domain-averaged 3-hour accumulated precipitation from the domain3 simulation and corresponding TRMM measurements during September 2014. The model well captures the occurrence of rainfall measured remotely by satellite. The regional rainfall events on 6, 8, 17 and 18 Sep are well predicted by the model with a slight underestimation, which reflects a better model performance compared with the evident model underestimation of precipitation at the ATTO site on these four days. Moreover, the modelled synoptic patterns corresponding to the precipitation episodes are consistent with the NCEP reanalysis data (not shown). The well-reproduced regional synoptic and precipitation conditions in the model serve to corroborate that the precipitation underestimation at the ATTO site is likely induced by a local bias of rainfall location and neglecting precipitation of sub-grid convection by the model. Generally, the simulated precipitation is comparable with TRMM observations in terms of time variation and intensity, which illustrates the model's ability to represent the convective activity during the study period.

Test S3

Evaluation of aerosol field

Table S3 shows the comparison of the modelled AOD against the AERONET observation at Manaus_EMBRAPA, a forest reservation site representative of the central Amazon environment (Artaxo et al., 2013). The model simulation generally captures the absolute value and the temporal variation of the observed AOD, with the mean bias and correlation coefficient being -0.03 and 0.54, respectively (Table S3). This is basically consistent with the AOD prediction accuracy in the Amazon by global models using the same fire emission inventory (Reddington et al., 2019; Pan et al., 2020). The slightly low bias in the AOD value could be related to an underestimated BB emission intensity due to errors in the detection of fires by satellite (Rosario et al., 2013) and/or an underestimation of the transatlantic transport from Africa (Holanda et al., 2020). Besides, the lack of SOA production in the model may also account for the bias in the AOD simulation (Bond and Bergstrom, 2006).

The simulated single scattering albedo (SSA) is compared with observations from previous studies, as shown in Table S3. Compared with the in-situ measured SSA of 0.87±0.06 at 637 nm at the TT34 tower (Rizzo et al., 2013) in the central Amazon, a slightly higher value of 0.89±0.01 is obtained by the model simulation. Similarly, the modeled monthly mean SSA of 0.90 for the location of the ATTO site is relatively higher than an extrapolated value of 0.88 at 550 nm from multi-year observations for the dry season at the ATTO site (Saturno et al., 2018b). Given the substantial influence of BB particles on the aerosol SSA (Saturno et al., 2018b), the difference between model results and observation may be associated with the mismatched average time periods for the comparison. Generally, the simulated SSA does not deviate greatly from the observed

Deleted: ,

Deleted: suggesting uncertainties in the ice-phase microphysical processes. T

Deleted: in the microphysical scheme may contribute to

Deleted: corroborating the hypothesis that the bias of surface air temperature and RH are

Deleted: The simulated SSA is compared with AERONET retrievals for Alta_Floresta and Ji_Paraná_SE and observations from previous studies in Table 4. The comparison at Manaus_EMBRAPA is excluded because of the scarcity of the data available. The simulated SSA is lower compared with AERONET retrievals for Alta_Floresta and Ji_Paraná_SE. However, the SSA observed on flights at Porto Velho, a site at the southwestern Amazon, during the SCAR-B campaign (Reid et al., 1998), is close to the simulated result.

Deleted: 0.90

Deleted: our

Deleted: slightly

Deleted: also possibly be caused by

value, which reflects a reasonable representation of the aerosol optical characteristics in the model. In Fig. S7 we compare the time variation of black carbon mass concentration measured at the ATTO site during the simulation period with the simulation outputs. The model results are in fair agreement with the observed BC concentrations, indicating a reasonable estimate of the influence from BB on this region.

The aerosol vertical distribution is evaluated using the CALIPSO-measured monthly mean clear-sky aerosol extinction profile averaged over the domain3 (Fig. S8). The simulation data was processed to align with the observation by using outputs corresponding to the passing time of the satellite, excluding cloudy grids with a cloud criterion of 1 g kg^{-1} and interpolating the extinction coefficient at 550 nm to 532 nm. The model reproduced the observed high aerosol extinction coefficient below 3 km and accurately captured the location of the two peaks at the surface and near 2 km respectively. Compared with the observation, the model overestimates the aerosol extinction above 3 km, which was also found in Wu et al. (2011). This discrepancy may be associated with an overestimated exchange between PBL and the free atmosphere by turbulent mixing and convective transport, an underestimation of precipitation scavenging, and/or an overestimated plume rise at some fire spots. Generally, the model reasonably simulated the aerosol vertical distribution, illustrating an acceptable performance of the plume rise parameterization. The ability of the model to reproduce the aerosol vertical pattern provides reliable aerosol input for investigating the aerosol-radiation-cloud interaction, given the important role of the vertical distribution of light-absorbing aerosols in affecting the aerosol radiative effect (Johnson et al., 2004).

A comparison of CCN concentrations at different supersaturations between in-situ observation and the WRF-Chem simulation for the ATTO site is presented in Fig. S9. The calculation of CCN number concentration at observed supersaturation level from model outputs followed the method in Su et al. (2010). The model results show an overall agreement in magnitude with observations for the supersaturation range of 0.2-0.5%, which represents the typical atmospheric conditions during the dry season in the Amazon (Archer-Nicholls et al., 2016). The variation of CCN number with supersaturation level matches the pattern obtained by observation (Pöhlker et al., 2018), indicating a reasonable sensitivity of aerosol activation ability to varying supersaturation situations.

Deleted: 2

Deleted: 8

References

Artaxo, P., Rizzo, L. V., Brito, J. F., Barbosa, H. M. J., Arana, A., Sena, E. T., Cirino, G. G., Bastos, W., Martin, S. T., and Andreae, M. O.: Atmospheric aerosols in Amazonia and land use change: from natural biogenic to biomass burning conditions, Faraday Discuss., 165, 203–235, doi:10.1039/c3fd00052d, 2013.

Baro, R., Jimenez-Guerrero, P., Stengel, M., Brunner, D., Curci, G., Forkel, R., Nea, L., Palacios-Pena, L., Savage, N., Schaap, M., Tuccella, P., van der Gon, H. D., and Galmarini, S.: Evaluating cloud properties in an ensemble of regional online

coupled models against satellite observations, Atmos. Chem. Phys., 18, 15183–15199, doi:10.5194/acp-18-15183-2018, 2018.

Durre, I., Vose, R. S., and Wuertz, D. B.: Overview of the Integrated Global Radiosonde Archive, J. Climate, 19, 53–68, doi:10.1175/Jcli3594.1, 2006.

Huffman, G. J., Adler, R. F., Bolvin, D. T., Gu, G. J., Nelkin, E. J., Bowman, K. P., Hong, Y., Stocker, E. F., and Wolff, D. B.: The TRMM multisatellite precipitation analysis (TMPA): Quasi-global, multiyear, combined-sensor precipitation estimates at fine scales, J. Hydrometeorol., 8, 38–55, doi:10.1175/Jhm560.1, 2007.

Holben, B. N., Tanré, D., Smirnov, A., Eck, T. F., Slutsker, I., Abuhassan, N., Newcomb, W. W., Schafer, J. S., Chatenet, B., Lavenu, F., Kaufman, Y. J., Castle, J. V., Setzer, A., Markham, B., Clark, D., Frouin, R., Halthore, R., Karneli, A., O'Neill, N. T., Pietras, C., Pinker, R. T., Voss, K., and Zibordi, G.: An emerging ground-based aerosol climatology: Aerosol optical depth from AERONET, J. Geophys. Res.-Atmos., 106, 12067–12097, doi:10.1029/2001jd900014, 2001.

Lee, C. B., Kim, J. C., Belorid, M., and Zhao, P.: Performance Evaluation of Four Different Land Surface Models in WRF, Asian J. Atmos. Enviro., 10, 42–50, doi:10.5572/ajae.2016.10.1.042, 2016.

Pan, X. H., Ichoku, C., Chin, M., Bian, H. S., Darmenov, A., Colarco, P., Ellison, L., Kucsera, T., da Silva, A., Wang, J., Oda, T., and Cui, G.: Six global biomass burning emission datasets: intercomparison and application in one global aerosol model, Atmos Chem Phys, 20, 969–994, doi:10.5194/acp-20-969-2020, 2020.

Platnick, S., et al.: MODIS Atmosphere L3 Monthly Product. NASA MODIS Adaptive Processing System, Goddard Space Flight Center, USA: http://dx.doi.org/10.5067/MODIS/MOD08_M3.006, 2015.

Pöhlker, M. L., Ditas, F., Saturno, J., Klimach, T., de Angelis, I. H., Araujo, A. C., Brito, J., Carbone, S., Cheng, Y. F., Chi, X. G., Ditz, R., Gunthe, S. S., Holanda, B. A., Kandler, K., Kesselmeier, J., Konemann, T., Kruger, O. O., Lavric, J. V., Martin, S. T., Mikhailov, E., Moran-Zuloaga, D., Rizzo, L. V., Rose, D., Su, H., Thalman, R., Walter, D., Wang, J., Wolff, S., Barbosa, H. M. J., Artaxo, P., Andreae, M. O., Pöschl, U., and Pöhlker, C.: Long-term observations of cloud condensation nuclei over the Amazon rain forest - Part 2: Variability and characteristics of biomass burning, long-range transport, and pristine rain forest aerosols, Atmos. Chem. Phys., 18, 10289–10331, doi:10.5194/acp-18-10289-2018, 2018.

Reddington, C. L., Morgan, W. T., Darbyshire, E., Brito, J., Coe, H., Artaxo, P., Scott, C. E., Marsham, J., and Spracklen, D. V.: Biomass burning aerosol over the Amazon: analysis of aircraft, surface and satellite observations using a global aerosol model, Atmos. Chem. Phys., 19, 9125–9152, doi:10.5194/acp-19-9125-2019, 2019.

Rizzo, L. V., Artaxo, P., Muller, T., Wiedensohler, A., Paixao, M., Cirino, G. G., Arana, A., Swietlicki, E., Roldin, P., Fors, E. O., Wiedemann, K. T., Leal, L. S. M., and Kulmala, M.: Long term measurements of aerosol optical properties at a primary forest site in Amazonia, Atmos. Chem. Phys., 13, 2391–2413, doi:10.5194/acp-13-2391-2013, 2013.

Rosario, N. E., Longo, K. M., Freitas, S. R., Yamasoe, M. A., and Fonseca, R. M.: Modeling the South American regional smoke plume: aerosol optical depth variability and surface shortwave flux perturbation, Atmos. Chem. Phys., 13, 2923–2938, doi:10.5194/acp-13-2923-2013, 2013.

Saturno, J., Ditas, F., Penning de Vries, M., Holanda, B. A., Pöhlker, M. L., Carbone, S., Walter, D., Bobrowski, N., Brito, J., Chi, X., Gutmann, A., Hrabe de Angelis, I., Machado, L. A. T., Moran-Zuloaga, D., Rüdiger, J., Schneider, J., Schulz, C., Wang, Q., Wendisch, M., Artaxo, P., Wagner, T., Pöschl, U., Andreae, M. O., and Pöhlker, C.: African volcanic emissions influencing atmospheric aerosols over the Amazon rain forest, Atmos. Chem. Phys., 18, 10391–10405, doi:10.5194/acp-18-10391-2018, 2018a.

Saturno, J., Holanda, B. A., Pöhlker, C., Ditas, F., Wang, Q. Q., Moran-Zuloaga, D., Brito, J., Carbone, S., Cheng, Y. F., Chi, X. G., Ditas, J., Hoffmann, T., de Angelis, I. H., Konemann, T., Lavric, J. V., Ma, N., Ming, J., Paulsen, H., Pöhlker, M. L., Rizzo, L. V., Schlag, P., Su, H., Walter, D., Wolff, S., Zhang, Y. X., Artaxo, P., Pöschl, U., and Andreae, M. O.: Black and brown carbon over central Amazonia: long-term aerosol measurements at the ATTO site, Atmos. Chem. Phys., 18, 12817–12843, doi:10.5194/acp-18-12817-2018, 2018b.

Su, H., Rose, D., Cheng, Y. F., Gunthe, S. S., Massling, A., Stock, M., Wiedensohler, A., Andreae, M. O., and Pöschl, U.: Hygroscopicity distribution concept for measurement data analysis and modeling of aerosol particle mixing state with regard to hygroscopic growth and CCN activation, Atmos. Chem. Phys., 10, 7489–7503, doi:10.5194/acp-10-7489-2010, 2010.

Su, L., and Fung, J. C. H.: Investigating the role of dust in ice nucleation within clouds and further effects on the regional weather system over East Asia – Part 1: model development and validation, Atmos. Chem. Phys., 18, 8707–8725, doi:10.5194/acp-18-8707-2018, 2018.

Tackett, J. L., Winker, D. M., Getzewich, B. J., Vaughan, M. A., Young, S. A., and Kar, J.: CALIPSO lidar level 3 aerosol profile product: version 3 algorithm design, Atmos. Meas. Tech., 11, 4129–4152, https://doi.org/10.5194/amt-11-4129-2018, 2018.

Tuccella, P., Curci, G., Visconti, G., Bessagnet, B., Menut, L., and Park, R. J.: Modeling of gas and aerosol with WRF/Chem over Europe: Evaluation and sensitivity study, J. Geophys. Res.-Atmos., 117, doi:10.1029/2011jd016302, 2012.

Wu, L., Su, H., and Jiang, J. H.: Regional simulations of deep convection and biomass burning over South America: 1. Model evaluations using multiple satellite data sets, J. Geophys. Res., 116, doi:10.1029/2011jd016105, 2011.

Zhang, Y., Zhang, X., Wang, K., He, J., Leung, L. R., Fan, J., and Nenes, A.: Incorporating an advanced aerosol activation parameterization into WRF-CAM5: Model evaluation and parameterization intercomparison, J. Geophys. Res.-Atmos., 120, 6952–6979, doi:10.1002/2014jd023051, 2015.

Zhuang, Y., Fu, R., Marengo, J. A., and Wang, H.: Seasonal variation of shallow-to-deep convection transition and its link to the environmental conditions over the Central Amazon, J. Geophys. Res., 122, 2649–2666, https://doi.org/10.1002/2016JD025993, 2017

Table S1. Monthly mean perturbations caused by the ARI effect of BB aerosols for the EMIS6 emission scenario.

	ARI in this study	PC3_EMISX - PCNR3_EMISX	difference
LWP (g m^{-2})	–3.8	–3.9	–0.1 (3%)
IWP (g m^{-2})	0.26	0.24	–0.02 (8%)

TableS2. Statistical indexes of the comparisons between modeled and observed surface air temperature (T), relative humidity (RH), and wind speed (WS) at the ATTO site over September 2014.

	MB	RMSE	r
T (°C)	0.2	1.5	0.86
RH (%)	–2.3	9.2	0.78
WS (m s^{-1})	–0.2	1.9	0.52

MB: the mean bias;
RMSE: the root mean square error;
r: the correlation coefficient.

Deleted: 3

Table S3. Comparison of AOD and SSA at 550 nm obtained from model simulation in domain3 and observation.

	Observation	Model[a]
	AOD	
Manaus_EMBRAPA (AERONET)	0.24±0.10 (average of Sep 2014)	0.21±0.05 (R^b=0.54)
	SSA	
TT34[c] (Rizzo et al., 2013)	0.87±0.06 (average of Jul–Dec 2008–2010)	0.89±0.01
ATTO[d] (Saturno et al., 2018b)	0.88 (average of Aug–Nov 2012–2017)	0.90±0.01

a) Model results with EMIS1, averaged for September 2014.
b) R represents the correlation coefficient between the observation and model simulation.
c) The SSA values at this site are for 637 nm. Calculation of SSA at 550 nm is not conducted due to incomplete information on Angstrom exponent in Rizzo et al. (2013).
d) The SSA observation for the ATTO site is obtained from Saturno et al. (2018b) by extrapolating the original value at 637 nm to that at 550 nm using the Angstrom exponents in Saturno et al. (2018b).

Deleted: **Table 4.** Comparison of SSA at 550 nm obtained from model simulation and observation.¶

Table S4. Estimates of radiative perturbation by biomass burning aerosols over the Amazon Basin in this study and from previous studies.

	Description	Radiative perturbation ($W\ m^{-2}$)*	AOD	Effect	Region of Amazon Basin	Model	Reference
Clear-sky	SW at TOA	–5.6±1.7	0.25±0.11	ARI	Southern	SBDART	Sena et al. (2013)
	SW at TOA	–3.33±0.89	0.67	total	Southern	HadGEM3-GA3	Thornhill et al. (2018)
	SW at TOA	[–0.7, –3.7]	0.2–0.6	ARI	Central	WRF-Chem	This study
All-sky	SW at TOA	1.35±1.8	0.67	total	Southern	HadGEM3-GA3	Thornhill et al. (2018)
	LW at TOA	–3.07±1.55					
	SW at surface	–5.46±1.93					
	SW at TOA	–1.75	0.8–1.2	ARI	Southwest	WRF-Chem	Archer-Nicholls et al. (2016)
		2.72	0.4–1.0				
		1.53	0.4–1.0				
	SW+LW at TOA	–4±1		ARI	Southern	MetUM	Kolusu et al. (2015)
	SW+LW at surface	–9±1					
	LW at TOA	–0.12		total	entire	WRF-Chem	Wu et al. (2011)
	SW at surface	–15.9					
	SW at surface	–28.23	0.633	total	Southern	GATOR-GCMOM	Ten Hoeve et al. (2012)
	LW at surface	8.6					
	SW at surface	–10	0.2–0.4	ARI	Northwest	CCATT-BRAMS	Rosario et al. (2013)
	SW at TOA	[–0.3, 0.6]	0.2–0.6	total	Central	WRF-Chem	This study
	LW at TOA	[0.1, 0.9]					
	SW at surface	[–6.7, –31.8]					
	LW at surface	[0.3, 1.9]					
	SW at TOA	[0.4, 2.0]	0.2–0.6	ARI	Central	WRF-Chem	This study
	LW at TOA	[0.1, 1.0]					
	SW at surface	[–5.7, –30.5]					
	LW at surface	[0.4, 2.0]					

*Radiative perturbation with standard deviation or in bracket for range obtained from simulations with emission intensity of EMIS1–EMIS6.

Deleted: 1

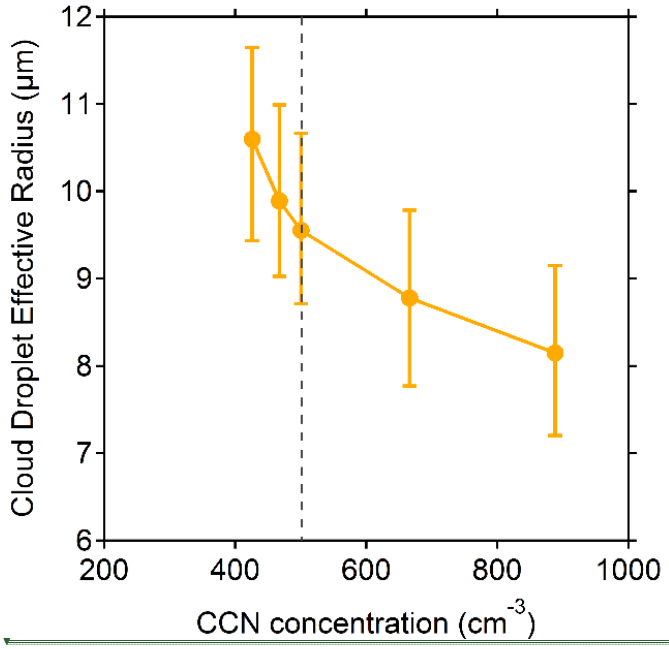

Figure S1. Relationship of monthly mean domain-averaged cloud droplet effective radius and cloud-base CCN concentrations for all emission scenarios derived from experiments of CCNR3 and PCNR3_EMISX. The dashed line indicates the EMIS1 scenario. Error bars represent the 25th and 75th percentiles of all domain-averaged data in each simulation.

Moved (insertion) [2]

Deleted: 5

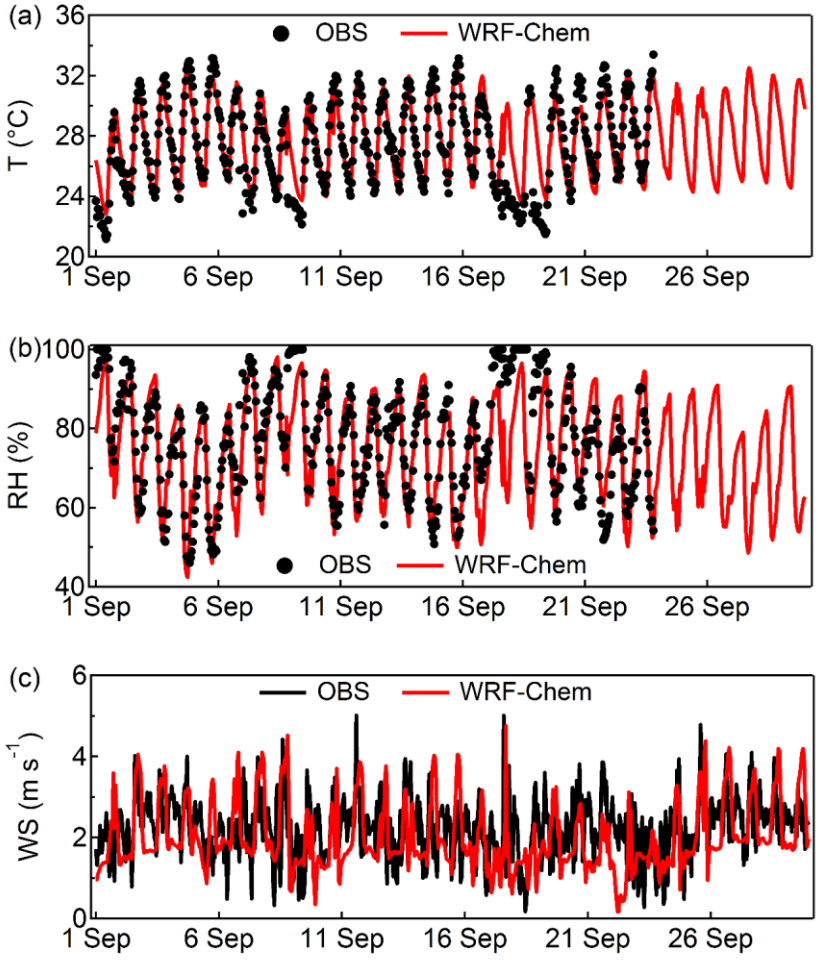

Figure S2. Time series of surface air temperature (a), relative humidity (b), and wind speed (c) from the domain3 simulation and the observations at ATTO during September 2014.

Deleted: 3

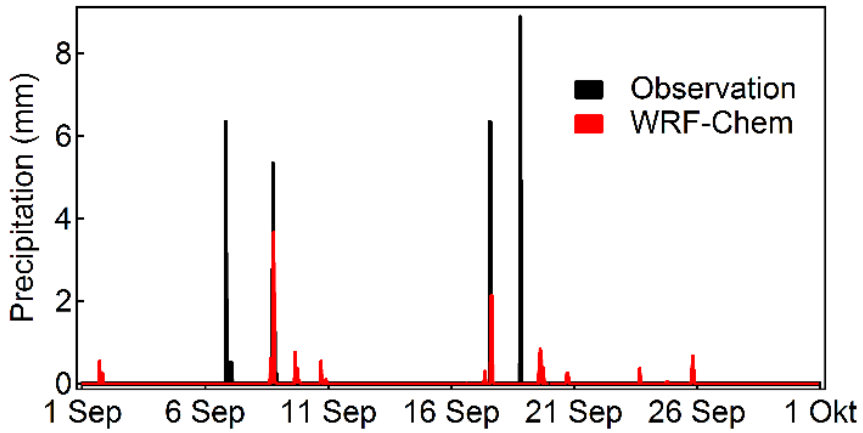

Figure S3. Time series of precipitation from observations at the ATTO site and WRF-Chem simulations during September 2014.

Deleted: 1

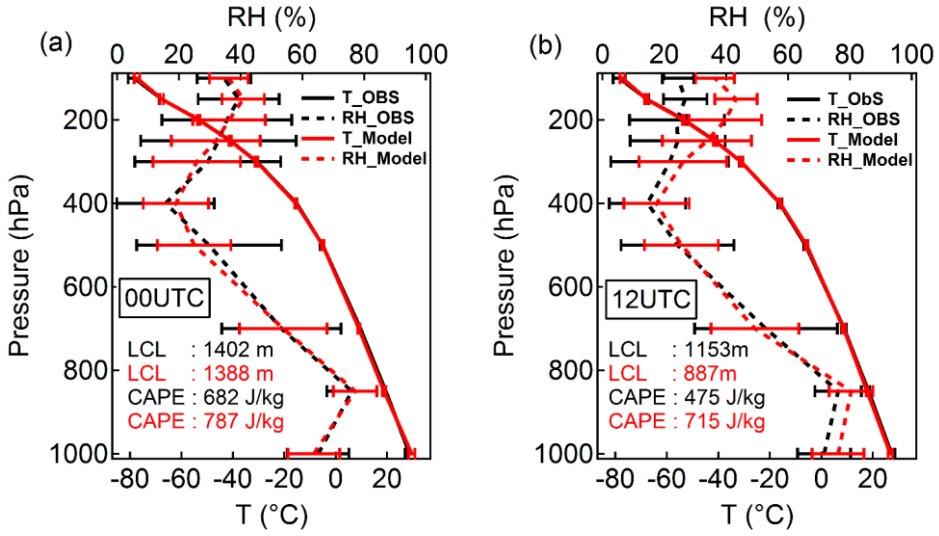

Figure S4. Vertical profiles of air temperature and relative humidity at standard levels, and retrieved CAPE and LCL values from radiosonde observations and WRF-Chem domain3 simulations at 00:00 UTC and 12:00 UTC at Manaus. Error bars at each pressure level represent the standard error at that level.

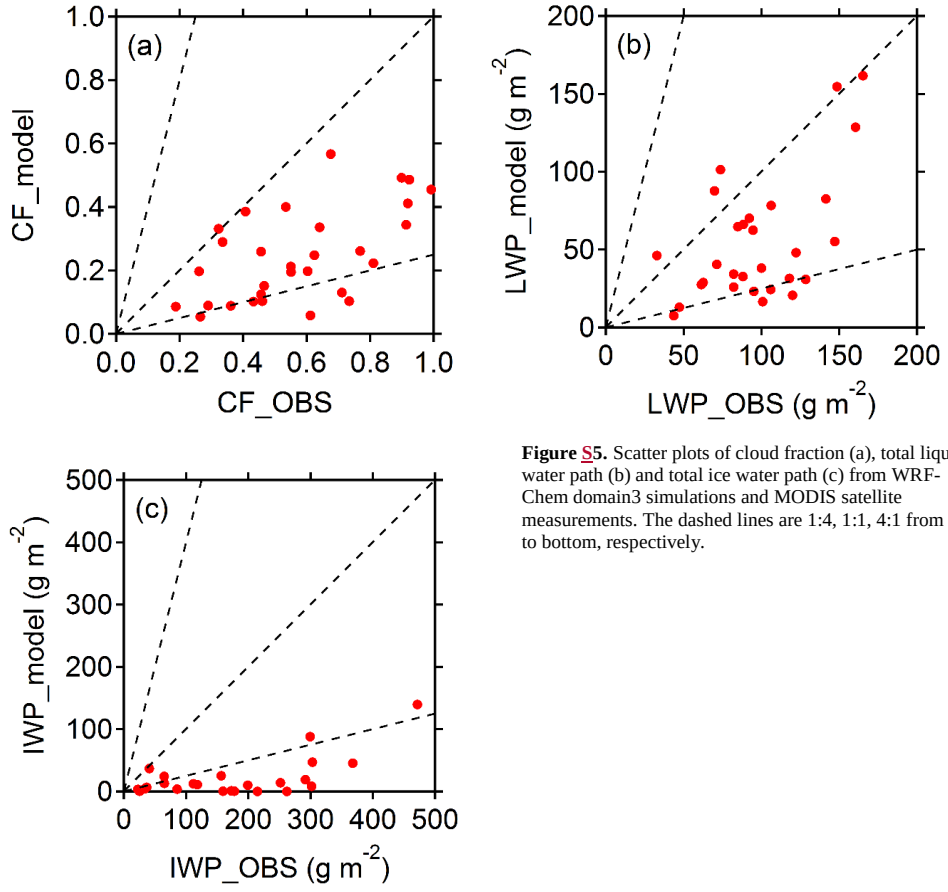

Figure S5. Scatter plots of cloud fraction (a), total liquid water path (b) and total ice water path (c) from WRF-Chem domain3 simulations and MODIS satellite measurements. The dashed lines are 1:4, 1:1, 4:1 from top to bottom, respectively.

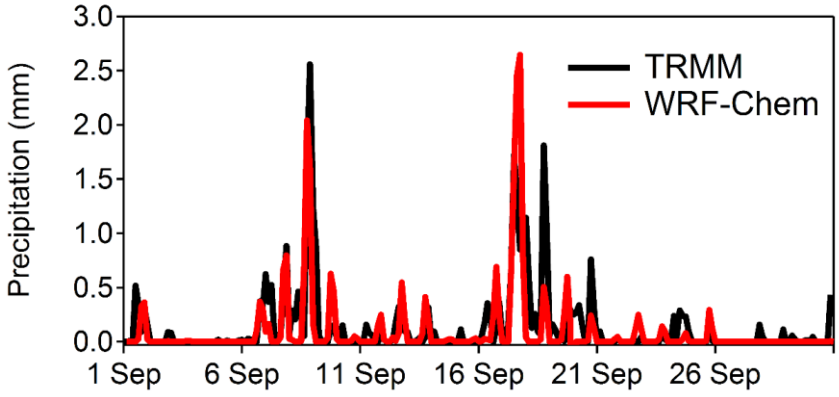

Figure S6. Time series of region averaged 3-hour accumulated precipitation (mm) over domain3 from TRMM satellite observations and WRF-Chem simulations during September 2014.

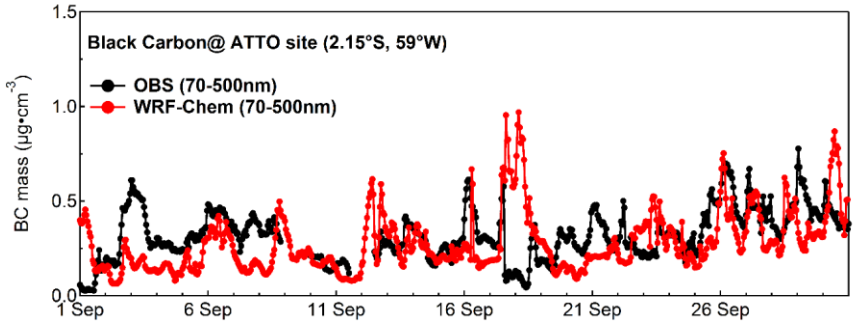

Figure S7. Time series of simulated and observed black carbon mass concentrations at the ATTO site.

Deleted: 2

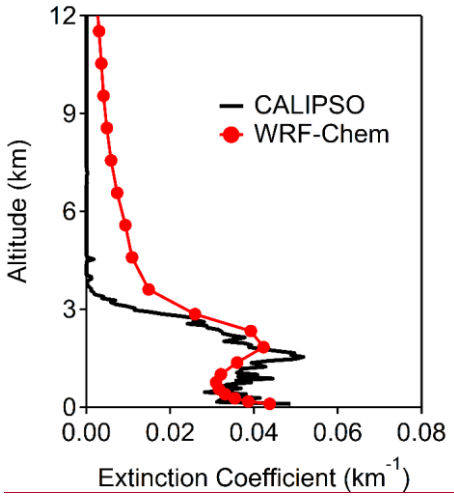

Figure S8. Monthly mean clear-sky aerosol extinction coefficient at 532 nm averaged over domain3.

Deleted:

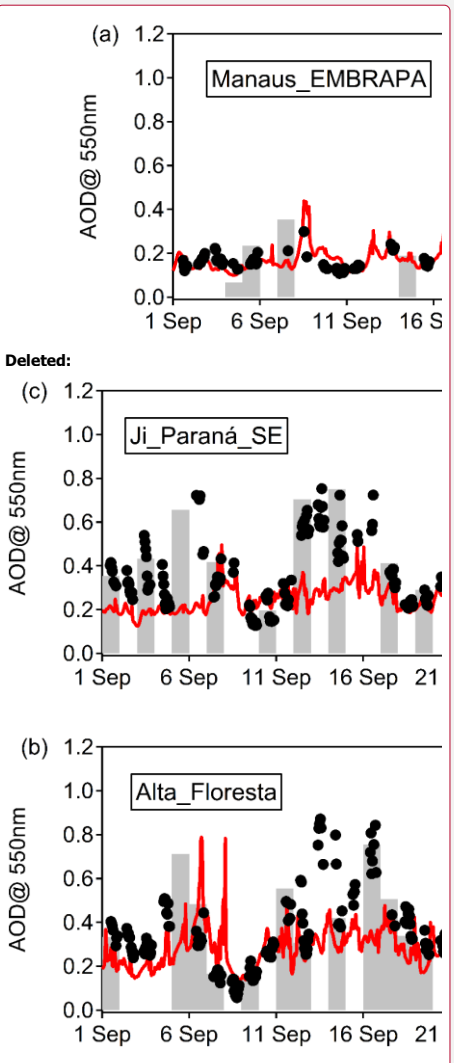

Figure 7. Time series of AOD at 550 nm from AERONET measurements, MODIS daily retrievals, and WRF-Chem simulations for three AERONET stations. The locations of the AERONET stations are shown in Figure 1.¶

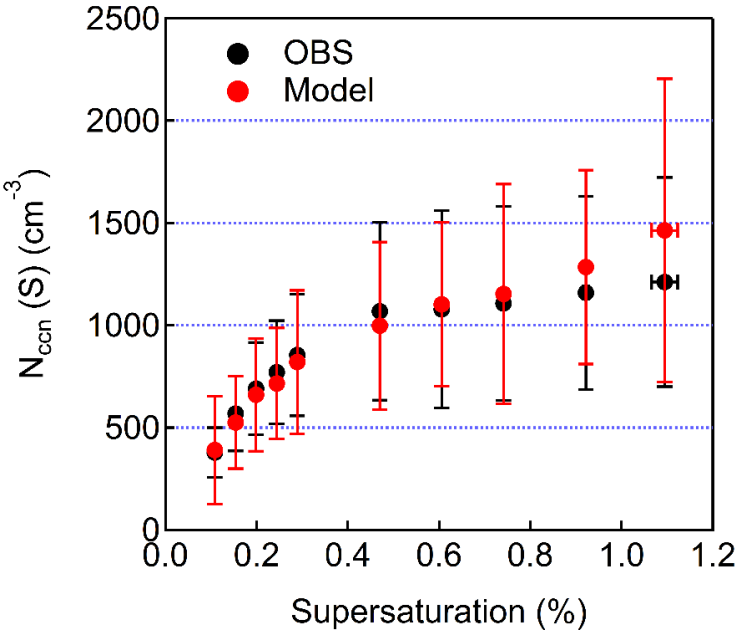

Figure S9. Monthly averaged CCN number concentrations at different supersaturations from ATTO observations and WRF-Chem simulations. Error bars represent the standard deviation.

Deleted: 8

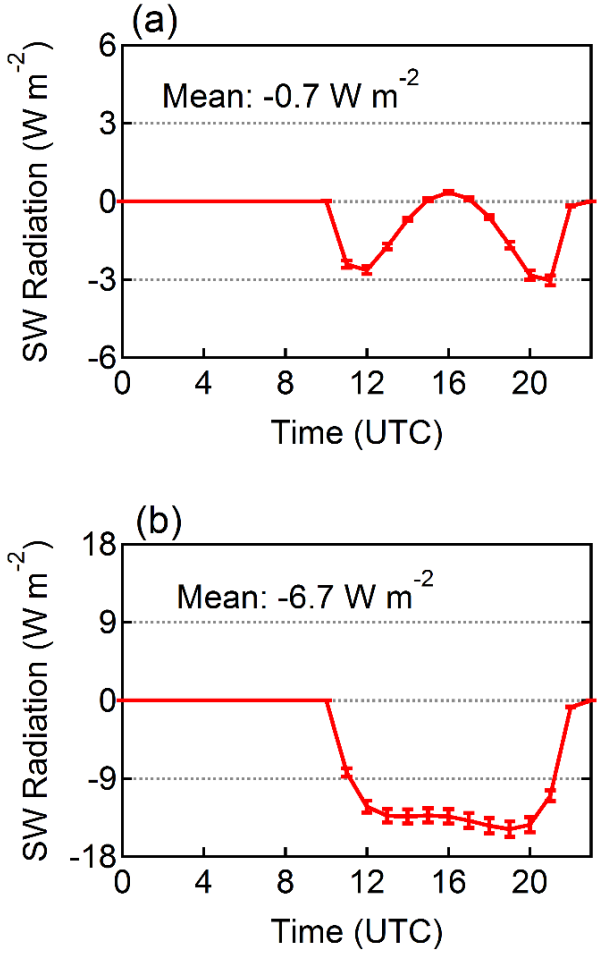

Figure S10. Diurnal variation of changes in clear-sky shortwave radiation at TOA (a) and at the surface (b) due to ARI in the EMIS1 emission scenario. Error bars denote the standard error.

Deleted: 3

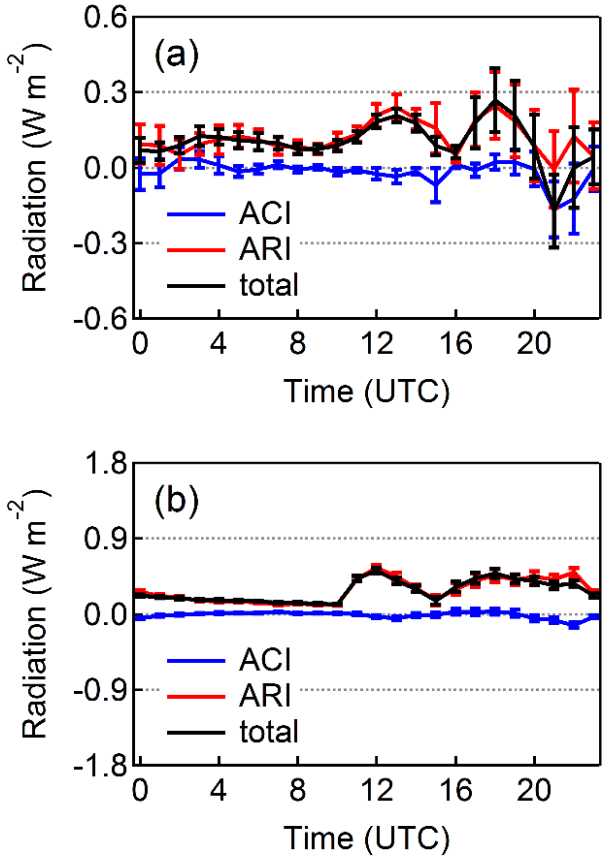

Figure S11. Diurnal variation of changes in all-sky longwave radiation at TOA (a) and at the surface (b) in the EMIS1 emission scenario. Error bars denote the standard error.

Deleted: 4

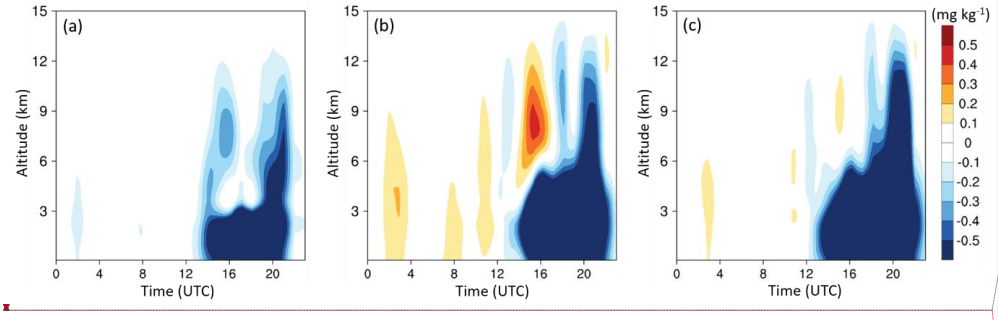

Figure S12. Diurnal variation of the vertical distribution of the domain-averaged difference in precipitating hydrometer (QRAIN+QSNOW+QGRAUP) concentrations caused by BB aerosols' ACI (a), ARI (b), and total effect (c) in the EMIS6 emission scenario.

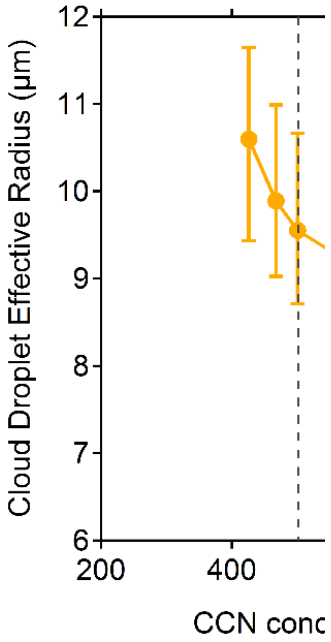

Moved up [2]:
Figure S5. Relationship of monthly mean domain-averaged cloud droplet effective radius and cloud-base CCN concentrations for all emission scenarios derived from experiments of CCNR3 and PCNR3_EMISX. The dashed line indicates the EMIS1 scenario. Error bars represent the 25th and 75th percentiles of all domain-averaged data in each simulation.¶

Deleted: Section Break (Next Page)

Deleted: 6

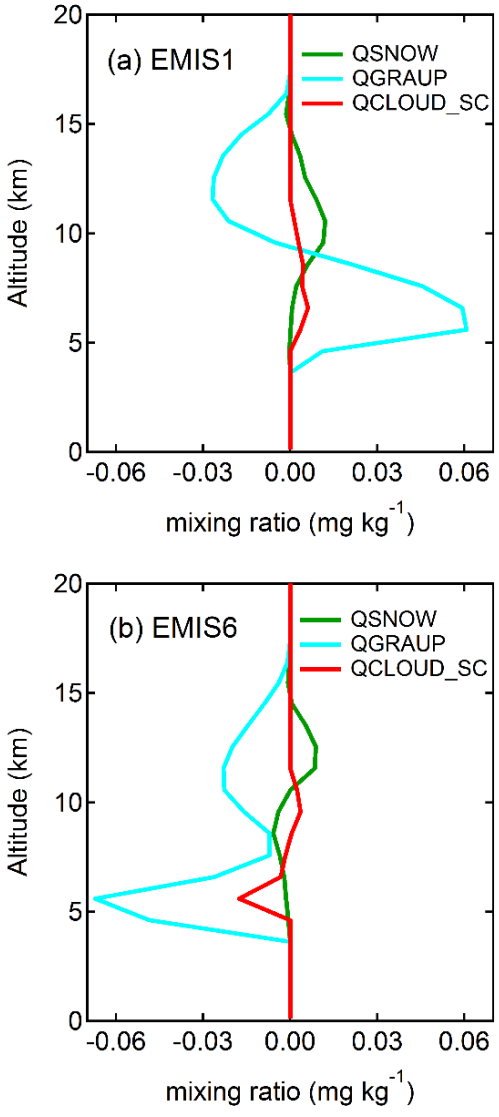

Figure S13. Profiles of ARI-induced changes in snow, graupel, and super-cooled cloud water mixing ratios for emission scenarios EMIS1 (a) and EMIS6 (b).

Deleted: 7

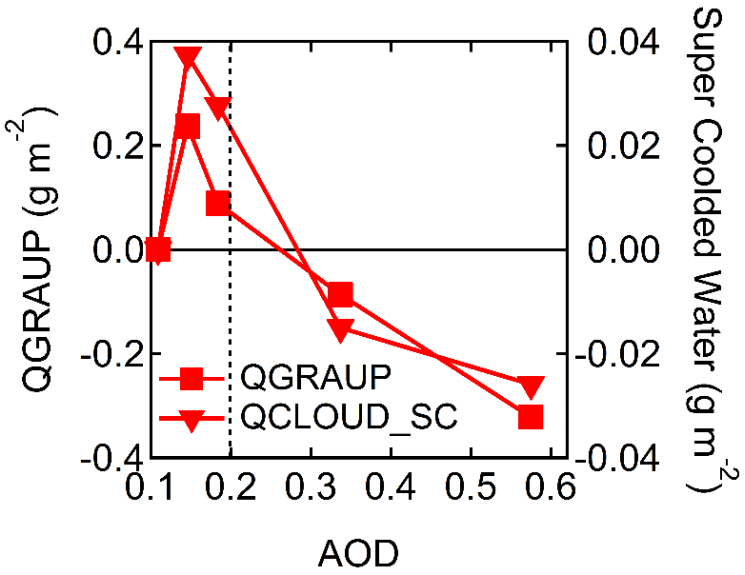

Figure S14. ARI-induced changes in column-integrated graupel and super-cooled cloud water content with increasing BB emission intensity (indicated by the domain-averaged AOD in each emission scenario). The vertical dotted line in each plot indicates the EMIS1 scenario.

Deleted: 8